T
~~SN251~~ 77-07 (T)

~~NOT FOR PUBLICATION~~

本資料は 43年 11月30日付けで登録区分変更する。
〔技術情報グループ〕

STUDIES ON WEAR AND FRICTIONAL BEHAVIOR BETWEEN FUEL RODS AND GRID SPACERS IN SODIUM

Feb., 1977

POWER REACTOR AND NUCLEAR FUEL DEVELOPMENT CORPORATION

~~NOT FOR PUBLICATION~~
T ~~S~~N251 77-07
Feb., 1977

STUDIES ON WEAR AND FRICTIONAL BEHAVIOR BETWEEN FUEL RODS AND GRID SPACERS IN SODIUM*

ISAO KAKEHI** SABURO TANI**
EIJI HUJII** HIDEHARU OKANO**
KINJI ENDO** TOSHIYUKI KAWADA**
KEIZO OGATA**

Abstract

Changes in the reactor power result in relative movements between the fuel rod bundle and grid spacers, due to thermal expansion of fuel rods.

Contact load, which is caused by deformation of fuel rods or axial alignment of grid spacers, is set up on the contact surfaces.

From this reason, changes in reactor power are the cause of galling between fuel rods and grid spacers.

In this work, wear between fuel rods and grid spacers in sodium was evaluated quantitatively under simulated reactor conditions, and a mock-up test in sodium was carricd out in order to evaluate designs of the fuel rod, grid spacers, and grid spacer mounting methods.

This is the translation of report, No. SJ201 76-23, issued in Sept., 1976

* The work performed under contracts between Power Reactor and Nuclear Fuel Development Corp. and Tokyo Shibaura Electric Co., Ltd.

** Tokyo Shibaura Electric Co., Ltd.

CONTENTS

Table List

Figure List

Photo List

1. Purpose of Experiment

Grid spacers and cladding tubes in the grid-type fuel assembly of an FBR are subject to axial relative displacement on their contracting surfaces caused by i) power ramp during normal operation and ii) power ramp at the time of abnormal operation. This is due to the difference in thermal expansion between the grid spacer holders (such as wrapper tube and tie-rods for instance) and fuel pins.

Even in the case where such a design consideration has been given as to provide a nominal dimensional gap between the grid spacer dimple and the cladding tube at the initial time of their manufacture, a load is produced on their contacting surfaces due to the following reasons:

i) Positional displacement of grid spacers which are axially arranged inside the wrapper tube.

ii) Bowing of the fuel pins within tolerance produced during fabrication.

iii) Bowing of fuel pins during reactor operation.

Because of the above phenomena, the relative movements caused by the power ramp of a reactor produce axial friction (galling) on the contacting surfaces between the grid spacer dimple and the cladding tube.

It is estimated that further load will be applied on the contacting surfaces at the time when the initial contact gap has disappeared as the result of swelling of the cladding tube caused by the progress of burn-up of the fuel.

Therefore, it is the purpose of this experiment to evaluate the wearing condition of the grid spacer holders and the cladding tubes by the repetition of galling in a series of in-sodium mockup tests, and thus to obtain the necessary design data for grid spacers and fuel pins.

2. Test Method

2-1. General Description of Test Method

The present experimental work involved the test of grid elements made and supplied by various fuel fabricators and the test of fuel assembly including grid spacers and full-bundles. The grid spacers and cladding tubes employed for this experiment have the same specifications as those of the prototype FBR, "MONJU".

The test of elements was performed to make quantitative evaluation of their correlations by combination of such parameters which are considered to affect the galling test results. And by grasping the wearing mechanism on the grid spacer dimple and the surface of cladding tubes by galling, evaluations of various grid elements were undertaken to provide useful data for design of grid spacers and fuel pins.

For the fuel assembly tests, the experimental conditions were prepared to simulate the real use conditions as much as possible, in order to observe the wearing phenomena caused by galling in an actual fuel and to reflect the results upon the design of grid type fuel assembly.

The tests were undertaken by exposing the test specimens comprising grid spacer and fuel pins to sodium in which the fuel pins or pin-bundles were moved up-and-down by a driving mechanism so that galling movements were created on the contacting faces between the grid spacer and the cladding tube. The measurement of the load was taken by the tension-compression type load cell which was installed on the axis of the driving mechanism.

2-2. Outline of Test Loop

The vertical driving mechanism installed to the Na test tank and the test specimens are as shown in Figs. 2-1 and 2-2. The photographs of the test loop and the test specimens are given in Photos 1 to 19.

2-2-1. Vertical Driving Mechanism

The vertical driving mechanism is coupled with the test specimen and the fuel pins, and is designed to move vertically the driving axis (crank shaft) to produce up-and-down crank movements so that galling can be created.

The main specifications are as follows:

Sliding stroke	10mm
Repetition velocity	3rpm
Max. load	100kg

2-2-2. Test specimen

a) Test of Elements

The specimens for the element test are as shown in Fig. 2-1 and Photos 4 to 13. But in this case, the test specimen is composed of grid elements, grid element spacer, fuel pins and the wrapper tube, and is able to hold six kinds of grid elements at a time in each test.

In respect of the load condition setup at the contact faces between grid element and fuel pin, it will be described in details in later pages. But referring to it briefly here, it is that, by moving slightly the grid element holes in the grid spacers which are arranged at 200mm intervals in the axial direction, the positions of fuel pins are forcibly changed to create load.

The list of the grid elements employed for this test is given in Table 2-1 and Fig. 2-11.

b) Test of Fuel Assembly

The test specimen of the fuel assembly is shown in Fig. 2-2 and Photos 14 to 19.

The mockup assembly employed for the test has the same specifications as those of prototype FBR, "MONJU". Two types of grid spacers such as the ring type grid spacer made by MAPI and the

combined grid made by Toshiba were used for the grid spacer test. (Photos 14 and 15, and Figs. 2, 12, and 13).

This test was aimed at observing the wearing condition of fuel pins and grid spacers in the actual assembly. Incorporating at the same time bowing fuel pins, application of the results of the element test was tried.

The positions of the bowing pins are shown in Fig. 2-10. Also for verification of grid spacer supporting technique, the screw fixing method which was proposed for "MONJU" was tested for the Toshiba-made combined grid, while the method whereby supporting framework holding both sides of the grid spacer was resistance spot welded to the wrapper tube was tested for the MAPI-made ring-type grid spacer. The outline of these methods are as given in Fig. 2-9 and Photos 18 and 19.

2-2-3. Sodium Purification Loop

For the impurity control of the sodium inside the test tank, a joint operation was performed for both the test loop and the cold trap loop.

The outline of the test loop and the cold trap loop is given in Fig. 2-3. The impurity control was carried out under the following conditions:

CT Operation Temperature	$<150\ ^{\circ}C$
PI Temperature	$<150\ ^{\circ}C$
Sodium Flow Rate	About 10ℓ/min

2-3. Test Loop Setup and Verification

2-3-1. Test of Elements

The load conditions for the element test were set up by forcibly displacing the fuel pins at the grid spacing position. The fuel rod

deformation mode under various load conditions are shown in Figs. 2-4 and 2-5. The load at this time is calculated theoretically as follows:

(1) Calculation Model

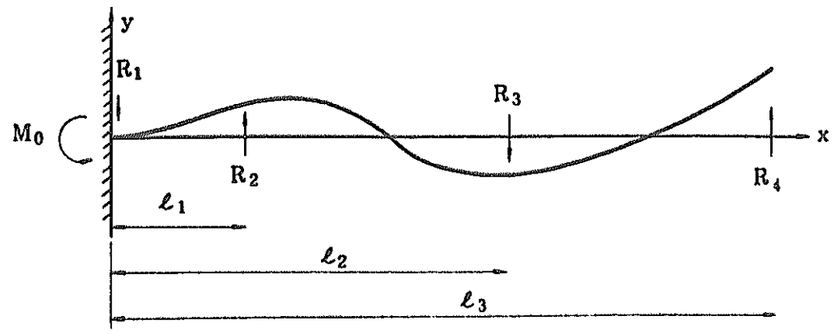

(2) Basic Equations

$$M_0 + \ell_3 R_1 + (\ell_3 - \ell_1) R_2 + (\ell_3 - \ell_2) R_3 = 0 \quad \cdots\cdots ①$$

$$R_1 + R_2 + R_3 + R_4 = 0 \quad \cdots\cdots ②$$

$$M_1 = M_0 + R_1 x \qquad 0 \le x \le \ell_1 \quad \cdots\cdots ③$$

$$M_2 = M_0 + R_1 x + R_2 (x - \ell_1) \qquad \ell_1 \le x \le \ell_2 \quad \cdots\cdots ④$$

$$M_3 = M_0 + R_1 x + R_2 (x - \ell_1) + R_3 (x - \ell_2)$$

$$\ell_2 \le x \le \ell_3 \quad \cdots\cdots ⑤$$

(3) Deflection

$$v_1 = \frac{1}{EI} \left(M_0 \frac{x^2}{2} + R_1 \frac{x^3}{6} \right) \qquad 0 \le x \le \ell_1 \quad \cdots\cdots ⑥$$

$$v_2 = \frac{1}{EI} \left(M_0 \frac{x^2}{2} + R_1 \frac{x^3}{6} + R_2 \left(\frac{x^3}{6} - \frac{\ell_1 x^2}{2} \right) + \frac{R_1 \ell_1^2}{2} x - \frac{R_2 \ell_1^3}{6} \right) \qquad \ell_1 \le x \le \ell_2 \quad \cdots\cdots ⑦$$

$$y_3 = \frac{1}{EI} \left(M_0 \frac{x^2}{2} + R_1 \frac{x^3}{6} + R_2 \left(\frac{x^3}{6} - \frac{\ell_1 x^2}{2} \right) + \frac{1}{2} (R_2 \ell_1^2 + R_3 \ell_2^2) x - \frac{1}{6} (R_2 \ell_1^3 + R_3 \ell_2^3) \right)$$

$$\ell_2 \le x \le \ell_3 \quad \cdots\cdots ⑧$$

Where, EI: Modulus of rigidity

(4) When load is sought from the deflection mode (Fig. 2-4 to Fig. 2-6 under various load conditions, it is as shown in Table 2-2.

After assembling the test specimen, the tensile load of the fuel pin was measured to verify the load condition. The tensile load of the fuel pin is calculated theoretically as follows:

i) Calculation Model

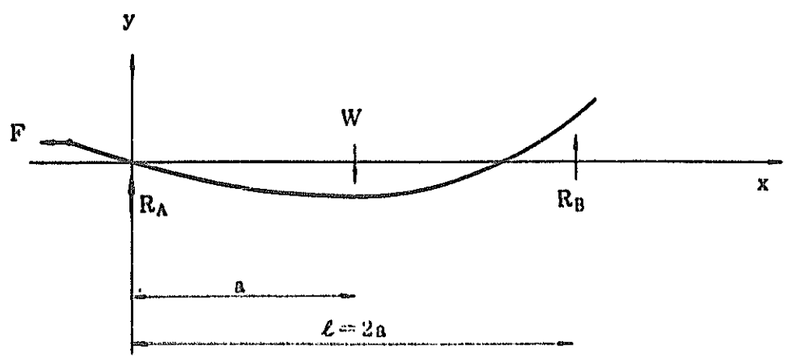

ii) Basic Equations

$$R_A + R_B + W = 0 \quad \cdots\cdots ①$$

$$W \cdot a + R_B \cdot \ell = 0 \quad \cdots\cdots ②$$

$$M_1 = R_A x \qquad 0 \leq x \leq a \quad \cdots\cdots ③$$

$$M_2 = R_A x + W(x - a) \qquad a \leq x \leq \ell \quad \cdots\cdots ④$$

iii) Deflection

$$y_{x=0} = 0 \quad \cdots\cdots ⑤$$

$$y_{x=a} = \frac{1}{EI}\left(\frac{W \cdot a^3}{12} + c_1 a\right) \quad \cdots\cdots ⑥$$

$$y_{x=\ell} = \frac{1}{6EI}\left(-3W \cdot a^3 + 6 C_1 a\right) \quad \cdots\cdots ⑦$$

Where, C_1 : Integral constant

EI : Modulus of rigidity

Calculated value of W, R_A and R_B under various load conditions, are as shown in Table 2-3. Consequently, assuming the in-air

coefficient of static friction for grid and cladding tube as μ = 0.2 to 0.4, the tensile load under various load conditions is then as given in Table 2-4.

The comparison between the above calculated results and the measured results is shown in Fig. 2-8 which indicates generally good consistency and the load condition setup is satisfied.

2-3-2. Test of Assembly

The load and deflection mode of the bowing fuel pins in an assembly are illustrated in Fig. 2-7.

Tensile tests were also undertaken the same as in the case of the element tests for the confirmation of load condition setup. The results are as shown in Fig. 2-8.

3. Measurement and Examination

3-1. Measurement of Changes in Frictional Force

The wear under repeated frictional motion of the fuel pins and grid spacers was observed at their contacting faces by measuring the tensile and compression load as mentioned in the previous section. The frictional force at the contact faces between fuel pins and grid spacers may be estimated by the following principle:

(1) The tension and compressed load measured by loadcell are the synthesized load with the following forces:

i) Force required for vertical movement by the vertical driving shaft alone, and

ii) Static frictional force and dynamic frictional force.

(2) The force required for driving the vertical driving shaft is estimated to produce some cyclic load since bellows are used for sealing of the driving shaft from the sodium test tank (Fig. 3-1-(a)). Actually the driving force is calculated as shown in Fig. 3-2-(a).

(3) In the next, the static frictional force is expected to have a peak at the time when grid spacers and fuel pin begin to slide on their contacting faces and also when their sliding motion finishes (Fig. 3-1-(b); A, B and C).

The dynamic frictional force is to be observed while in their sliding motion (Fig. 3-1-(b).

(4) Consequently, both the static and the dynamic frictional forces may be obtained as Fs, Fk from the synthesized load curve shown in Fig. 3-1-(c). In the actual case, this synthesized load curve is the same as shown by Fig. 3-2-(b).

3-2. Measurement of Wear

3-2-1. Measurement of Wear at Grid Dimple

The wear at grid dimple in the element test was measured as a change of the height from the standard level of the grid dimple before and after the test using a multipurpose projector. Photo 20 shows the main part of the apparatus.

The evaluation of the wear at the grid spacer dimple in the fuel assembly test was performed by examining the changes before and after the test in the internal contacting circle formed by the dimples.

3-2-2. Measurement of Wear of Cladding Tube

For the measurement of the wear at a cladding tube was conducted by use of three-dimensional measuring apparatus, and an electric micrometer was employed as the measuring sensor. The edge of the feeler was in a spherical form of 0.5^{R}. The apparatus used for this measurement is as shown in Photos 21 and 22.

3-3. Observation of Surface Condition

Examination of morphology of wear and degeneration on the friction-worn surfaces of the cladding tube and the grid dimple was conducted by scanning electron microscopic surface observation and metallographic microscopic observation.

3-4. Strength Test

3-4-1. Hardness Test

The hardness change on the worn surfaces of cladding tube and grid dimple before and after the testing was examined by Micro-Vickers hardness tester to see strength change and existence of degenerated layer.

3-4-2. Rupture Test of Cladding Tube

A hydraulic burst test was performed on the cladding tube after

galling test to examine the rupture strength.

3-4-3. Compression Test of Grid Dimple

A compression load test to measure the spring constant and yield strength was performed on grid dimple after galling test in order to examine its strength deterioration.

3-5. Fuel Assembly Test and Integrity Test of Grid Spacer

For the evaluation of integrity of grid spacers after the test of fuel assembly, the spacing of each grid element and external appearance were examined.

4. Assessment of Test Conditions

4-1. Temperature Condition

The test temperatures were set in consideration of the design temperature ranges of grid spacers and fuel pins as shown below:

i) 400 °C Equivalent to the temperature at the core inlet

ii) 550 °C Equivalent to the mean temperature for the entire assembly

iii) 650 °C Equivalent to the temperature on the surface of cladding tube

The design temperatures of fuel pin, wrapper tube and coolant are shown in Fig. 4-1.[27)]

4-2. Repetition Times

According to the recent studies on fretting wear, it is reported that the wear behavior changes at around the fretting amplitude of 70 μm, and that above this level, the wear increases drastically.[23)]

Therefore, those wear phenomena which are caused by the power ramp during reactor operation of which fretting amplitude is extremely small should be considered as fretting wear.

This experimental work handles such galling phenomena as caused by comparatively large power ramp during FBR operation. The power ramp of "MONJU" is represented by Table 4-1.[27)]

According to this table,

i) Frequency of power ramp under normal operation is about 1,200 times*

ii) Frequency of power ramp under abnormal operation is about 30 times*

Most of the power ramps are those due to the load following operation of the reactor, which is believed to occur about 1,000 times during the life of a fuel. The test cycle numbers were set as follows

considering the above:

(a) 500 times, (b) 1,000 times, (c) 1,500 times

4-3. Load Conditions

(1) The loading condition of fuel pin which has the severest contact load condition in the MONJU's adjustment design stage II is as shown in Fig. 4-2. According to which, the maximum contact load at the initial life cycle is about 0.5kg, and at the end life cycle about 1.0kg.

(2) From the above viewpoint, it will be good enough to evaluate the contact load up to the range of the maximum load of 1kg. But since this experimental work has to evaluate various grid elements within the given period of time, it is difficult to obtain its correlation with wear rate within the load below 1kg when considering the established accuracy of the load conditions.

(3) In this respect, it is thought desirable to obtain data over the wider range of load condition taking high fluence core in the future reactors into consideration.

(4) The load conditions were set as follows considering the above items:

(a) 0.5 kg, (b) 1.0 kg, (c) 2.0 kg.

4-4. Other Conditions

4-4-1. Sliding Length

The sliding length was set at 10mm in this experiment. This experiment. This width was calculated from the temperature distribution of the fuel assembly as shown in Fig. 4-1 and from the thermal expansion gap between the fuel rod and the grid spacer holding materials (wrapper tube, for instance).

According to this calculation, although the designwise conceivable sliding length is about 5mm, considering the accuracy of the wear

measuring technique (responding capacity of measuring technique to the wearing variation of the sliding length), it is set at 10mm for the present experiment. This treatment is thought to be not wrong since the wear of cladding tube depends only on the number of repetition.

The wear of the grid dimple was arranged not by cycle number but by friction distance (sliding length x 2 x cycle number).

4-4-2. Effect of Repetition (Friction) Velocity

As was stated before, the load following operation is the most frequent case of the power ramp operation of a reactor. The power ramp rate in this reactor operation is ± 5%/min.according to "MONJU" plant design. The friction velocity is about 10μm/sec at 100% of reactor power if the sliding length is 10mm. The repetition friction velocity in the present experiment is 1mm/sec.

However, when friction velocity is extremely low as in the case of this experiment or in the real reactor system, it can be assumed there is no much difference in the wear rates[25),26)]

That is, it will be all right to consider the effect of temperature on the friction surfaces by friction velocity Ws (θ) as shown below is constant, and wear rate ΔW proportionates to contact pressure ΔP and friction distance ΔL, etc.

$$\Delta W = Ws(\theta) \cdot P \cdot \Delta L$$

Hardly any difference was observed between static frictional force and dynamic frictional force in the actual measurement of frictional force. This, therefore, may be said an experiment of static friction.

4-5. Fuel Assembly Test Conditions

It can be said that the present experiment is a general test where the wear and frictional behavior of fuel pins and grid spacers in the

fuel assembly were tested and measured.

Consequently, temperature conditions and load conditions were selected so that they would constitute average conditions of a fuel assembly in the reactor core. Also, in order to observe the effect of displacement of various grid spacers axially arranged inside the wrapper tube to wear and frictional phenomena, the tests were conducted by installing both straight and bowed pins to apply load.

The above mentioned test conditions are summarized as follows:

Temperature condition	:	550 °C
Contact load condition	:	0.3 kg max.
Cycle No.	:	1500

5. Inspection Data of Test Specimens Prior to In-Sodium Testing

5-1. Cladding Tube

(1) The results of the inspection of the outer diameter of the cladding tube which was exposed to test are in Fig. 5-1.

(2) The hardness of the cladding tube prior to test is as shown in Fig. 5-6.

(3) The results of the burst test of the cladding tube prior to in-sodium test and also those of after in-sodium test are shown in Fig. 6-19.

5-2. Grid Elements

(1) The results of the inspection of the internal contact surface circle diameter of various grid elements which were subjected to test are in Figs. 5-2 to 5-5.

(2) Fig. 5-6 shows the pre-test hardness of various grid elements.

(3) The results of the compression test of dimples of various grid elements before in-sodium test are illustrated together with those of post-in-sodium test in Fig. 6-20.

5-3. Grid Spacer

(1) The results of the inspection of the internal contacting surface circle diameter of the combined grid of Toshiba and the ring-type grid of Mitsubishi are in Figs. 6-22 to 6-23.

(2) Similarly, the results of the inspection of the fuel pin arrangement pitches in various grids are shown for both before and after in-sodium testing in Figs. 6-24 to 6-25.

5-4. Fuel Pin Bundle Holders

The results of the fuel pin arrangement pitches of fuel pin bundle holders which were subjected to the fuel assembly test are as shown in Fig. 5-7.

6. Results

6-1. Test of Elements

6-1-1. Measurement of Frictional Force

(1) Figs. 6-1 to 6-3 represent the estimation of the variation of frictional force during its two-way sliding motion on the contacting faces between grid spacer and fuel pin. This estimation was made from the load obtained by loadcell and using the theory given in Fig. 3-1.

(2) Estimating the static friction coefficient between fuel pin and grid spacer in sodium from this measurement of frictional force, it is as follows:

$$\mu s = 0.40 - 0.60^{14)}$$

(3) The results of the load at this time were analyzed according to the theory given in Fig. 3-1. It was shown that there was no difference between statical friction force and kinetic friction force, and that the condition of the two-way sliding velocity in this test was the coefficient of static friction.

6-1-2. Wear and Wear Rate of Cladding Tube

(1) The test results of the wear of cladding tube under the test conditions of sodium temperature at 400 °C, load 0.5 ~ 2 kg, and cycle number 500 ~ 2000 are as shown in Fig. 6-4.

(2) The test results of the wear of cladding tube under the test conditions of sodium temperature at 550 °C, load 0.5 ~ 2 kg, and cycle number 500 ~ 1500 are as shown in Fig. 6-6.

(3) The test results of the wear of cladding tube under the test conditions of sodium temperature at 650 °C, load 0.5 ~ 2 kg, and cycle number 500 ~ 1500 are as shown in Fig. 6-8.

(4) The wear of cladding tube can be expressed as follows by use of wear rate K_C:[3),8)]

$$d = K_C \cdot N \cdot W$$

Where, d = Wear of cladding tube (measured value) (μm)

K_C = Wear rate (μm/cycle·kg)

N = Number of repetition

W = Load on contacting surface (kg)

(5) The relations between wear rate and cycle number at various temperatures are shown in Figs. 6-5, 6-7 and 6-9 respectively with load condition as parameter.

(6) From these data, it is known that the wear rate K_C becomes small under the test conditions of 2kg load and 1500 cycle. Consequently, wear is thought to make no abrupt increase when conditions reach this stage and that thereafter it remains at normal and constant wearing.

(7) Fig. 6-10 shows the temperature effect on the wear rate K_C with contacting load and cycle number as parameters.

6-1-3. Wear and Wear Rate of Grid Dimple

(1) The test results of grid dimple wear under the conditions of sodium temperature 400 °C, load 0.5 ~ 2 kg, and cycle number 500 ~ 2000 (equivalent to frictional distance of 10 ~ 40 m) are as shown in Fig. 6-11.

(2) The test results of grid dimple wear under the conditions of sodium temperature 550 °C, load 0.5 ~ 2 kg, and cycle number 500 ~ 1500 (equivalent to frictional distance of 10 ~ 30 m) are as shown in Fig. 6-13.

(3) The test results of grid dimple wear under the conditions of sodium temperature 650 °C, load 0.5 ~ 2 kg, and cycle number 500 ~ 1500 (equivalent to frictional distance of 10 ~ 30 m) are as shown in Fig. 6-15.

(4) Grid dimple wear can be expressed as follows by use of wear rate K_g same as in the case of cladding tube:[3),8)]

$$d = K_g \cdot L \cdot W$$

Where, d = Wear of grid dimple (measured value) (μm)

K_g = Wear rate (μm/m·kg)

L = Frictional distance (m)

W = Load on contact surface (kg)

(5) The relations between wear rate K_g and frictional length at various test temperatures are as shown in Figs. 6-12, 6-14 and 6-16 with load condition as parameter.

(6) The wearing phenomena of grid dimple showed small wear rate K_g similarly to the cladding tube under the test conditions at 2.0kg load and 1500 cycle number, and is estimated to have transitted to normal and constant wearing.

(7) Fig. 6-17 represents the temperature effect of wear rate using contact surface load and cycle number as parameters.

6-1-4. Observation of Surface Condition of Worn Section

(1) The typical external appearances of surface wearing of cladding tube and grid dimple are represented in Photos 23 and 24.

(2) Scanning electron microscopic observation of surface conditions and wear morphology of both cladding tube and grid dimple was conducted, of which results are as shown in Photos 25 ~ 30. This electron microscopic observation revealed the following points:

*shear-breaking traces considered to have been caused by coagulational friction were observed in the cladding tube and grid dimple.

*On both ends of the sliding direction on the sliding surfaces, deposition of abrased particles was observed. In particular, on the contacting surface of cladding tube, this type of deposition

was quite evident.

*No difference in wear morphology by the difference of configuration of grid dimple was observed. Difference in the contacting surface area was evident particularly in the observation photographs of grid dimples.

(3) Metallographic Cross Sectional Observation

Longitudinal and transverse cross sectional metallographic observation was performed on the worn surfaces of cladding tube and grid dimple for the purpose of examining wear morphology and surface degenerated layer. The results are as shown in Photos 31 and 32, which indicate the following points:

*The transverse cross sectional metallographic pictures clearly present rough surface of worn section, while the longitudinal cross sectional metallographic pictures indicate deposition of abrased particles.

*This cross sectional metallographic observation revealed no compositional or structural changes on the abrased surfaces.

6-1-5. Strength Test

(1) Measurement of Hardness Change in Abrased Sections

Changes of surface hardness on the worn surfaces of cladding tube and grid dimple before and after testing were examined in order to verify the strength change and existence of degenerated layers.

The results are as shown in Fig. 6-18.

The measured positions were the five locations as indicated in Fig. 6-18. Each location had three measuring points, and the mean value of so measured values is shown in terms of hardness. The measured results were compared with the pre-test data given in Fig. 5-6 to observe the changes in surface hardness. This

comparative observation revealed no evident change indicating good consistency with the results of the cross sectional metallographic observation.

(2) Rupture Test of Cladding Tube

Hydraulic pressure burst test was performed to examine strength deterioration in the abrased section of cladding tube after testing (pressurization rate about 100kg/cm^2/sec.) The results are as shown in Fig. 6-19. The test result indicated that the tested rupture strength exceeded the manufacturing specifications of the cladding tube for "MONJU". Rupture took place even in other sections than the worn section. But the worn section indicated high rupture probability. Rupture pressure was low for the test specimen at the sodium temperature of 650 °C. This was thought as the result of annealing phenomenon taken place during the galling test.

(3) Compression Test of Grid Dimple

The spring constant and yielding load were measured in order to examine the strength deterioration of grid dimple after testing. The results are as shown in Fig. 6-20. The measured data were compared with the pre-test data to observe changes. But no obvious change was presented.

6-2. Fuel Assembly Test

6-2-1. Measurement of Frictional Force

(1) The changes in frictional force during two-way slidding frictional motion estimated from the load obtained by use of tension compression type load cell for 100 kg load by the same technique as applied to the element test, and the results are shown in Fig. 6-21. The so measured frictional force in this case was for the

load at the contact points of 169 fuel pins with grid (3 points in axial direction).

(2) The measured results of frictional force were 15 ~ 30 kg in the initial cycle period and 50 ~ 70 kg in the end cycle period (1500 cycles) as shown in Fig. 6-21.

(3) The average contact load between fuel pin and grid spacer, from the coefficient of friction of $\dot{\mu}$ ~ 0.50 to 0.60 estimated from the element test at 550 °C, was estimated about 0.07 ~ 0.12 kg for the initial cycle period and about 0.16 ~ 0.28 kg for the end cycle period.

(4) The contact load of the bowed pin incorporated into the fuel assembly was 0.07 ~ 0.3 kg as shown in Fig. 2-7. The gross total of the frictional force (for 28 bowed pins) was 15 kg, and indicated generally reasonable value in the initial cycle period. The reason for comparatively large values for the combined grid was that, due to the finish of the weld-assembling of wave beam type plates with the surrounding honeycome type grid, there were some places where fuel pin charging was not smoothly done at the time of the assembling of the test specimen.

(5) The frictional force in the end cycle period of the test had reached equilibrium, but its value was considerably large. This is approximately equivalent to 169 bowing pins having maximum contact load of 0.3 kg.

This phenomenon is thought to indicate the variation of contact load created during the galling motion within the assembling tolerance between fuel bundles and grid spacers (for instance, by the positional displacement of the axially arranged grid spacers, there was created contact load between fuel pins and grid). Frictional coefficient indicated small value as shown in Fig. 6-21

and had reached equilibrium.

6-2-2. Wear Rate of Cladding Tube

(1) To facilitate the observation of the wear condition of cladding tube after test, metallographic photographs of external appearance are presented in Photos 33 and 34.

(2) For the measurement of wear of cladding tube, a total microscope was employed since both the width and depth of flaw are so small that it was impossible to measure them by the same measuring technique as employed for element test.

(3) The wear of cladding tube was observed as 20 to 40 μm for bowed pins (max. contact load about 0.3 kg) and <5 to 20 μm for straight pins. These values are approximately consistent with the results of the element test.

(4) No difference in wear was observed between the central cell section and the surrounding cell section of the straight pins.

6-2-3. Wear of Grid

(1) The internal contact diameter formed by the grid dimple was measured before and after test in order to facilitate the examination of wear rate of grid after test. The results are as shown in Figs. 6-22 and 6-23.

(2) The frequency distribution of the internal contact diameter changes as shown in Figs. 6-22 and 6-23 were measured taking the samples of the entire contacting sections of both the straight and bowed pins of grid spacers. But in the case of the combined grid, only the surrounding honeycomb grid was taken as sample. On the right shoulder of the diagram, there are shown the mean value and standard deviations of the data expressed in frequency distribution, and at the same time, the mean value and the standard deviations of the bowed pin contact section only were presented to show its effect.

(3) It is concluded that there was no evident change in grid wear, judging from the bundle average data.

The max. changes of internal contact diameter before and after test was about 40 μm for Toshiba combined grid and about 50 μm for Mitsubishi ring type grid.

6-2-4. Integrity of Grid Spacers

(1) For the evaluation of the integrity of grid spacers after the assembly test, grid arrangement pitches and external configuration were examined to see whether there had been any changes. The results are as shown in Figs. 6-24 ~ 6-27.

(2) The post-test grid spacers were observed to have changed the configuration of lattice due to mechanical interaction between fuel pin bundle and grid spacers as considered in the previous Paragraph 6-2-1 (Photo 35).

The configurational changes of Toshiba-made combined grid and Mitsubishi-made ring-type grid are as indicated in Figs. 6-28 ~ 6-29. There was found no immediate relation between the deformed sections and the location of the bowed pins. The following reasons can be considered for the deformation of lattice:

(a) In the case of Mitsubishi-made ring-type grid, dimples are forcibly deployed in the weaker section in the peripheral area as shown in Fig. 6-28.

(b) In the case of Toshiba-made combined grid, since charging of fuel pins during the assembling work had not been smoothly done due to the finish up the weld-assembly of wave beam lattice plates forming the peripheral honeycomb and central grid, the constraining load in this area remained as a load.

(c) This mechanical interaction is considered due to the end-plug holding technique of the fuel pin bundle and the tolerance

clearance of this end-plug holder. But in this test, it was held tightly by use of the holders with such pitch arrangement as shown in Fig. 5-7. Refer to Fig. 2-2 and Photo 17 for the holding method.

6-2-5. Integrity of Grid Spacer Holding Method

Integrity of the grid spacer holding method was verified after the test. Both of the two holding methods were confirmed good. Photo 35 shows the post-test grid spacer holders.

7. Evaluation of the Results

7-1. Wear of Cladding Tube

(1) As to the wear of cladding tube, the results of its post-test evaluation are summarized in Fig. 6-10.

(2) Based on the above data on the wear of cladding tube applicable to fuel design are given in Figs. 7-1 and 7-3.

7-2. Wear of Grid Dimple

(1) The wear of grid dimple as evaluated from the results of the test are summarized in Fig. 6-17.

(2) Based on the above data, the wear of grid dimple applicable to fuel design are given in Figs. 7-4 to 7-5.

(3) No prediction was possible for the abrupt increase of grid dimple wear during low cycle test unlike in the case of cladding tube. For this reason, a low cycle test of 100 cycle at 650 °C was performed to make up the evaluation data. As the result, it was known that the wear of grid dimple progressed considerably even in the initial cycle period contrary to the case of cladding tube. Its data are as shown in Fig. 7-5.

7-3. Configuration Effect of Grid Spacer Dimple

(1) As to the effect of the configuration of grid spacer dimple to the wear of cladding tube and of the spacer dimples themselves, it is very effective to the wear of cladding tube at 400 °C in the case of the wave beam type as seen in Fig. 6-4, but at 550 °C and 650 °C, its effect shows a trend of decline. But no visible wear was noticed on the dimples themselves as shown in Photo 24.

(2) Even in respect of oval-shaped dimple, its effect to cladding tube is almost the same as in the case of semi-circular dimples.

For its own dimple wear, as seen from Fig. 6-11, 6-13 and 6-15, its wear is smaller than in the case of semi-circular dimples.

7-4. Strength of Cladding Tube and Grid after Galling Test

(1) Hardness

Hardness of the worn surfaces of cladding tube and grid dimple after and before the test were examined to see their hardness change and existence of degenerated layers. No conspicuous changes were observed within the conditions of measurement (Na temperature at 550 °C, wear 20 to 75 μm), which concurred with the results of the cross sectional metallographic observation.

(2) Rupture Strength of Cladding Tube

Strength deterioration of the worn section of cladding tube before and after test was examined by hydraulic burst test. No conspicuous strength deterioration was noticed upto the wear of 100 μm level. But it may be said that rupture at the worn section took place with a high probability. The test specimens after sodium exposure at 650 °C showed lower rupture pressure. This may be because of the annealing effect.

(3) Compression Strength of Grid Dimple

Compression test was made for the post-test grid dimple to check its strength deterioration. No conspicuous changes were observed within the measured conditions (Na temperature at 550 °C, wear 20 to 70 μm).

(4) No information was obtained as to the mechanical property changes (especially hardness) of cladding tube and grid. Further studies are necessary for that purpose.

7-5. Evaluation and Verification of "MONJU" Fuel Assembly from It's Galling Behavior

(1) Wear of cladding tube was 20 to 40 μm in bowed pins (max. contact load about 0.3kg) and 5 to 20 μm in straight pins.

From the results of the assembly test, the wear of cladding tube in the assembled form by galling effect approximately agreed with the data obtained in the element test.

The wear by the mechanical interaction between fuel pin bundle and grid spacer during the galling movement was about 20 μm max, when both of them were within the tolerance limit.

(2) The wear of the grid spacer dimple presented little problem within the conditions of the present assembly test.

(3) From the above, it is considered that the knowledge on the wear behavior of cladding tube and grid spacer during galling movement in fuel assembly can be mostly obtained from the data of the element test.

(4) But, as judged from the measurement of frictional force, the contact load generated in the fuel assembly was observed to have caused some deformation of grid during the galling movement, even if the fuel was assembled within the tolerance limits. It will therefore be necessary to pay more attention to the design and quality control of fuel fabrication from this view point (for instance, clearance between fuel pin and grid).

(5) In respect of the grid supporting method, the integrity of the two methods which had been tested has proved to be acceptable.

8. Conclusion

(1) The present element test proved it possible to quantitatively evaluate the wear behavior of cladding tube and grid spacer dimples during the galling between fuel pins and grid spacers as a function of such parameters as Na temperatures, repetition times, contact load conditions, etc.

(2) It was possible by the fuel assembly test to evaluate grid type fuel assembly for "MONJU" with regard to its galling behavior, and to obtain data for its verification.
The assembly test indicated that the data obtained from the element test could be effectively utilized.

(3) In respect of the utilization of the evaluation data obtained from the results of the present experiment to the fuel design, it is considered that the design wear rate should be determined after giving discrete consideration to the contact load between cladding tube and grid spacer, temperatures, cycle numbers, frictional distance, etc., within the strength of the worn cladding tube (especially creep characteristics) and the tolerable wear of the verified integrity of the worn grid spacer.

References

1) "Friction and Lubrication of Solid" by F.P. Bowden & D. Tabor, Translated by Masuda, Maruzen.

2) Masuda, "Stories of Friction", Iwanami.

3) "Lubrication Handbook", Nippon Junkatsu Gakkai.

4) Chikuzoe "Surface Roughness and Friction" Junkatsu Vol. 19, No. 2, 1974.

5) Kohashi, "Corrosion of Stainless Steel 316 304 and 2¼Cr-1Mo Steel in Liquid Sodium and Their Mechanical Properties", Toshiba, SR-283.

6) Toshiba SR-392.

7) R.N. Johnson, "Wear Resistant Coating for Reactor Components in Liquid Sodium Environments" J. Vol. Sci. Technol. Vol. 11, No. 4, 1974.

8) W.A. Glaeser, "Wear and Friction Characteristics of Structural Materials in Liquid Sodium", Reactor Technol. Vol. 15, No. 1, 1972.

9) E. Rabinowicz, "Friction and Wear of Materials", John Wiley & Sons, Inc., New York, 1965.

10) LMEC-70-10, "Friction and Wear Screening Tests of Materials in Sodium", 1970.

11) SN941, 73-20, "Fretting Corrosion Test in High Temperature Sodium (I)" June, 1973.

12) SN941, 75-52, "Fretting Corrosion Test in High Temperature Sodium (II) and Temperature Dependency of Fretting Phenomena", June, 1975.

13) SN941, 75-12, "Self-Weld Test in High Temperature Sodium (III) and Temperature Dependency of Self-Welding Phenomena" Jan. 1975.

14) SN941, 74-80, "In-Sodium Wear Test of FBR Materials (IV) and Metallographic Test of Hard Alloy Carbite", October, 1974.

15) Sata, "Wear Behavior of Mechanical Materials and Measures to be Taken", The Japan Society of Mechanical Engineers, 381th Lecture Course, June, 1973.

16) Kawagoshi et al. "Relations between High Temperature Hardness and Tensile Properties of 50 - 754 Steel Materials", Material Test Technology Vol. 20, No. 1, Jan., 1975.

17) Yoshizawa et al. "Meaning of Material Strength of Hardness", Journal of Japan Society of Mechanical Engineers, Vol. 64, No. 513, Oct., 1961.

18) Nakajima, "Metal Surface and Its Observation" Journal of Japan Society of Mechanical Engineers, Vol. 79, No. 693, Aug., 1976.

19) Kayaba, "Surface Roughness and Deposition", Junkatsu Vol. 19, No. 2, 1974.

20) Noro, "Friction and Abrasion", Junkatsu Vol. 20, No. 7, 1975.

21) Wada, "Coefficient of Friction of UO_2 Pellet and Cladding Tube", Toshiba RM-14418, Oct., 1975.

22) K. Kleefeldt, "Untersuchungen Zum Verschleis und zum Reibverhalten Zwischen Brennestbbundel und Abstandshaltergittern in Natrium", KFK-1290, Oct., 1970.

23) N. Ohmae, "The Effect of Slip Amplitude on Fretting Wear", 27 (1974) 281-294.

24) K. Natesan, "Effect of Sodium on Mechanical Properties and Friction Wear Behavior of LMFBR Materials", Reactor Technol. Vol. 15, No. 4, Winter 1972 - 1973.

25) Japan Institute of Metals, "Metal Handbook".

26) Asakura Shoten, "Material Strength Engineering Handbook".

27) PNC, Adjusting Design for "MONJU", Phase II.

Table 2-1 List of Grid Elements

Makers	Type	Material	Height (mm)	Plate Thickness (mm)	Configuration of Dimple	Cold Work Rate (%)	Mechanical Strength		
							Tensile Strength (kg/mm^2)	Yeild Point (kg/mm^2)	Elongation (%)
NFI	Honeycomb	SUS316	10	0.15	Hemispherical	17	—	—	—
MAPI	Honeycomb	SUS316	15	0.20	Hemispherical (two-stage)	—	60	—	60
	Ring	SUS316	15	0.15	Hemispherical	20	59	—	56
TOSHIBA	2-stage Honeycomb	SUS316	20	0.20	〃	—	120.0	113.3	12.0
	Rohmbus	SUS316	25	0.20	No Dimple	—	120.0	113.3	12.0
	Honeycomb	SUS316	15	0.15	Oval shaped sphere	—	86.8	58.3	24.6

Makers	Type	Chemical Compositions (%)								
		C	Si	P	Co	Mn	S	Ni	Cr	Mo
NFI	Honeycomb	0.05	0.70	0.031	—	1.45	0.010	13.59	17.74	2.36
MAPI	Honeycomb	0.06	0.52	0.025	—	1.56	0.006	13.00	16.35	2.22
	Ring	0.06	0.52	0.026	—	1.60	0.009	13.00	16.60	2.07
TOSHIBA	2-stage Honeycomb	0.08	0.73	0.029	0.16	0.97	0.030	10.58	16.97	2.66
	Rohmbus	0.08	0.73	0.029	0.16	0.97	0.030	10.58	16.97	2.26
	Honeycomb	0.03	0.61	0.020	0.03	1.61	0.006	13.90	16.21	2.15

Table 2.2 Calculation Results of Contact Loads

Load (kg)	0.5	1.0	2.0
ℓ_1 (mm)	100	100	100
ℓ_2 (mm)	300	300	300
ℓ_3 (mm)	500	500	500
EI ($kg \cdot mm^2$)	6×10^5	6×10^5	6×10^5
$y_{x=\ell_1}$ (mm)	± 0.0	± 0.0	± 0.0
$y_{x=\ell_2}$ (mm)	− 0.5	− 0.5	− 1.5
$y_{x=\ell_3}$ (mm)	+ 0.5	+ 2.0	+ 2.0
R_2 (kg)	+ 0.9	+ 1.3	+ 2.7
R_3 (kg)	− 0.6	− 1.0	− 2.0
R_4 (kg)	+ 0.2	+ 0.4	+ 0.7

Table 2.3 Caluculation Results to Confirm the Load Conditions

Load (kg)	0.5	1.0	2.0
a (mm)	200	200	200
ℓ (mm)	400	400	400
EI(kg·mm^2)	6×10^5	6×10^5	6×10^5
$y_{x=a}$ (mm)	− 0.5	− 0.5	− 1.5
$y_{x=\ell}$ (mm)	+ 0.5	+ 2.0	+ 2.0
W (kg)	− 0.13	− 0.32	− 0.45
R_A (kg)	+ 0.064	+ 0.16	+ 0.23
R_B (kg)	+ 0.064	+ 0.16	+ 0.23
$\Sigma = \|W\| + \|R_A\| + \|R_B\|$	0.26	0.64	0.90

Table 2.4 Caluculation Results of Tensile Force

Load (kg)	0.5	1.0	2.0
$F_{\mu=0.2}$	0.052	0.13	0.18
$F_{\mu=0.4}$	0.10	0.26	0.36

Table 4.1 Changes in The Reactor Power

Classification No.	Typical case	No. of occurrence	Operation Mode	Remarks
N 1	Start-up	34	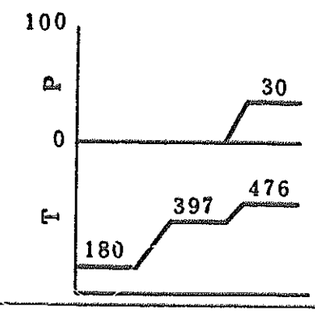	MP-57245 N 1 50℃/hr
N 2	Regular Reactor Shutdown	6	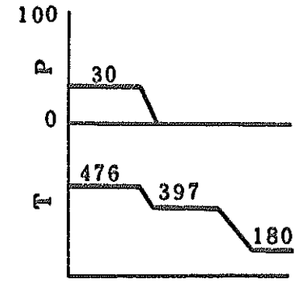	MP-57245 N 2 50℃/hr
N 3	Ramp type Power Change	1,000	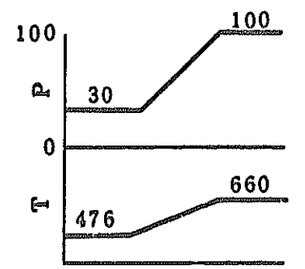	MP-57245 N 3 ±5%/min
N 4	Step type Power Change	100	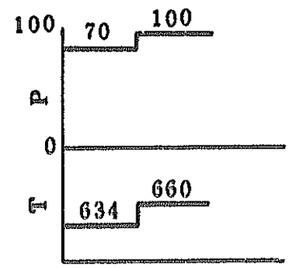	MP-57245 N 4 Δ = ±10%

Table 4.1 Changes in The Reactor Power (continued)

Classification No.	Typical case	No. of occurrence	Operation Mode	Remarks
N 5	Steam Damp	3 4	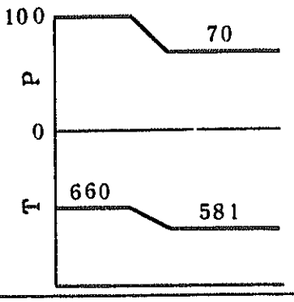	MP-57245 N 5 −5%/min
U 1	Outside Power Failure	8	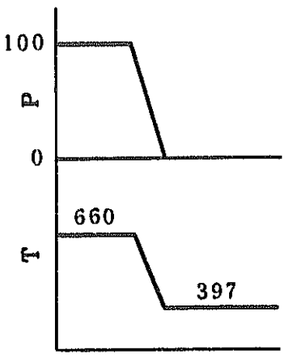	MP-57245 U 1 ~ U 6
U 2	In-premises Power Failure	4		
U 3	Erroneous Scrum	1 0		
U 4	Reactivity Insertion Accident	1		
U 5	Trip Accident in One Primary Circulation Pump	2		
U 6	Trip Accident in One 2ndry Circulation Pump	2		

R-101	Assembly of Test Specimen Cover
R-102	Test Specimen Fixing Flange
R-41	Fuel Pin Assembly
R-103	Guide Rod
R-43	No. 1 Nut
R-104	Grid Support plate G
R-105	No. 1 Grid Support plate B
R-106	No. 1 Grid Support plate F
	No. 3 Grid Support plate G
R-107	Grid Stopper
R-108	No. 1 Support Tube A
R-108	No. 2 Support Tube B

R-109	Toshiba Combined Grid
R-112	Toshiba 2-stage Honeycomb
R-111	Toshiba New Grid
R-115	Rotation stop
	Pan-head screw
	Spring pin

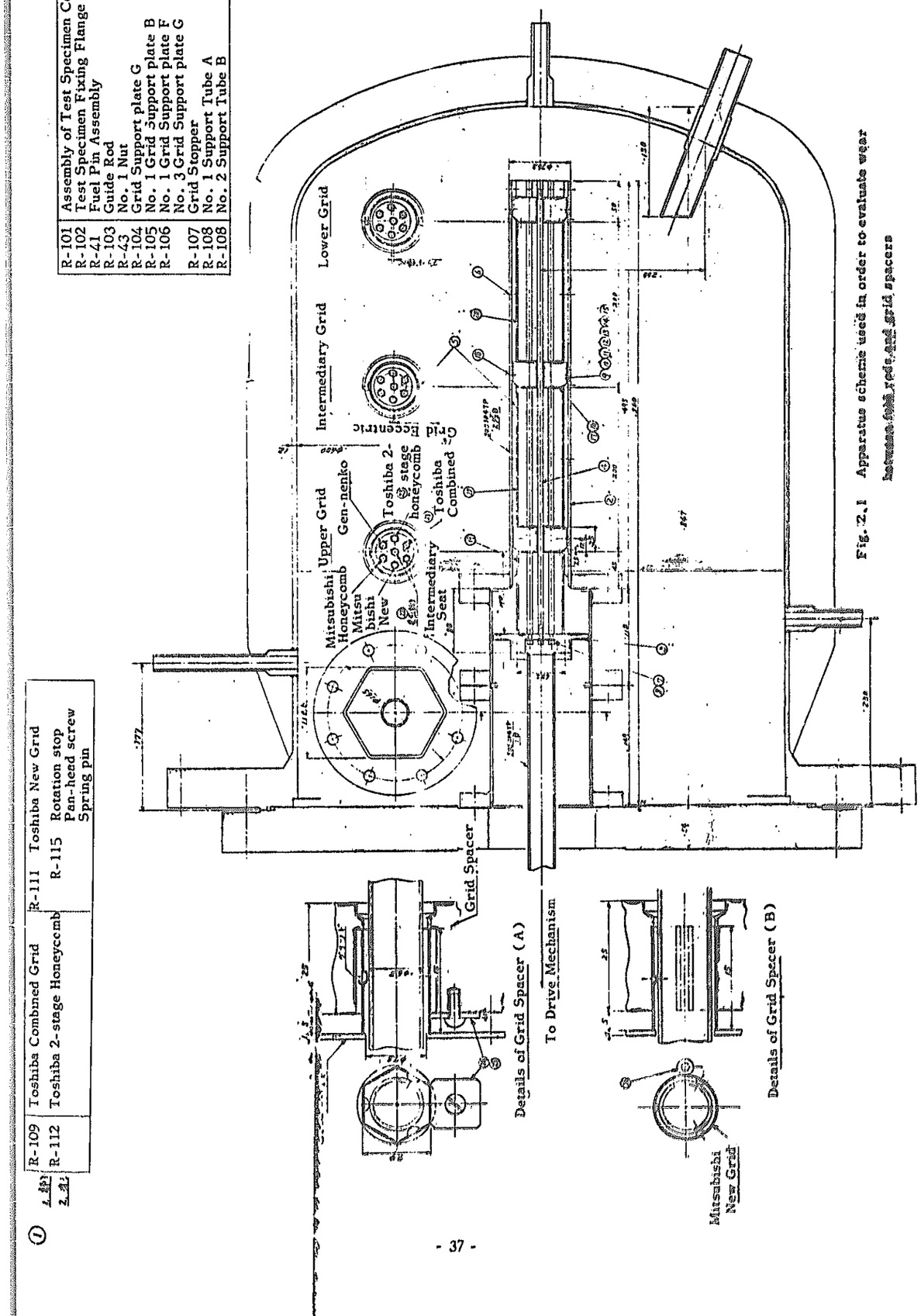

Fig. 2.1 Apparatus scheme used in order to evaluate wear between fuel rods and grid spacers

R-1	Stand	S-1 #1	Motor
R-2	Test Tank Cover	S-1 #2	Shinko Reduction Gear
R-4	Coupling Rod Assembly	S-2 #4	Bellow-type Unit
R-8	Assembly of Crank		
R-15	Mounting Seat for Test Specimen		
R-16	Intermediary Seat		
R-17	Change Gear Assembly	S-4 #1	Metal O-ring
R-33	Crank Shaft	S-4 #2	Metal O-ring
R-36	Coupling A	S-4 #3	Metal O-ring
R-37	Coupling B	R-39	Test Specimen Assembly
R-38	Coupling C	R-44	Thermocouple Grid
		R-46	Wrapper Tube Assembly
		R-48 #1	Grid Stop Screw
		R-48 #2	Feeler Type Wave Surface Gauge

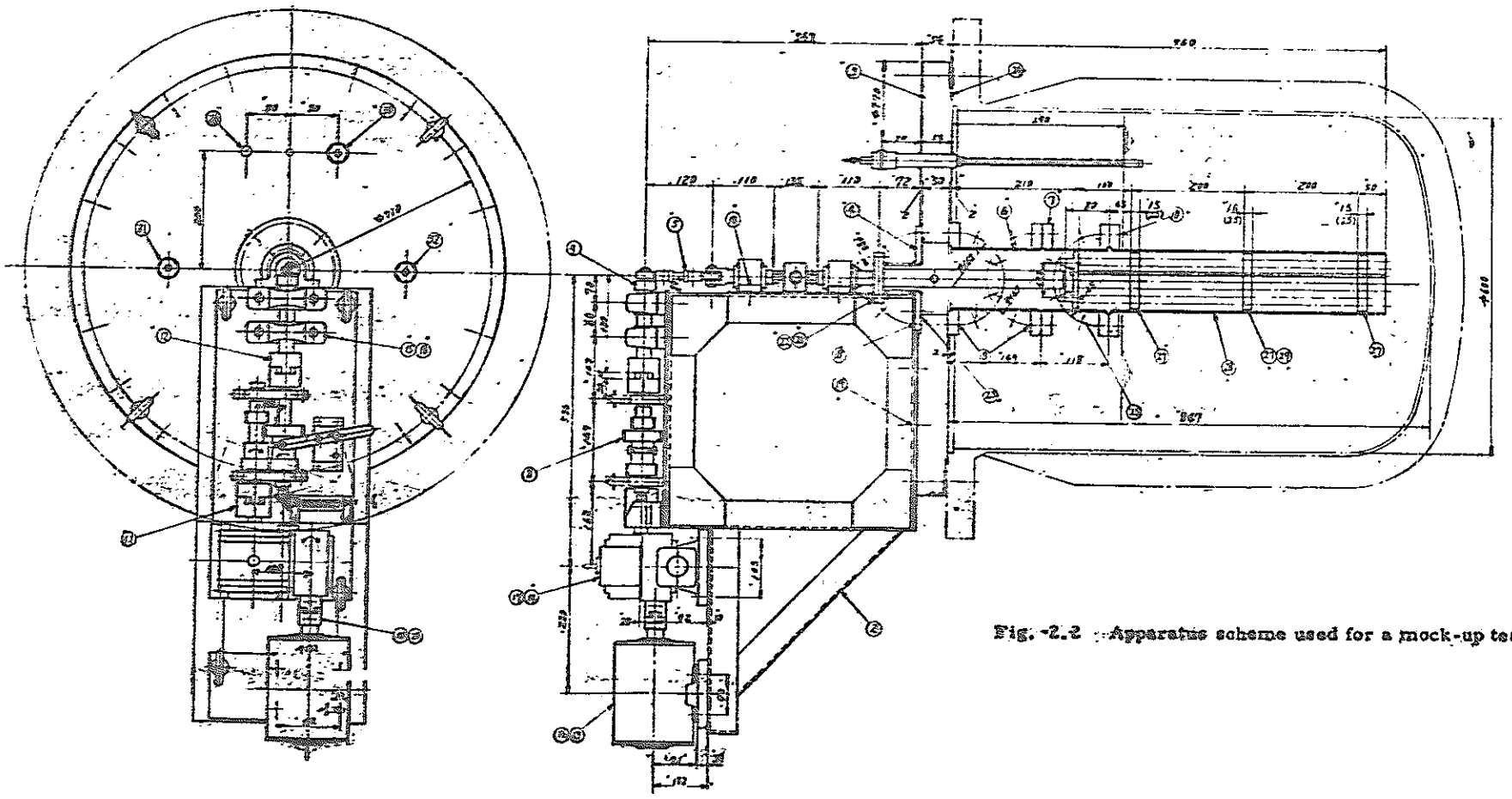

Fig. 2.2 Apparatus scheme used for a mock-up test in sodium

CTL : Cold Trap Loop

MEL: Mechanical Element Test Loop

EFM: Electric Flow Meter

EMP: Electromagnetic Pump

DT : Dump Tank

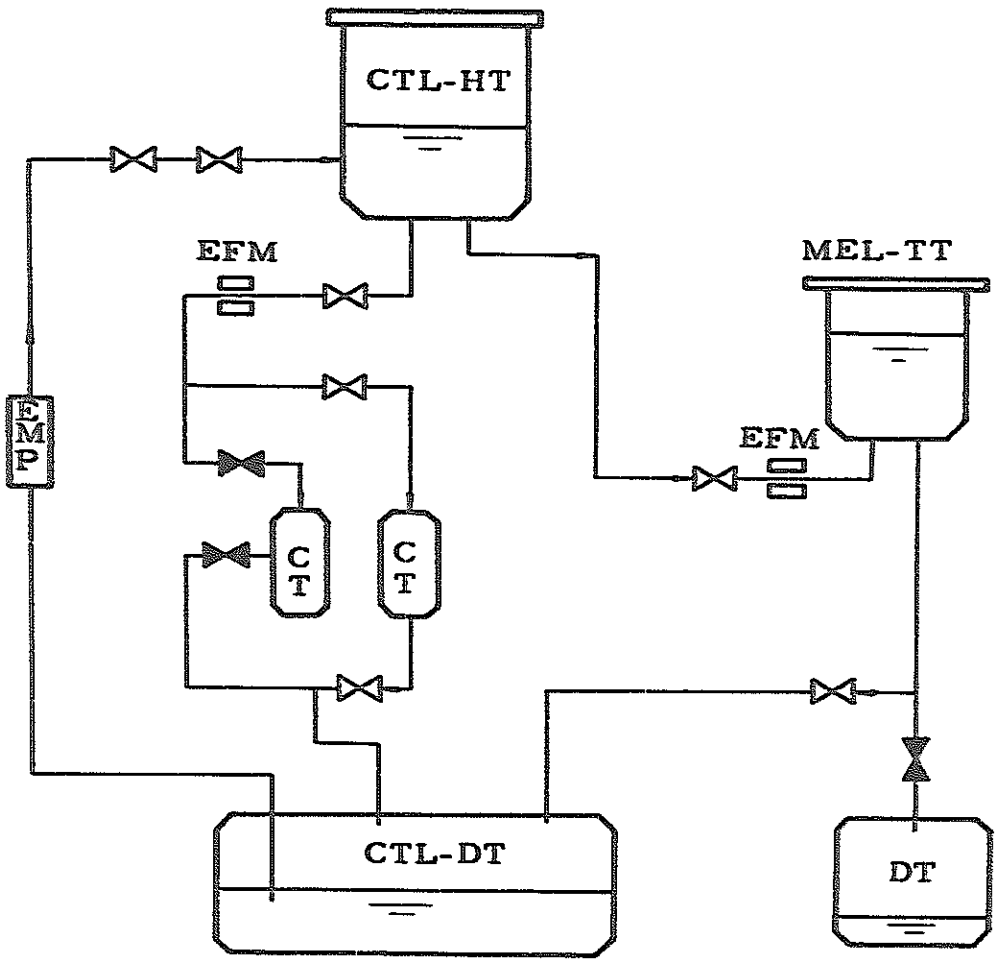

Fig. 2.3 Sodium test loop

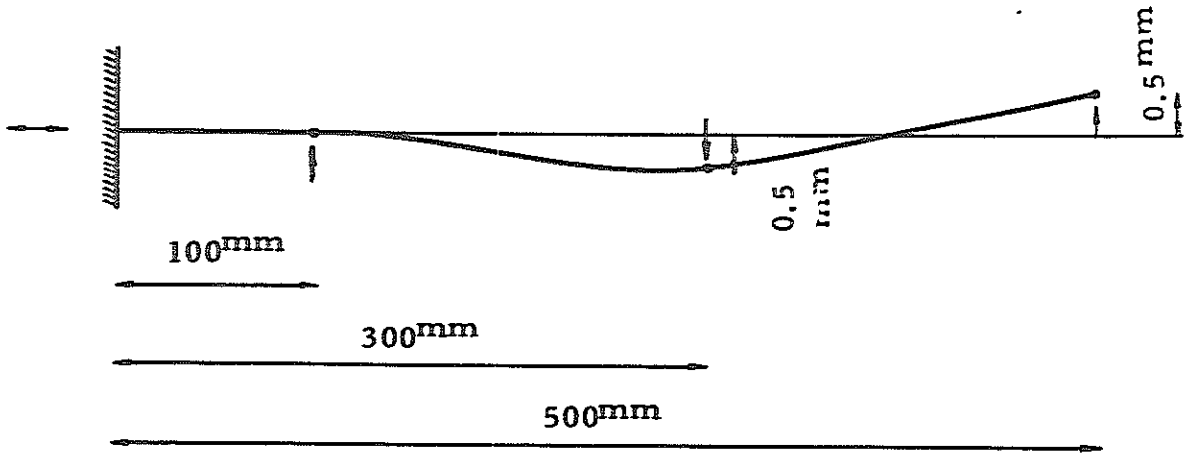

Fig. 2.4 Fuel rod deformation mode on the load condition 0.5 kg.

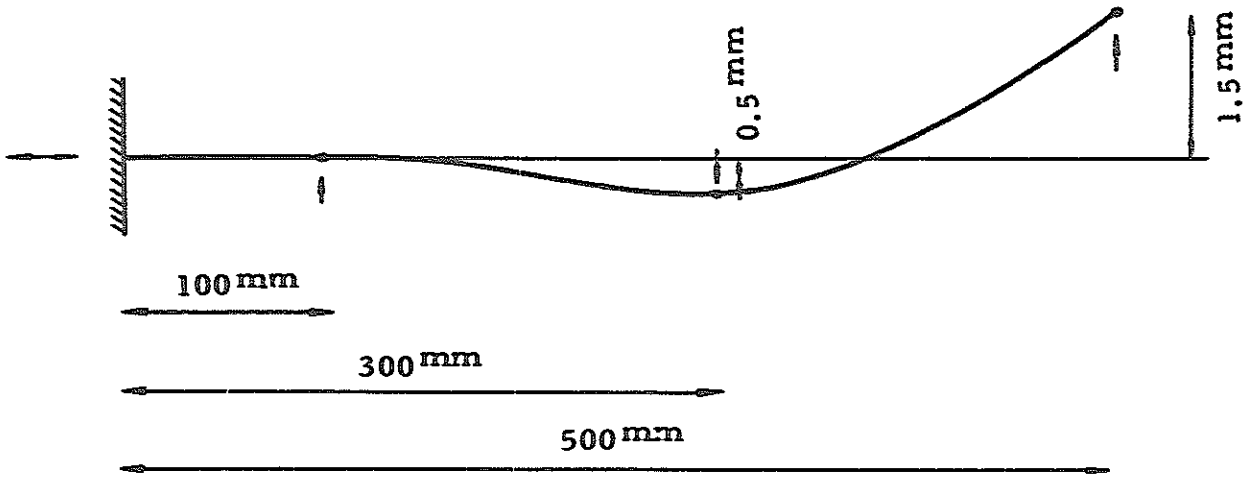

Fig. 2.5 Fuel rod deformation mode on the load condition 1.0 kg.

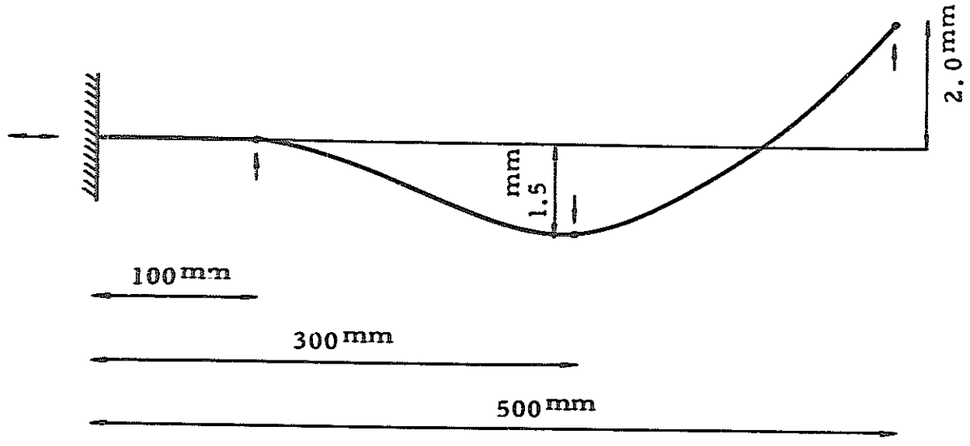

Fig. 2.6 Fuel rod deformation mode on the load condition 2.0 kg.

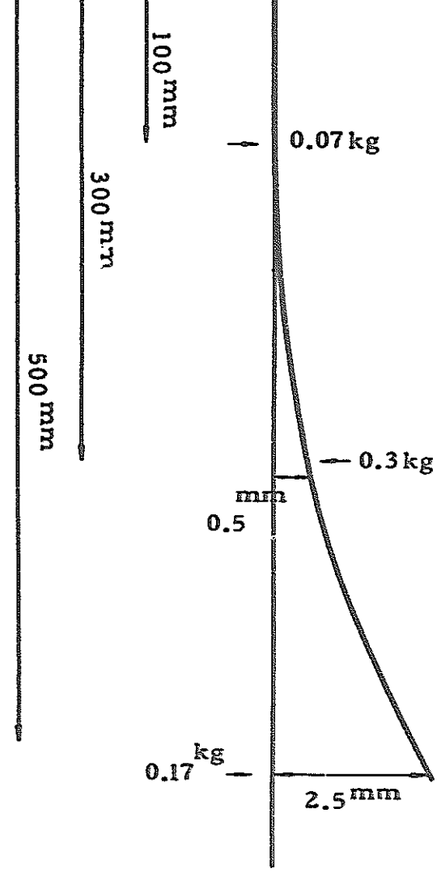

Fig. 2.7 Bowing rod deformation mode

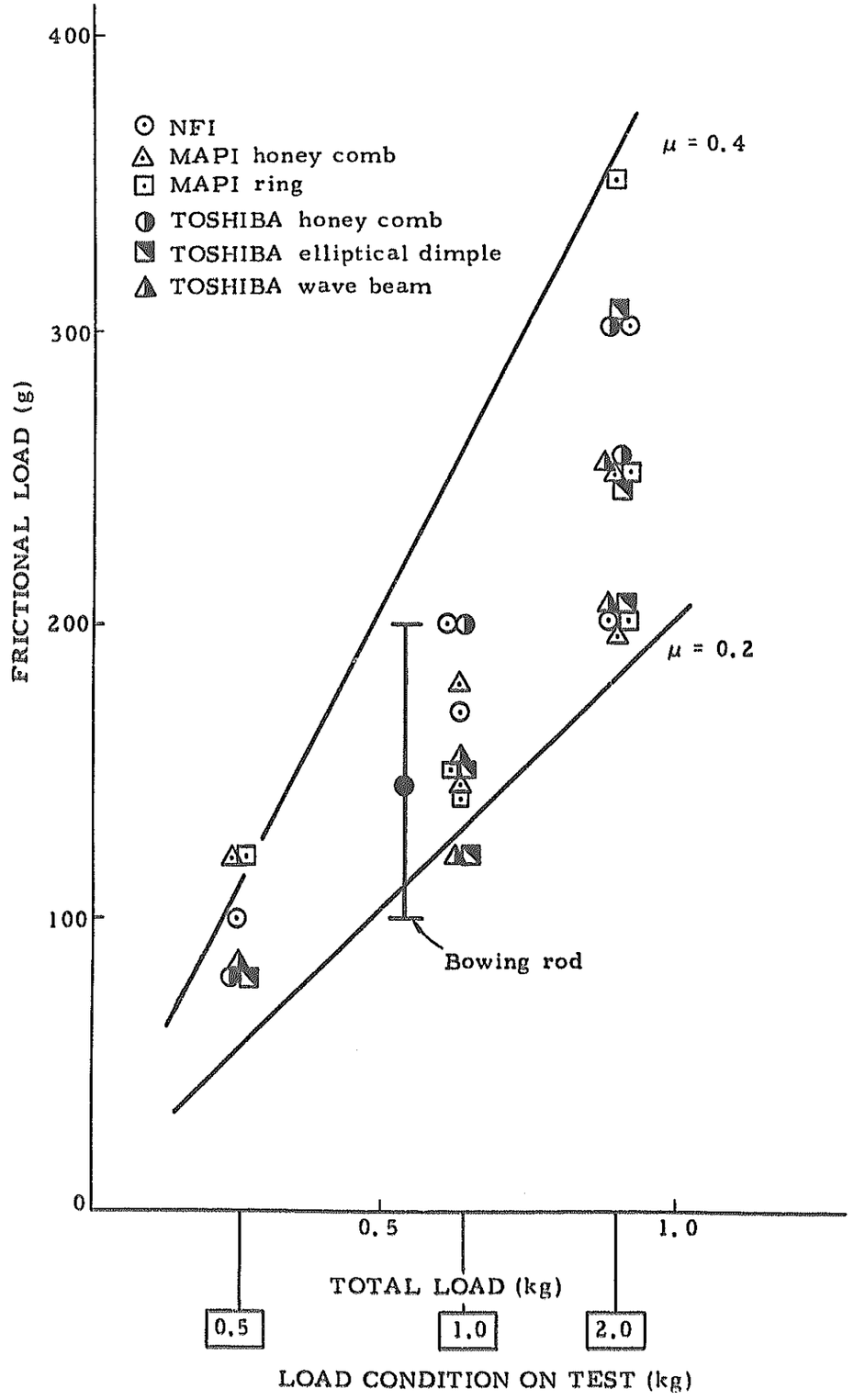

Fig. 2.8 Data to confirm the load condition

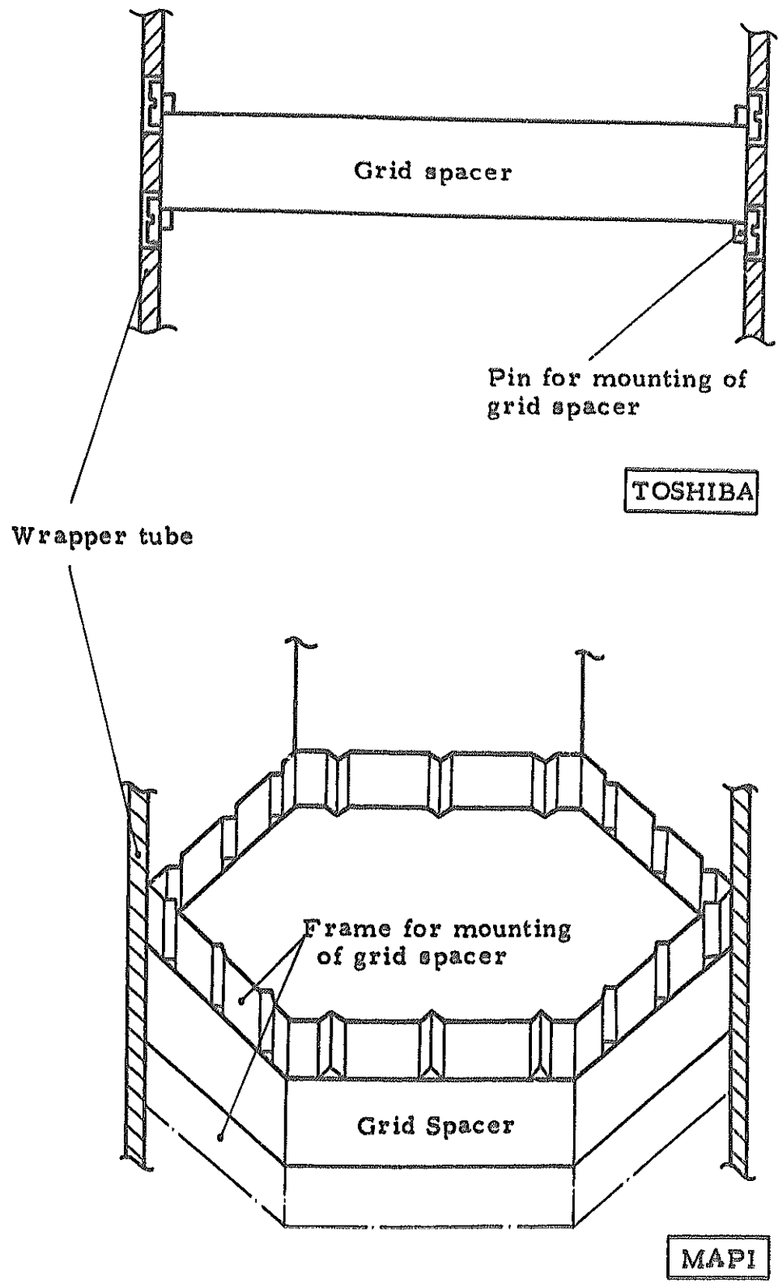

Fig. 2.9 Grid spacer mounting methods

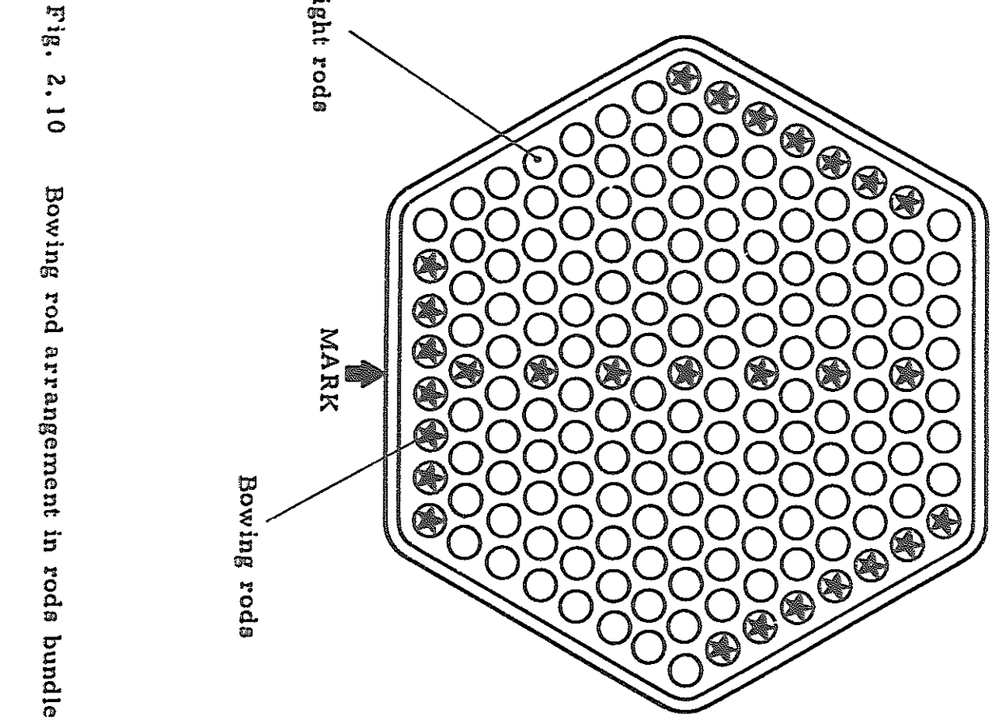

Fig. 2.10 Bowing rod arrangement in rods bundle

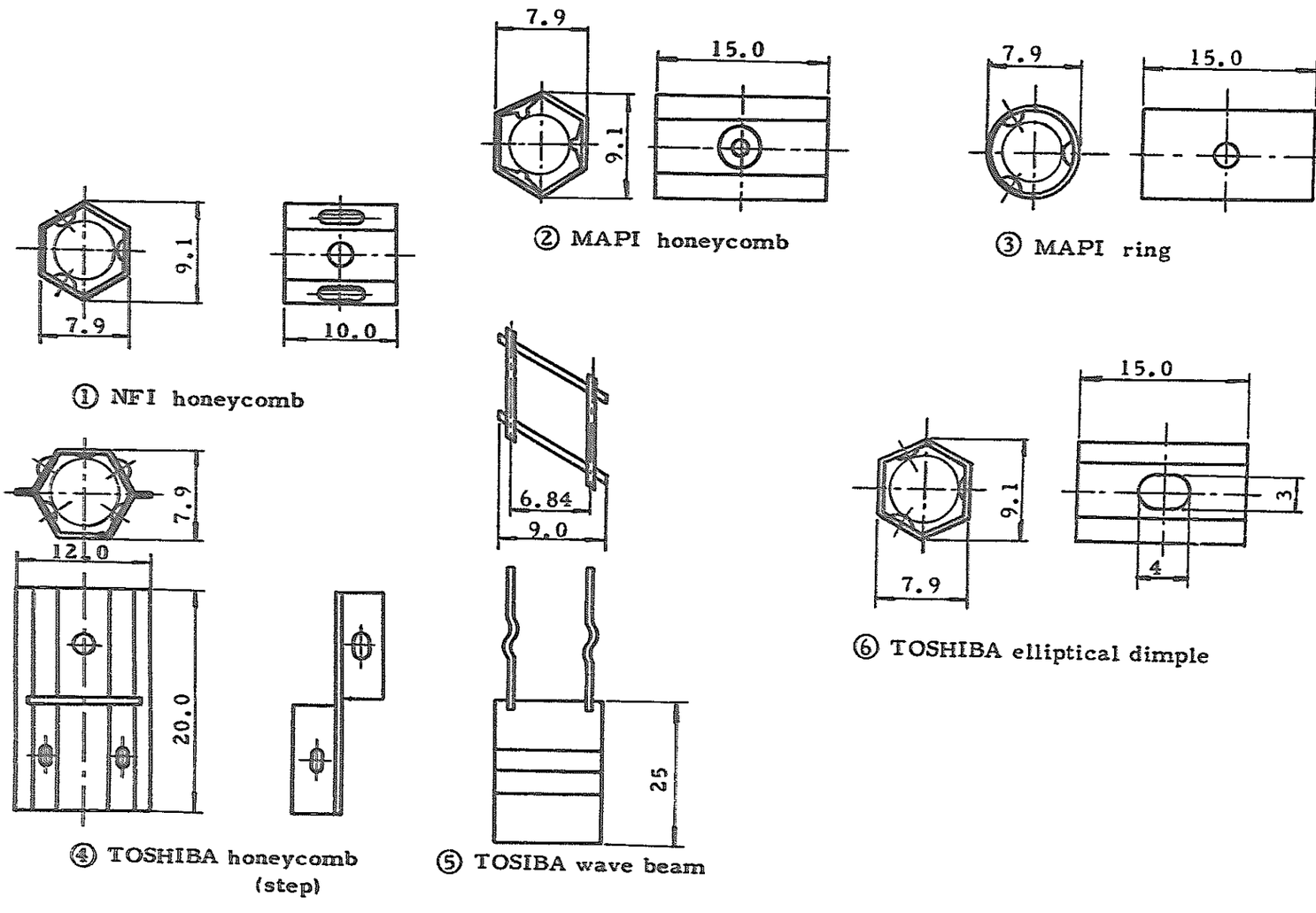

Fig. 2.11 Grid elements

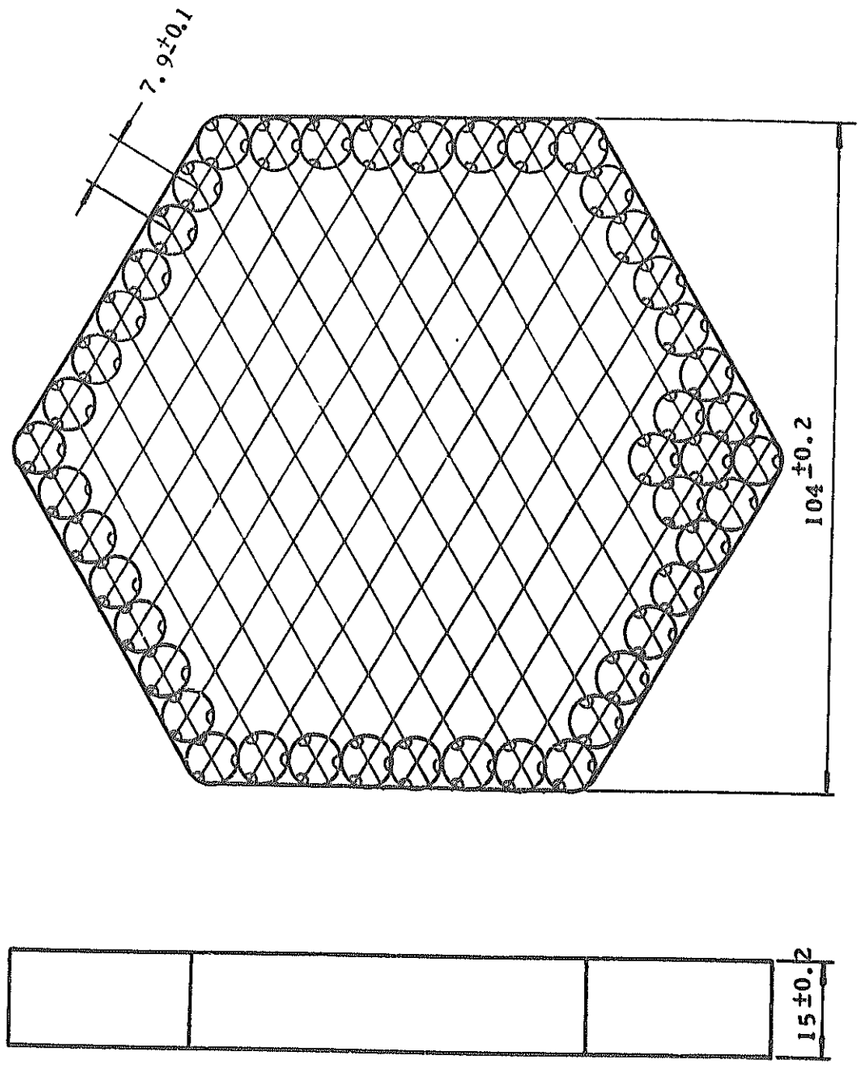

Fig. 2.12 MAPI ring type grid spacer

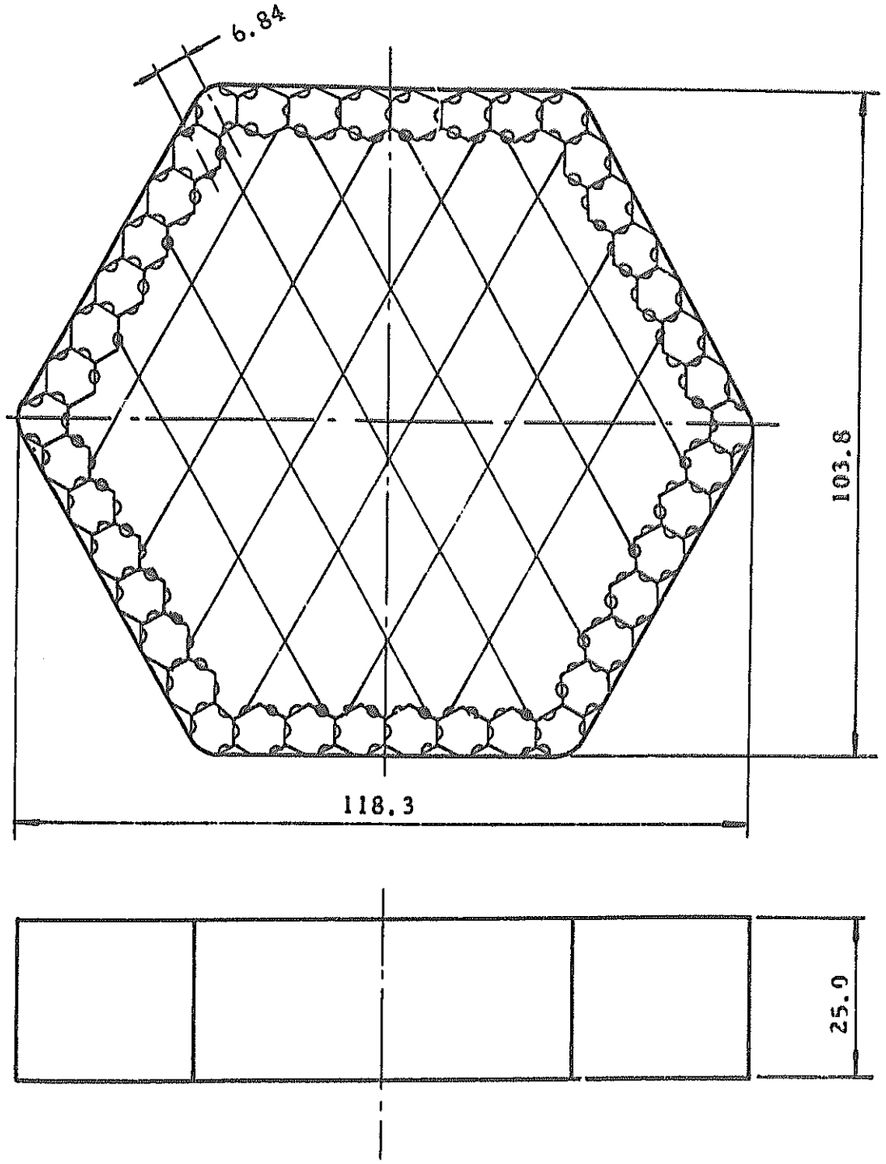

Fig. 2.13 TOSHIBA grid spacer

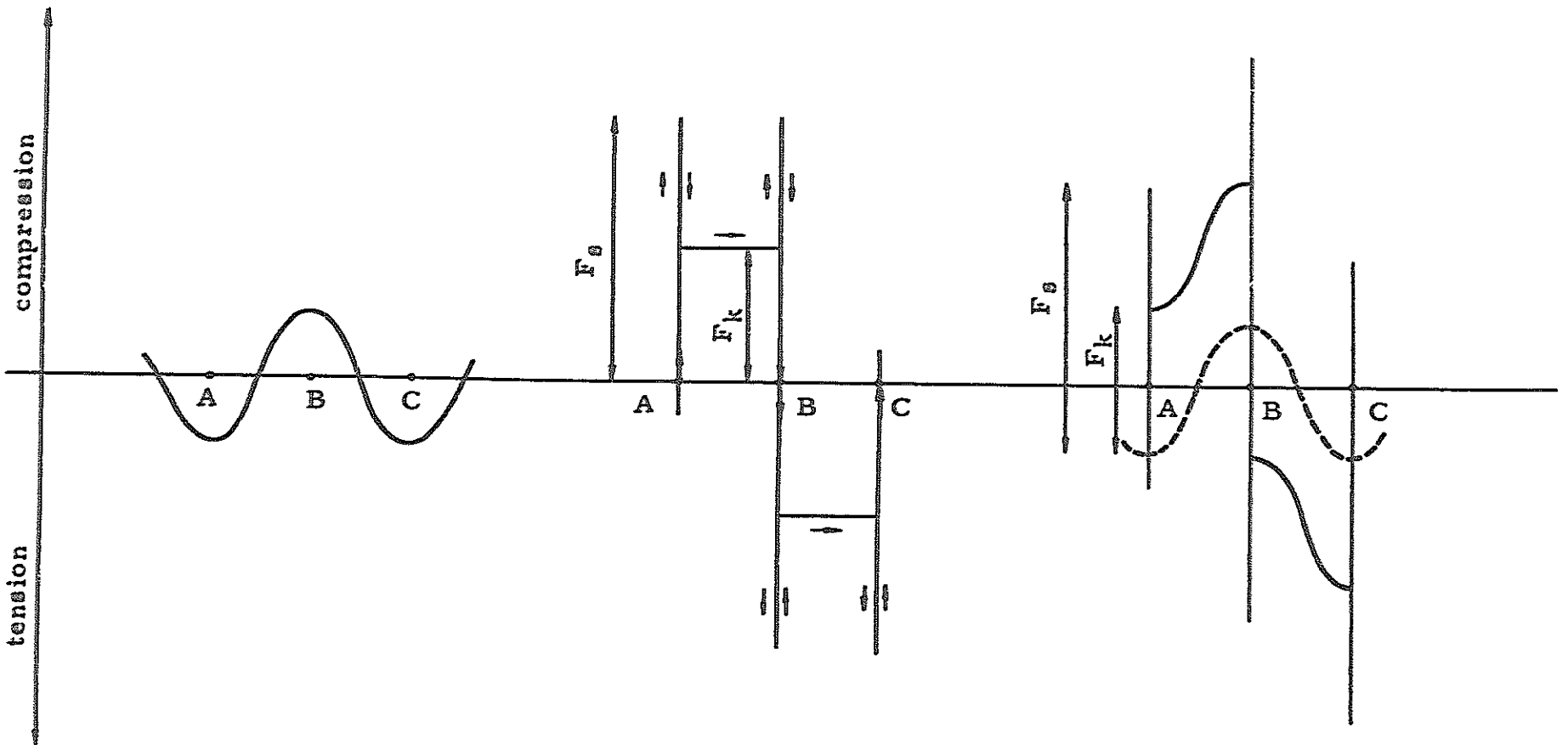

(a) driving force (b) frictional force (c) composed force

Fig. 3.1 Measurement procedure of frictional force by the tensile and compressive force transducer.

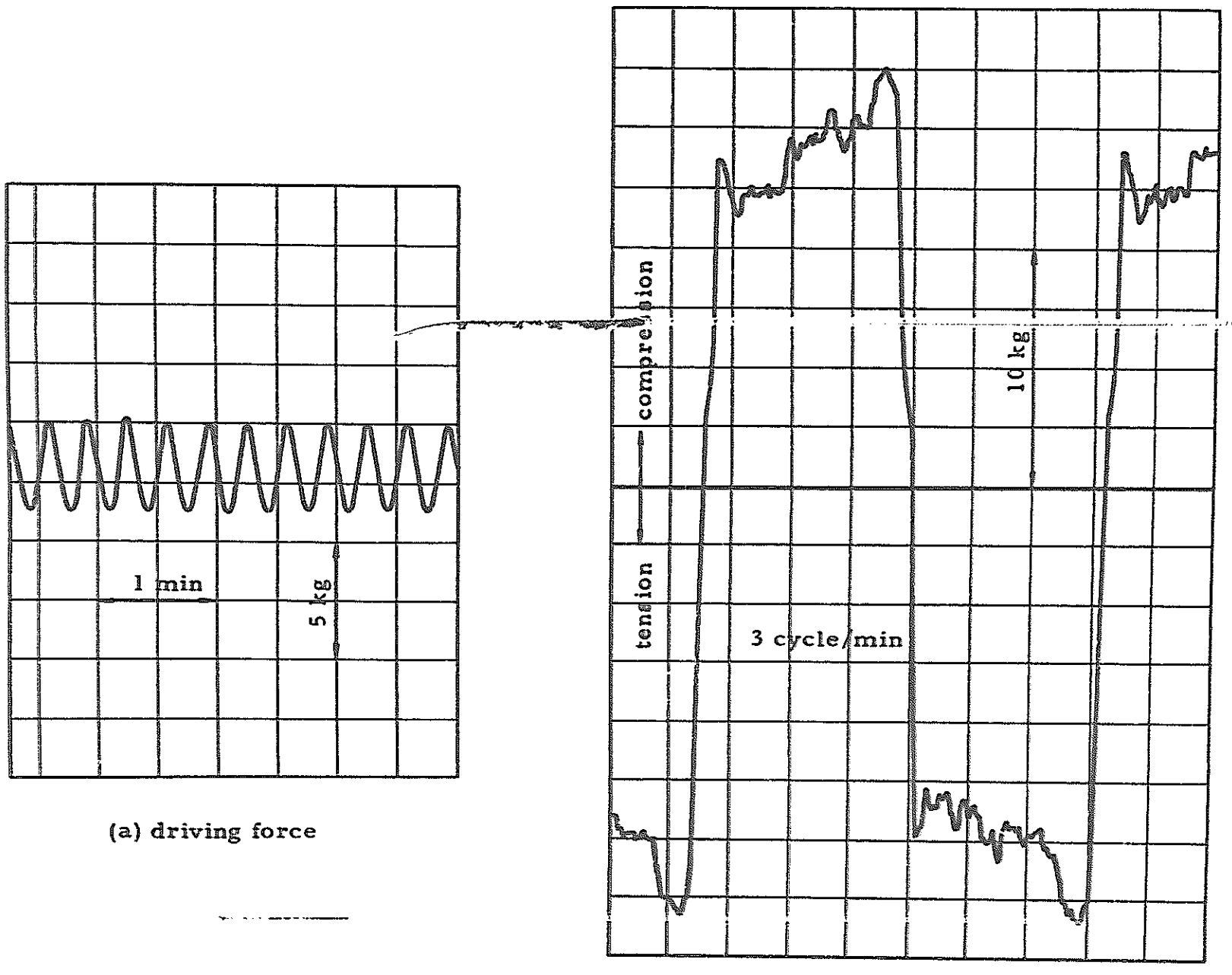

(a) driving force

(b) composed force

Fig. 3.2 Example of frictional force (measured)

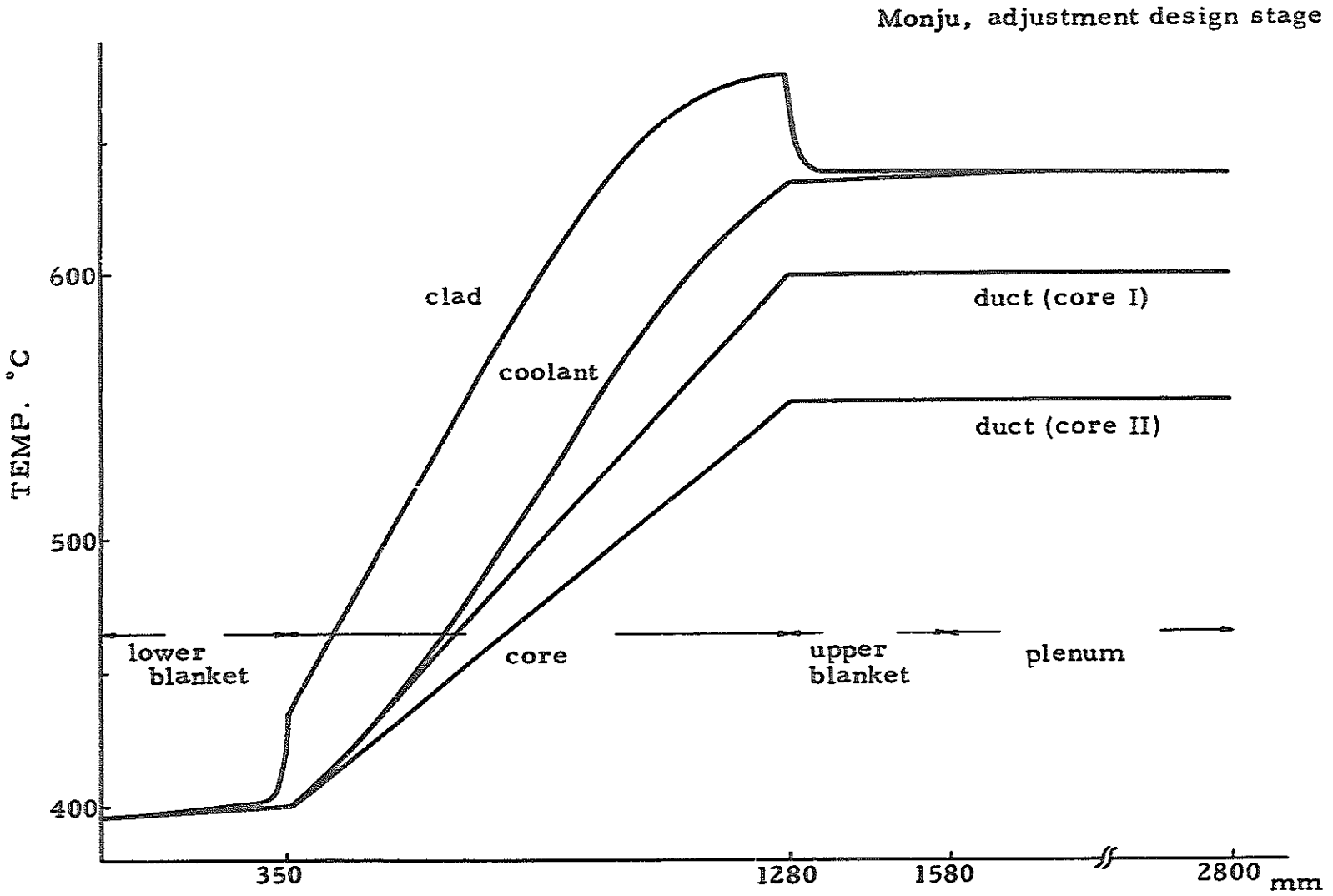

Fig. 4.1 Temperature distribution of fuel assembly

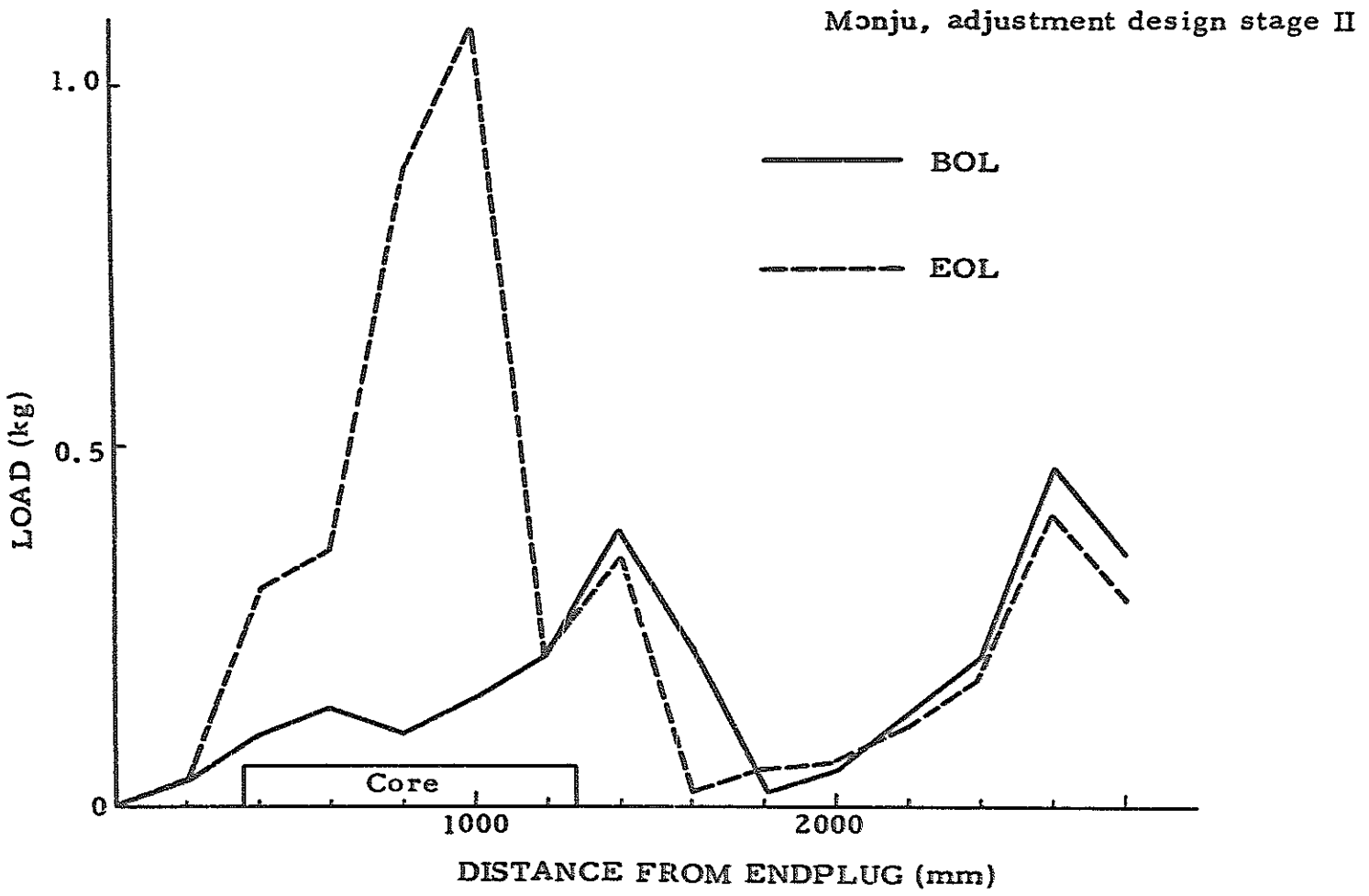

Fig. 4.2 Contact load between fuel rods and grid spacers in the fuel life time.

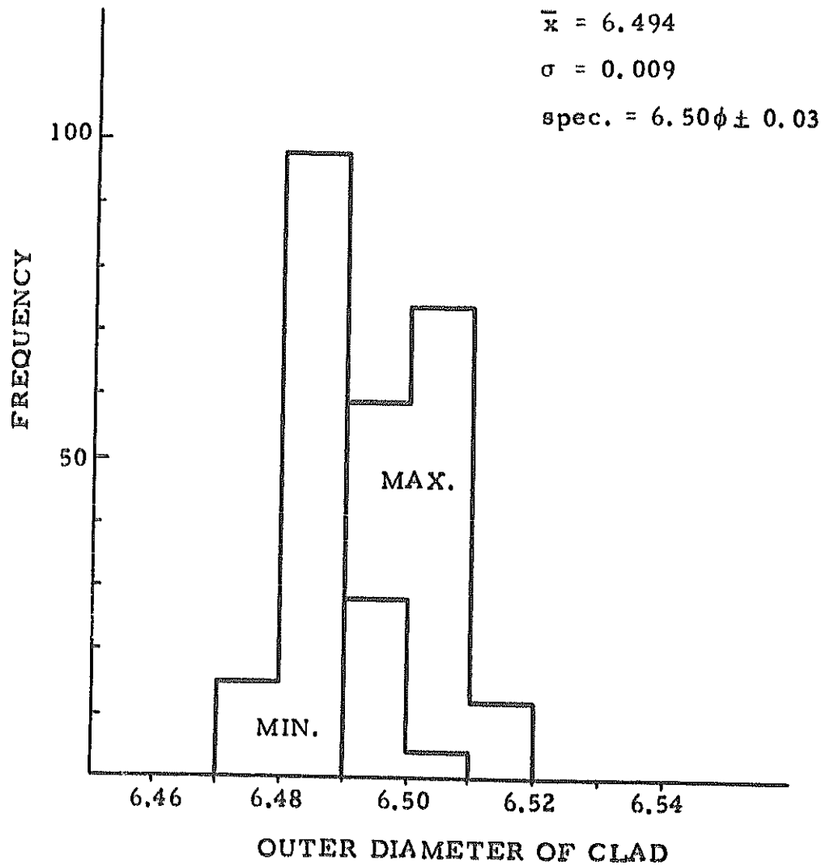

Fig. 5.1 Frequency data of clad outer diameter.

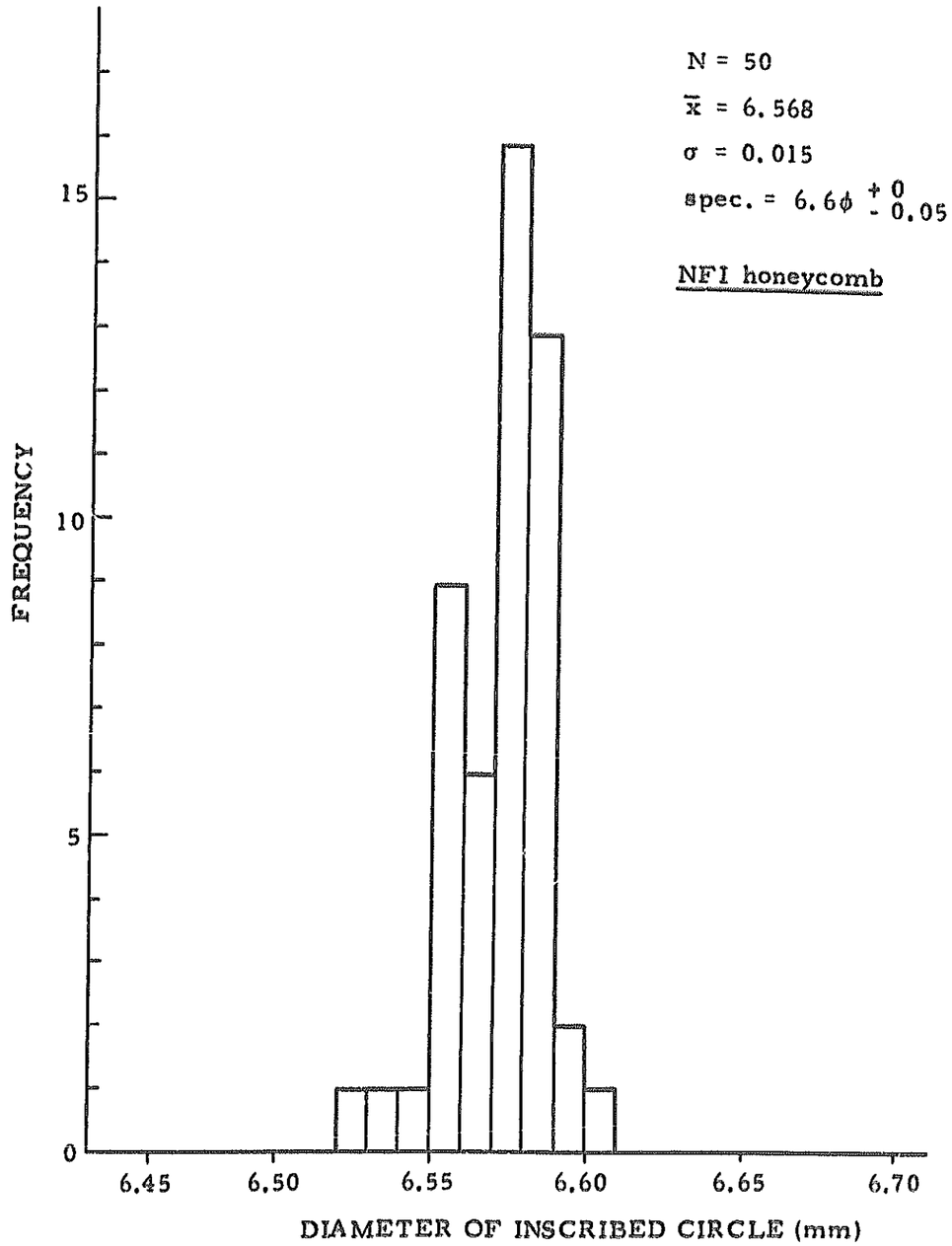

Fig. 5.2 Frequency data of grid inscribed circle diameter (1).

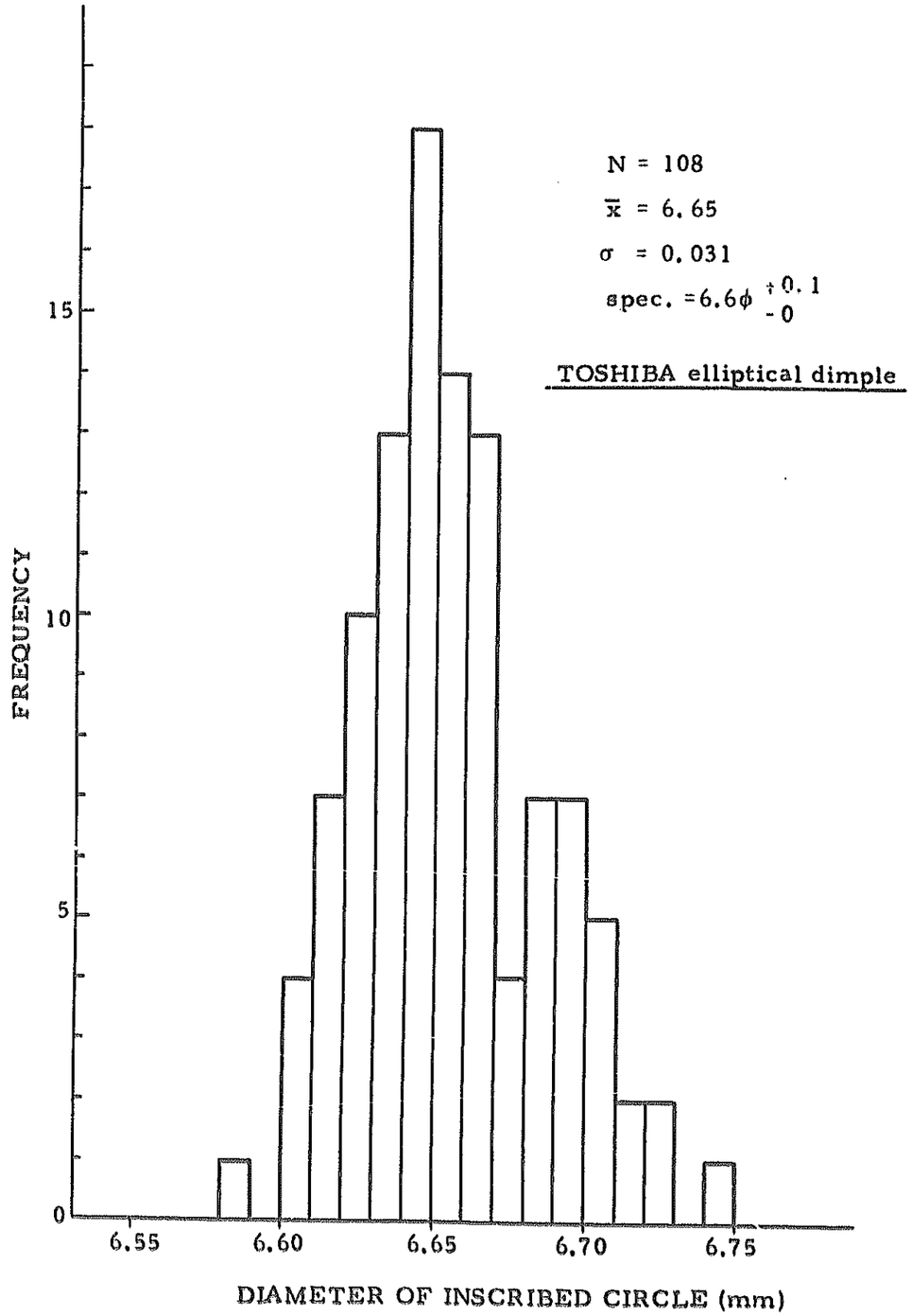

Fig. 5.3 Frequency data of grid inscribed circle diameter (2).

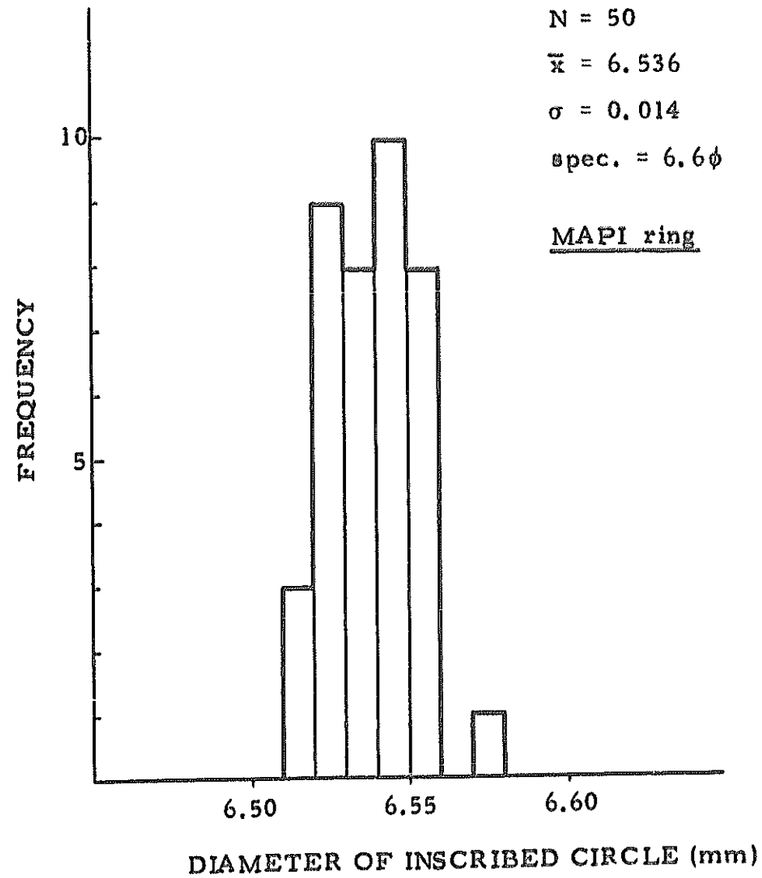

Fig. 5.4 Frequency data of grid inscribed circle diameter (3)

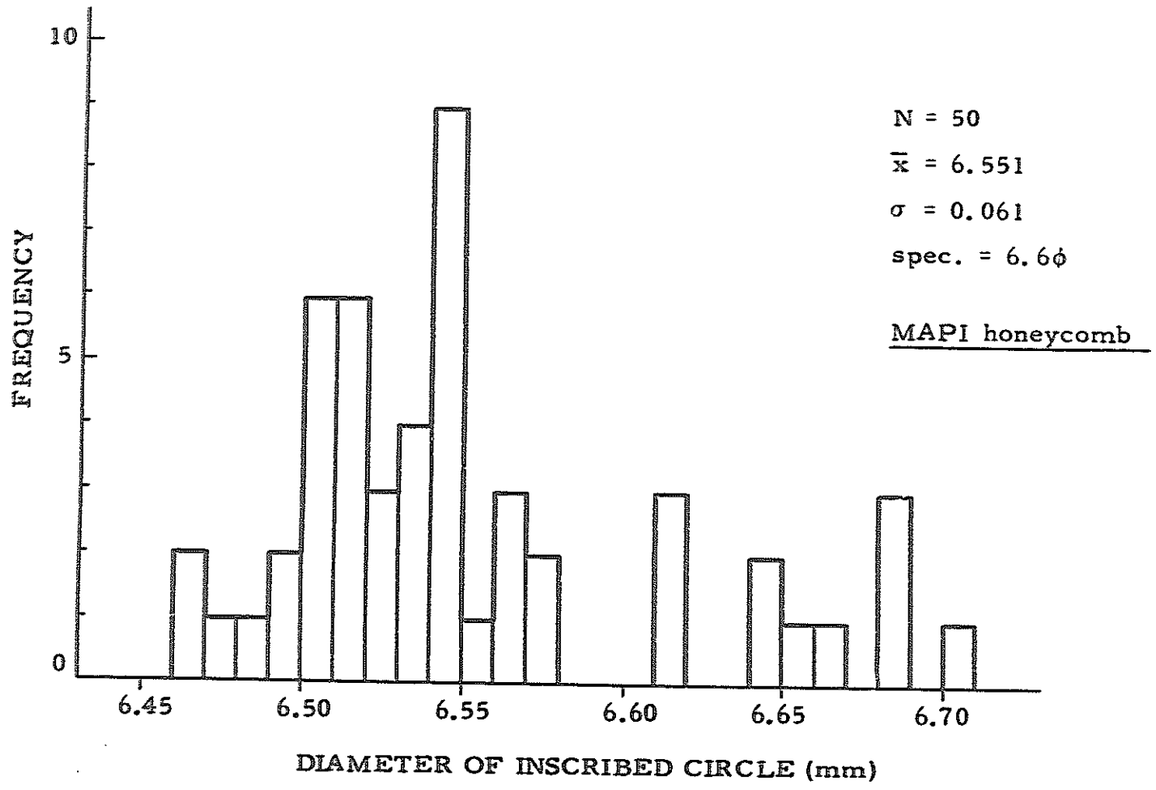

Fig. 5.5 Frequency data of grid inscribed circle diameter (4).

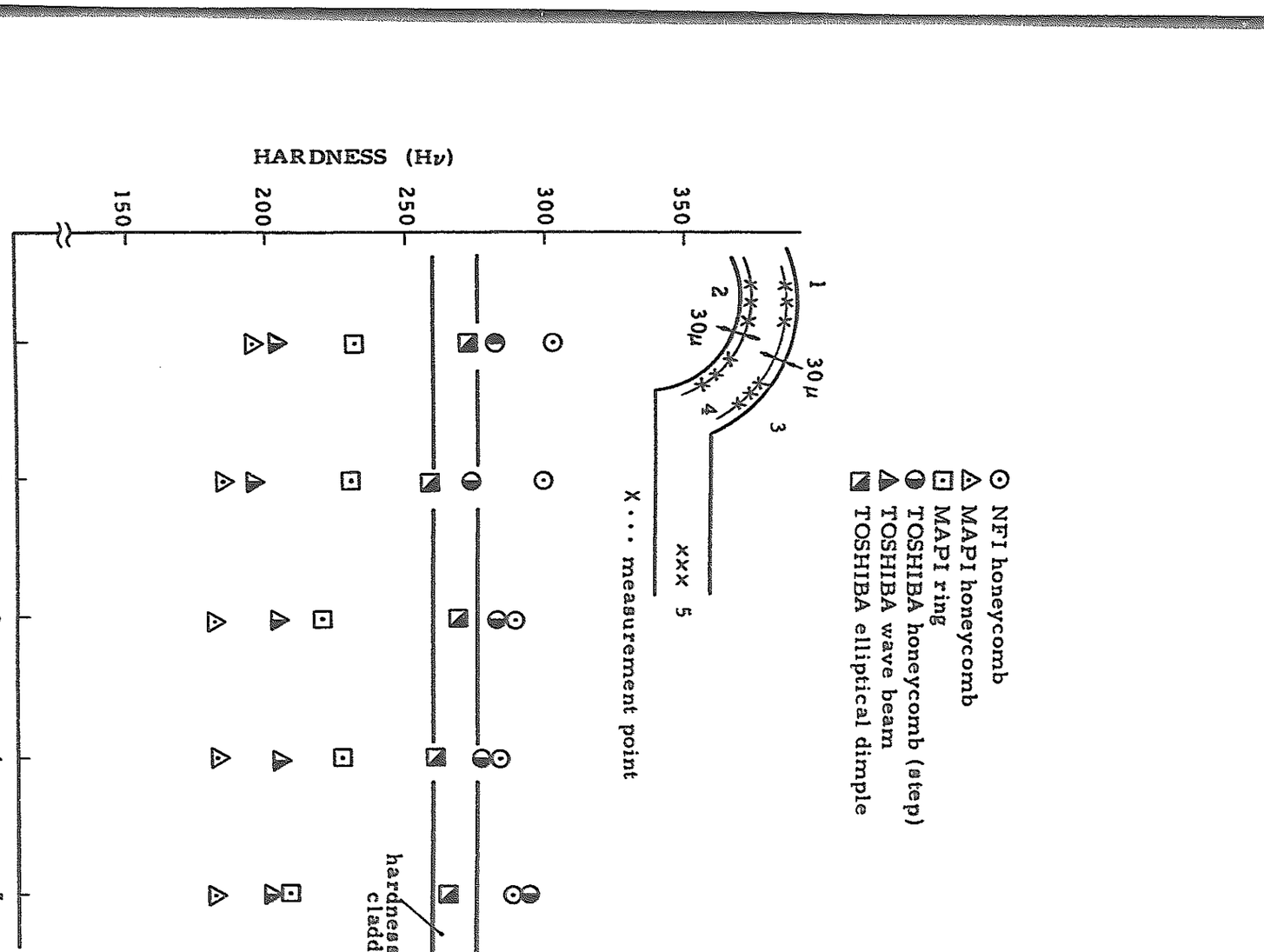

Fig. 5.6 Hardness of grid dimple and cladding. (before galling test)

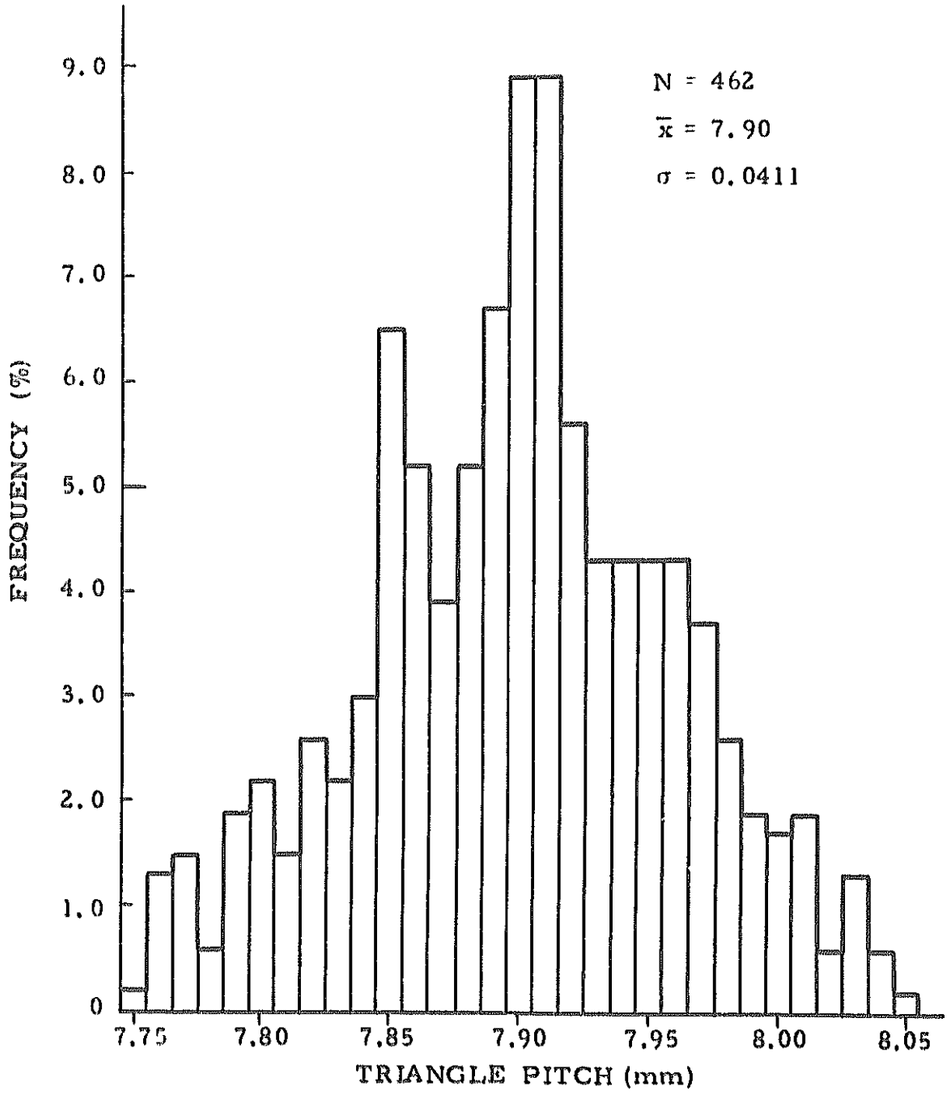

Fig. 5.7 Fixed triangle pitch of rod bundle.

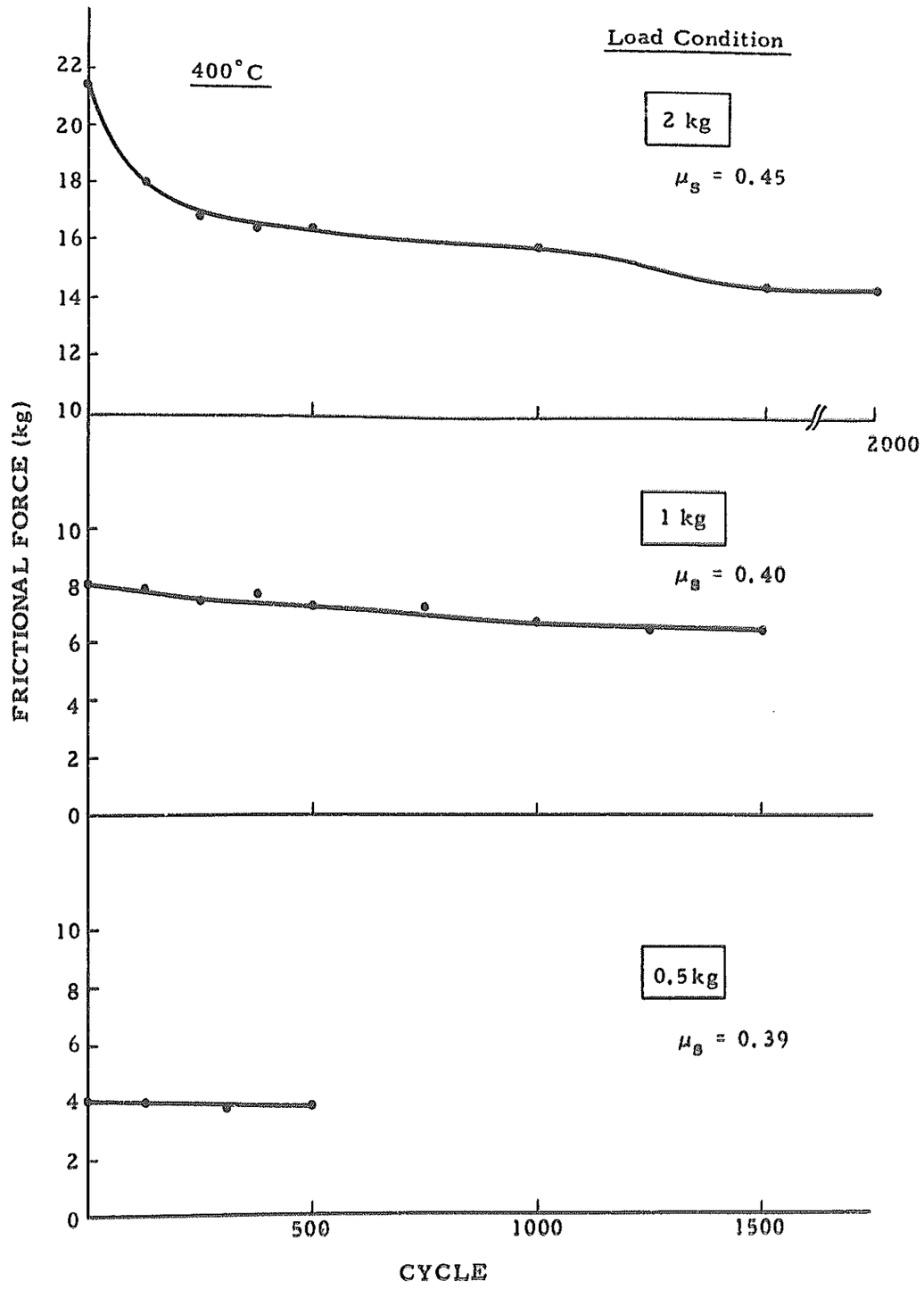

Fig. 6.1 Change of frictional force vs operational cycle and contact load at 400°C.

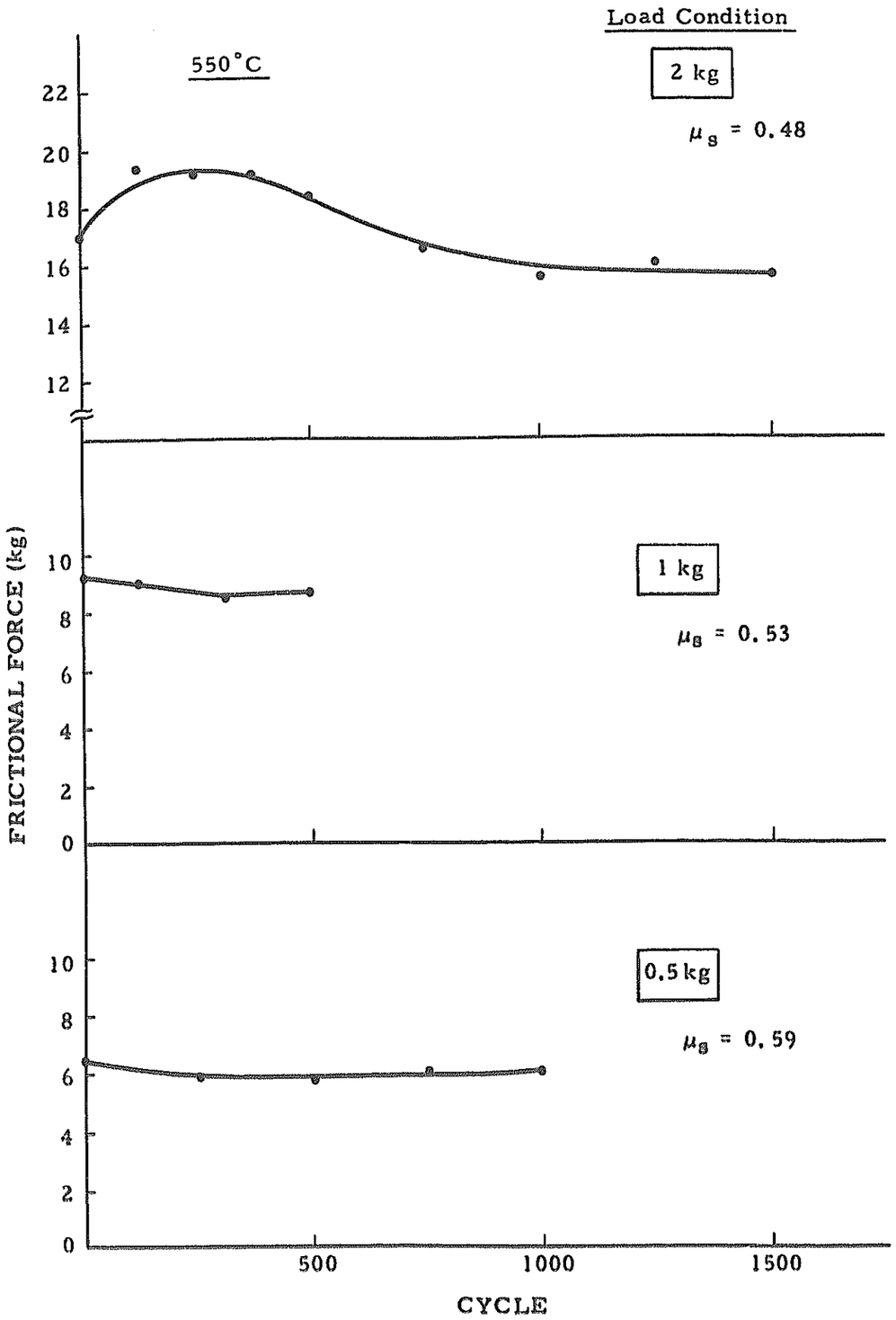

Fig. 6.2 Change of frictional force vs operational cycle and contact load at 550°C.

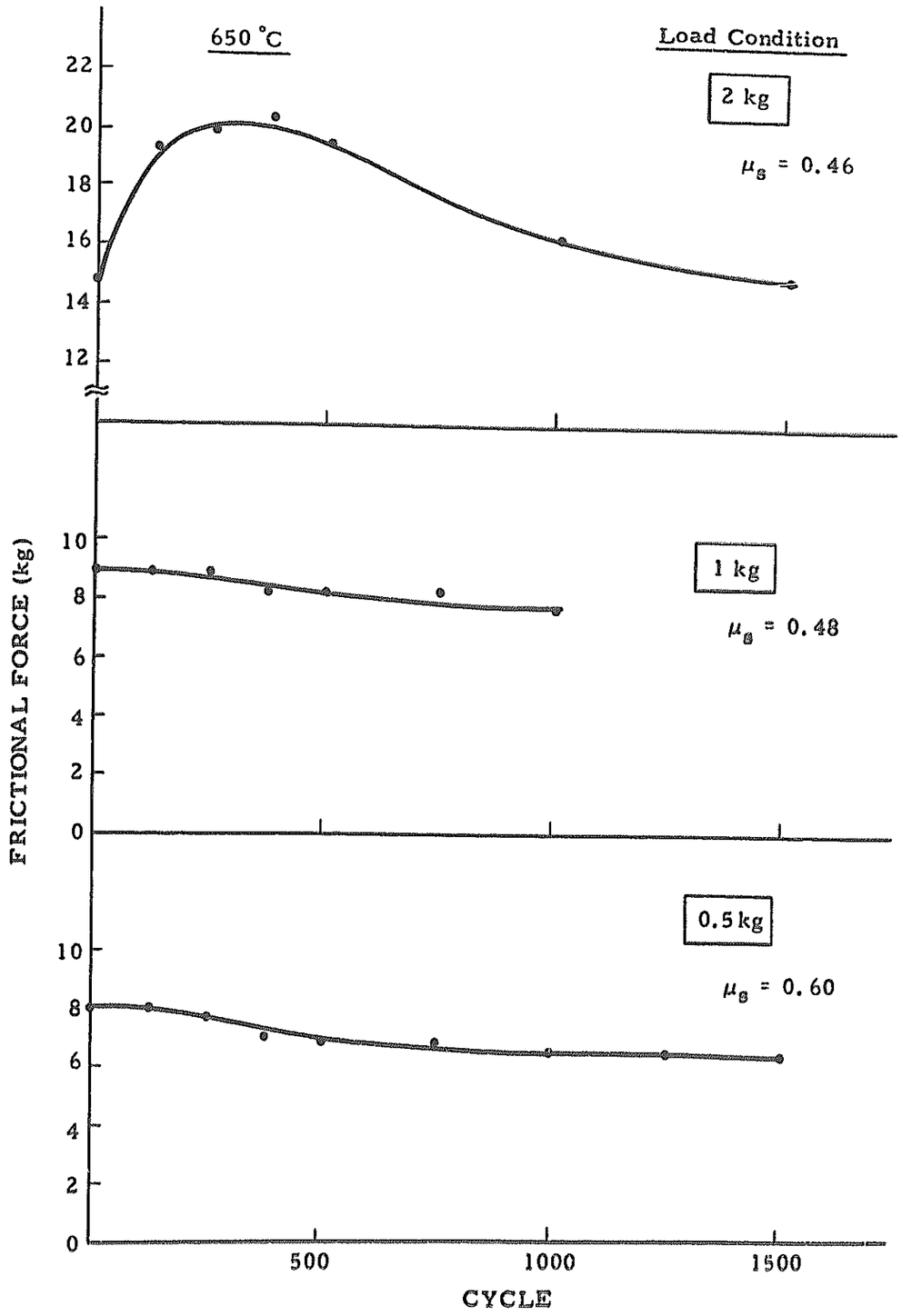

Fig. 6.3 Change of frictional force vs operational cycle and contact load at 650°C.

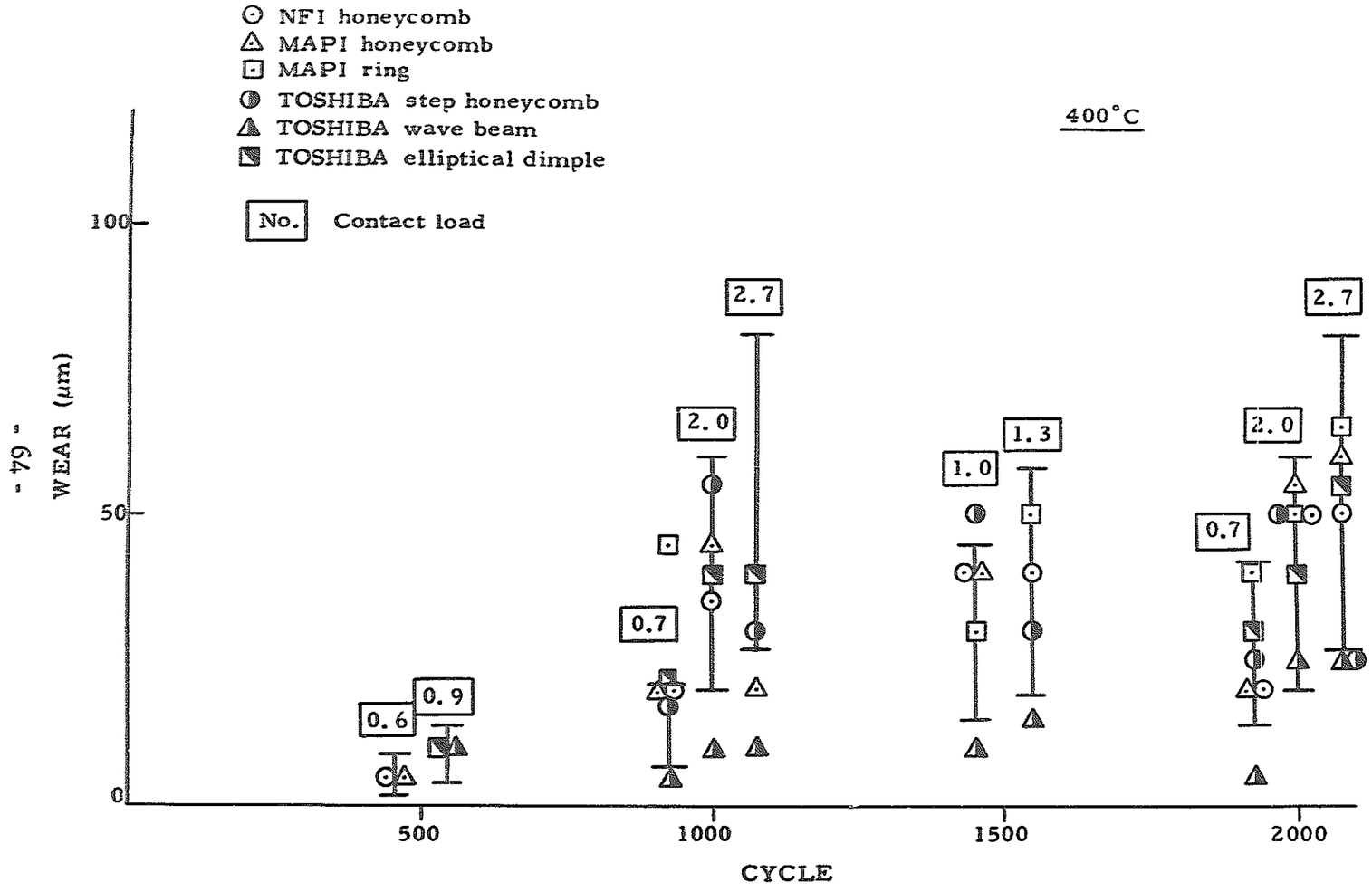

Fig. 6.4 Cladding wear at 400°C.

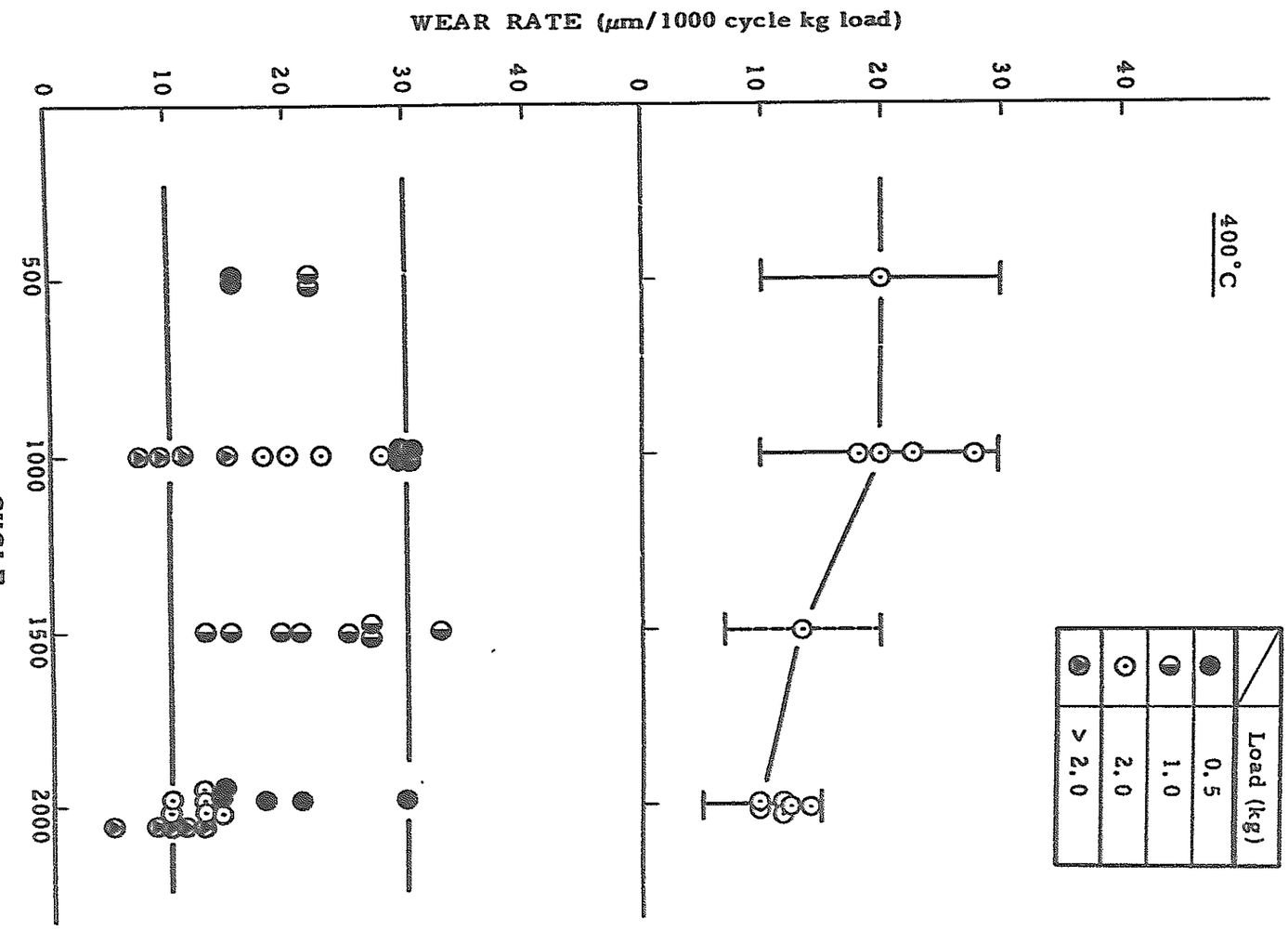

Fig. 6.5 Cladding wear rate at 400°C.

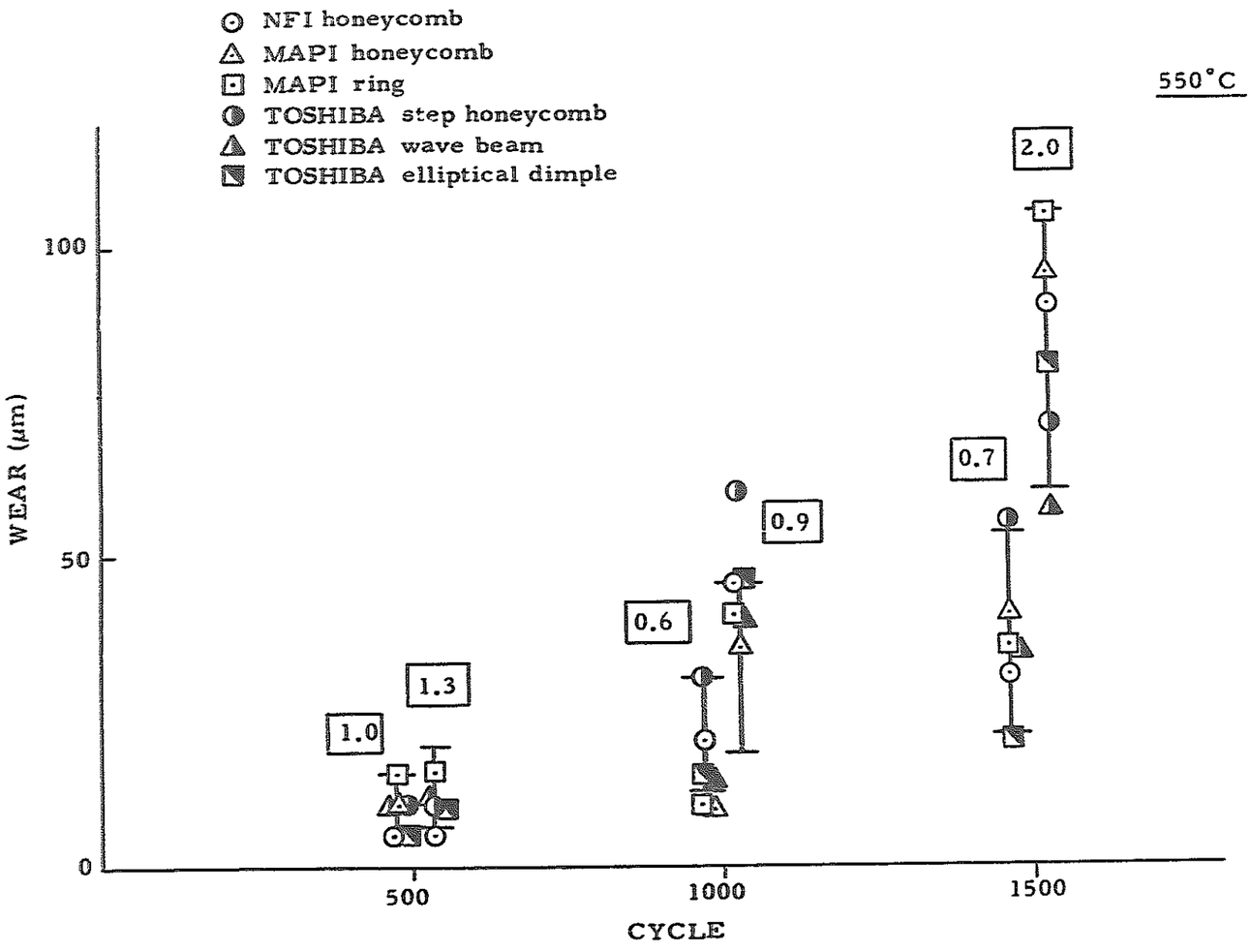

Fig. 6.6 Cladding wear at 550°C.

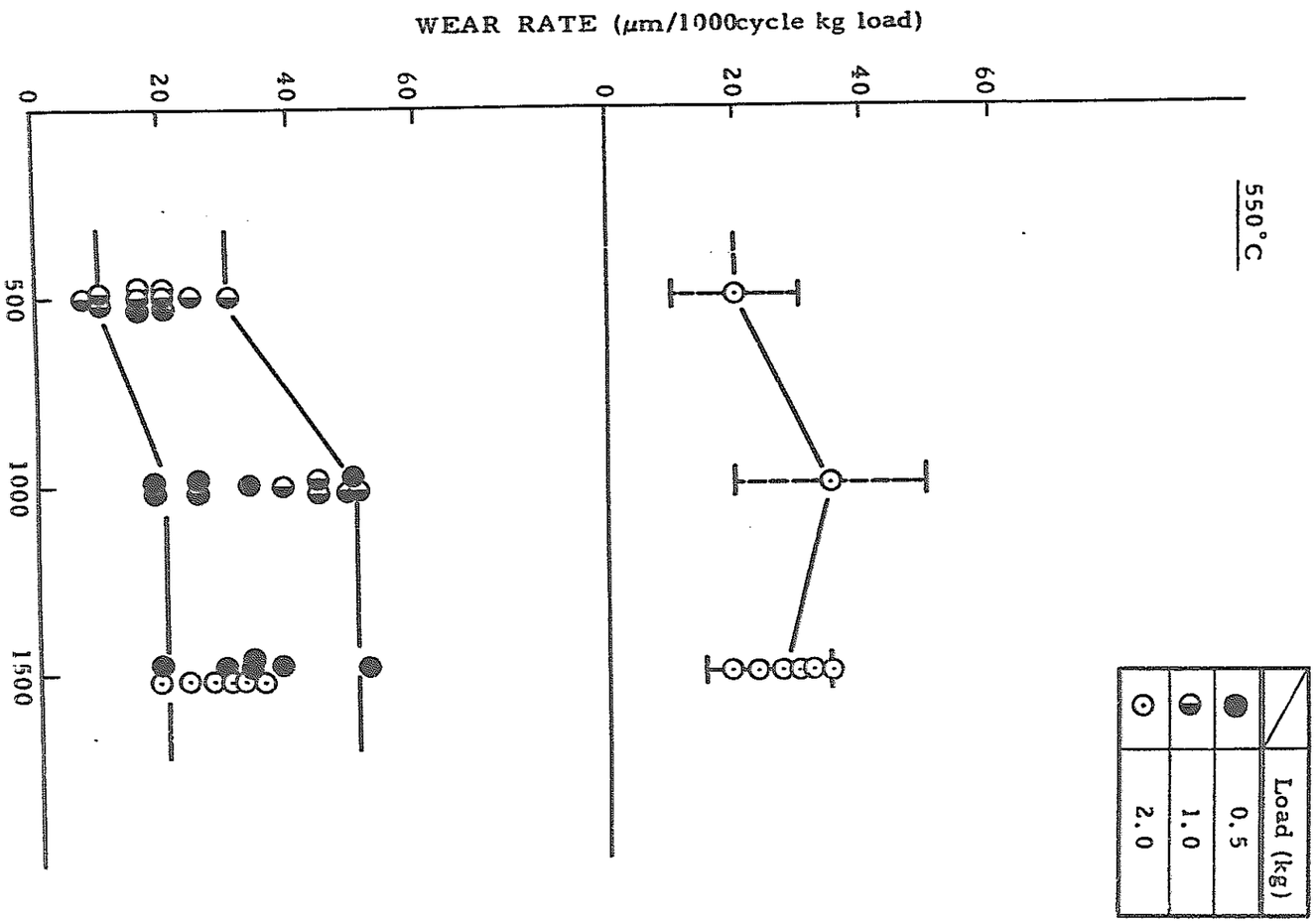

Fig. 6.7 Cladding wear rate at 550°C.

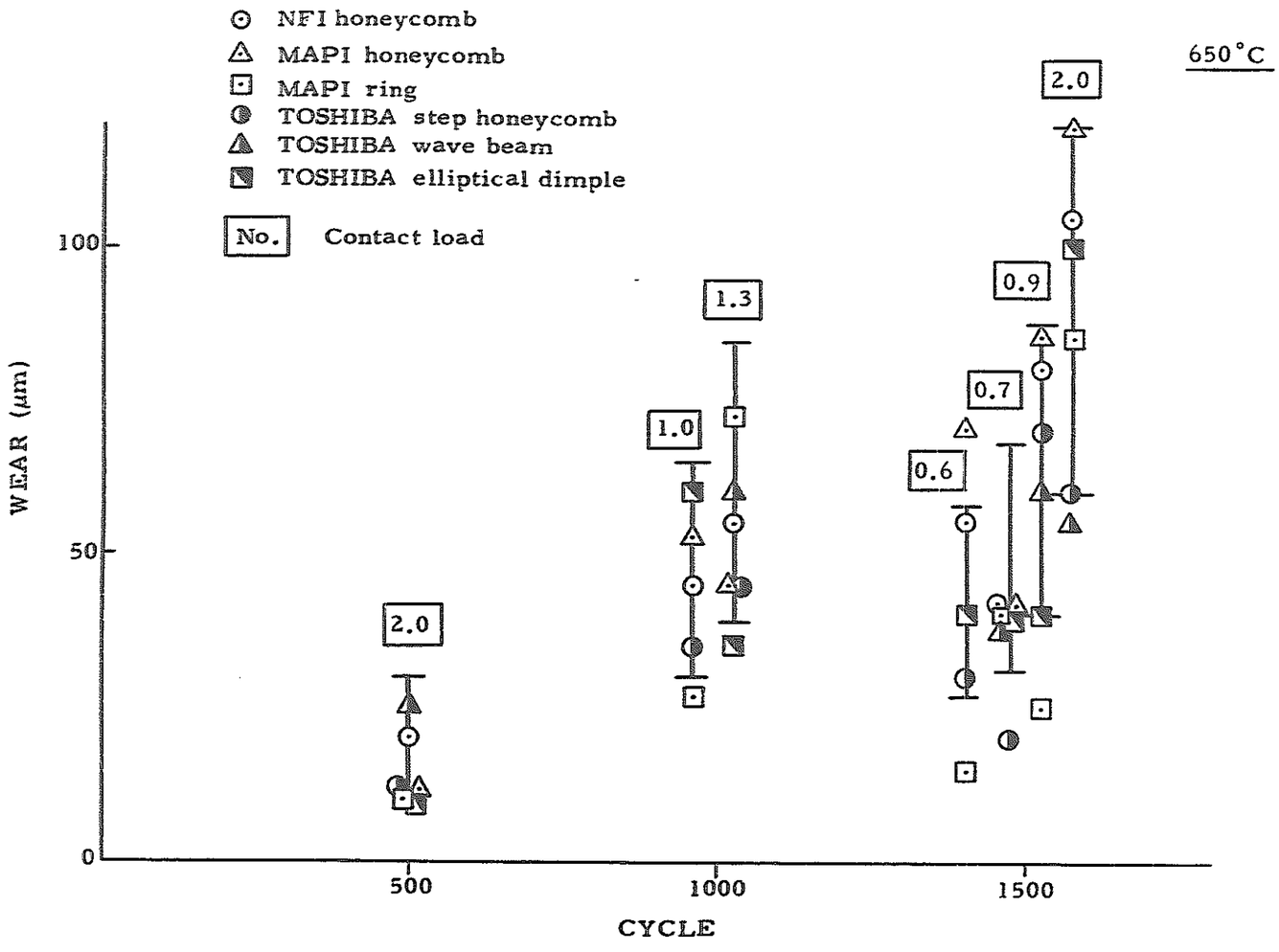

Fig. 6.8 Cladding wear at 650°C.

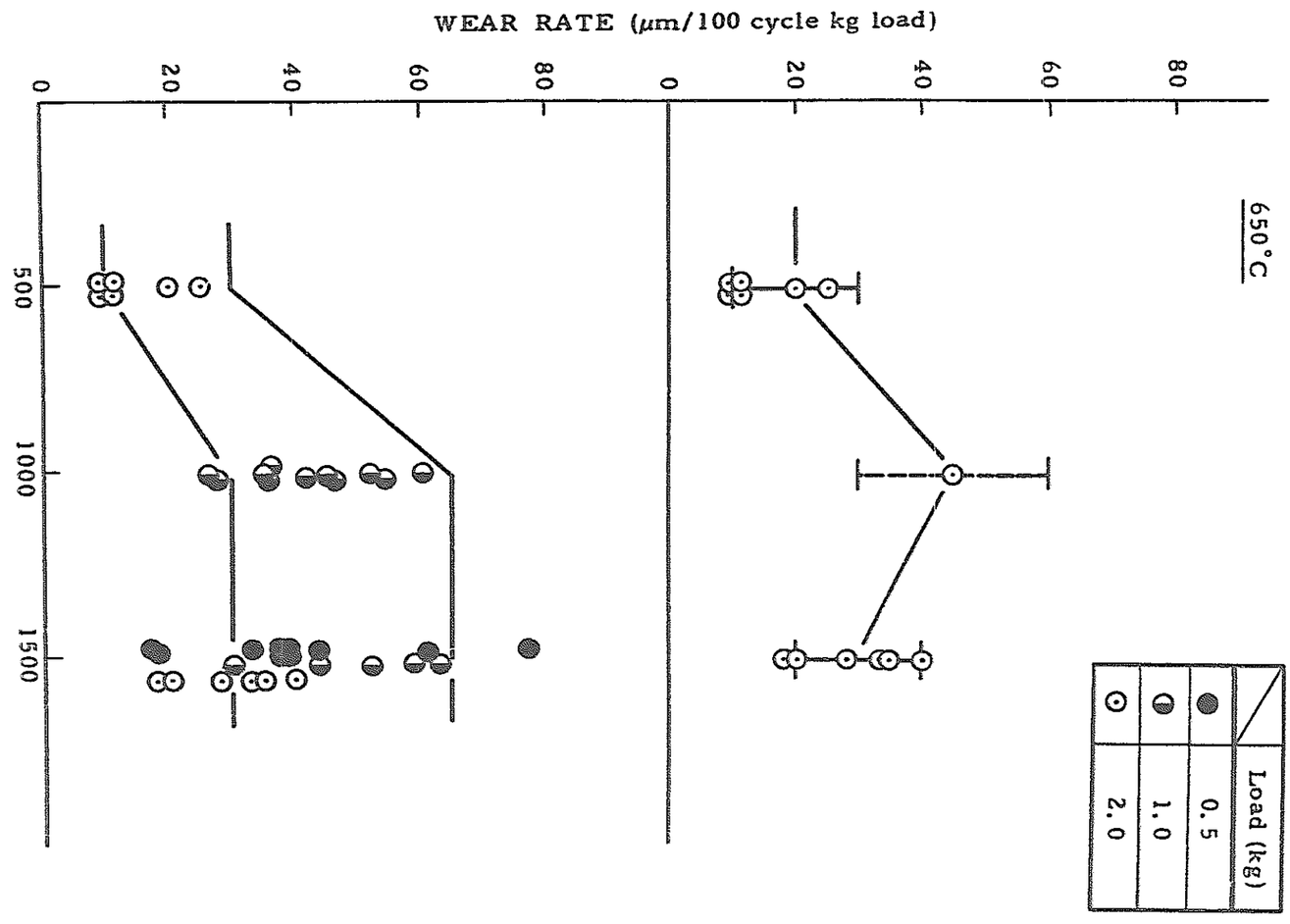

Fig. 6.9 Cladding wear rate at 650°C.

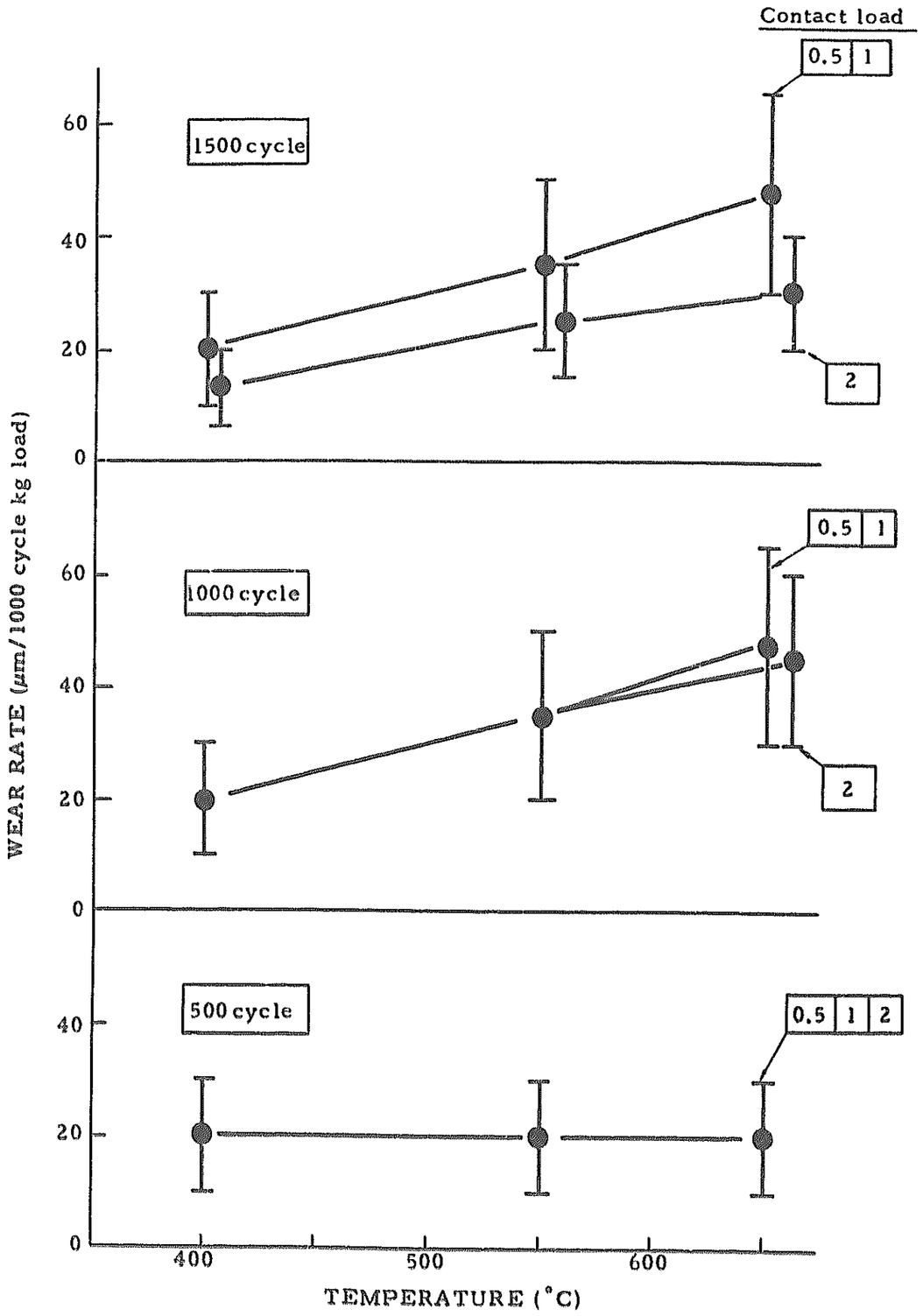

Fig. 6.10 Cladding wear rate vs sodium temp. and contact load.

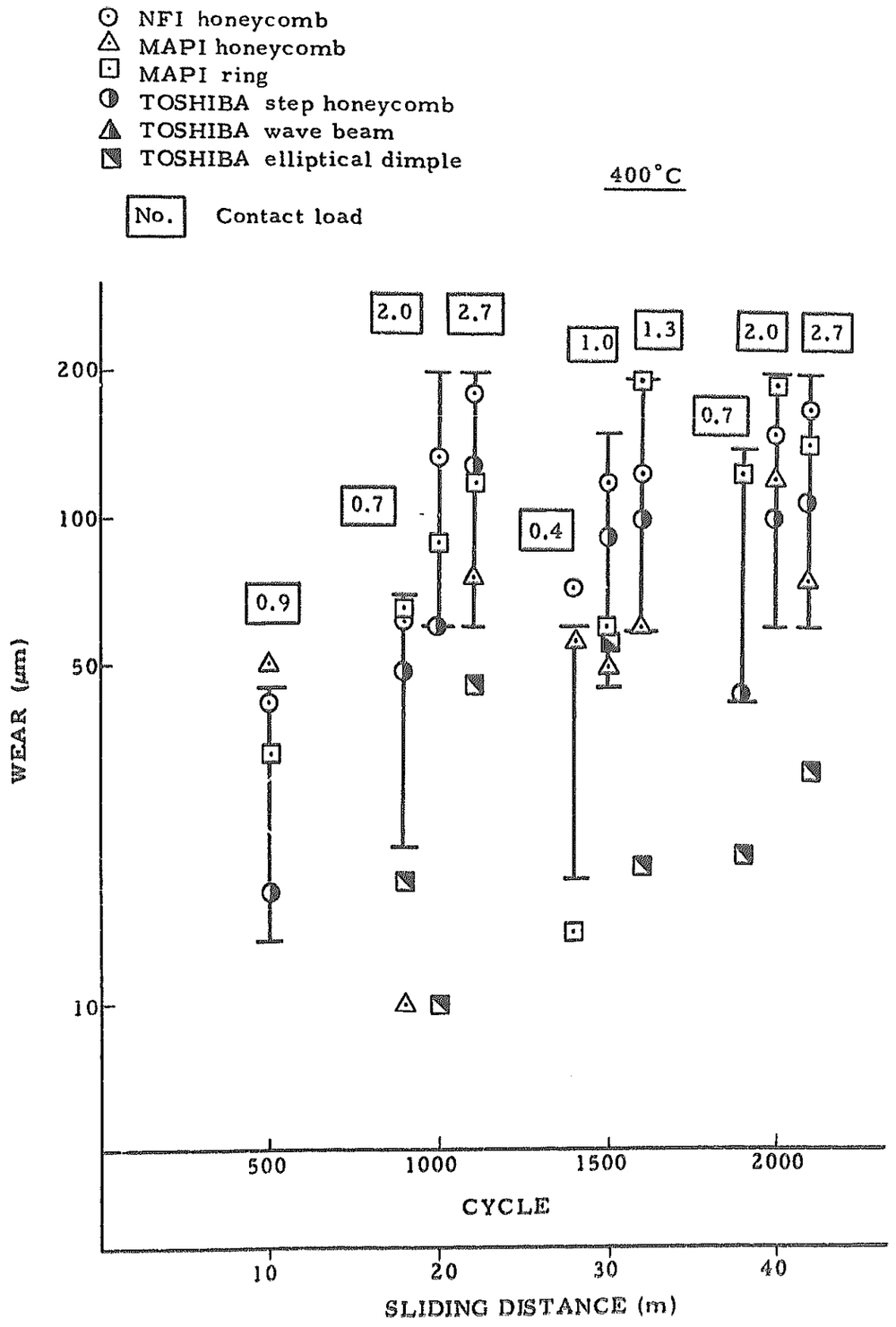

Fig. 6.11 Wear of grid dimple at 400°C.

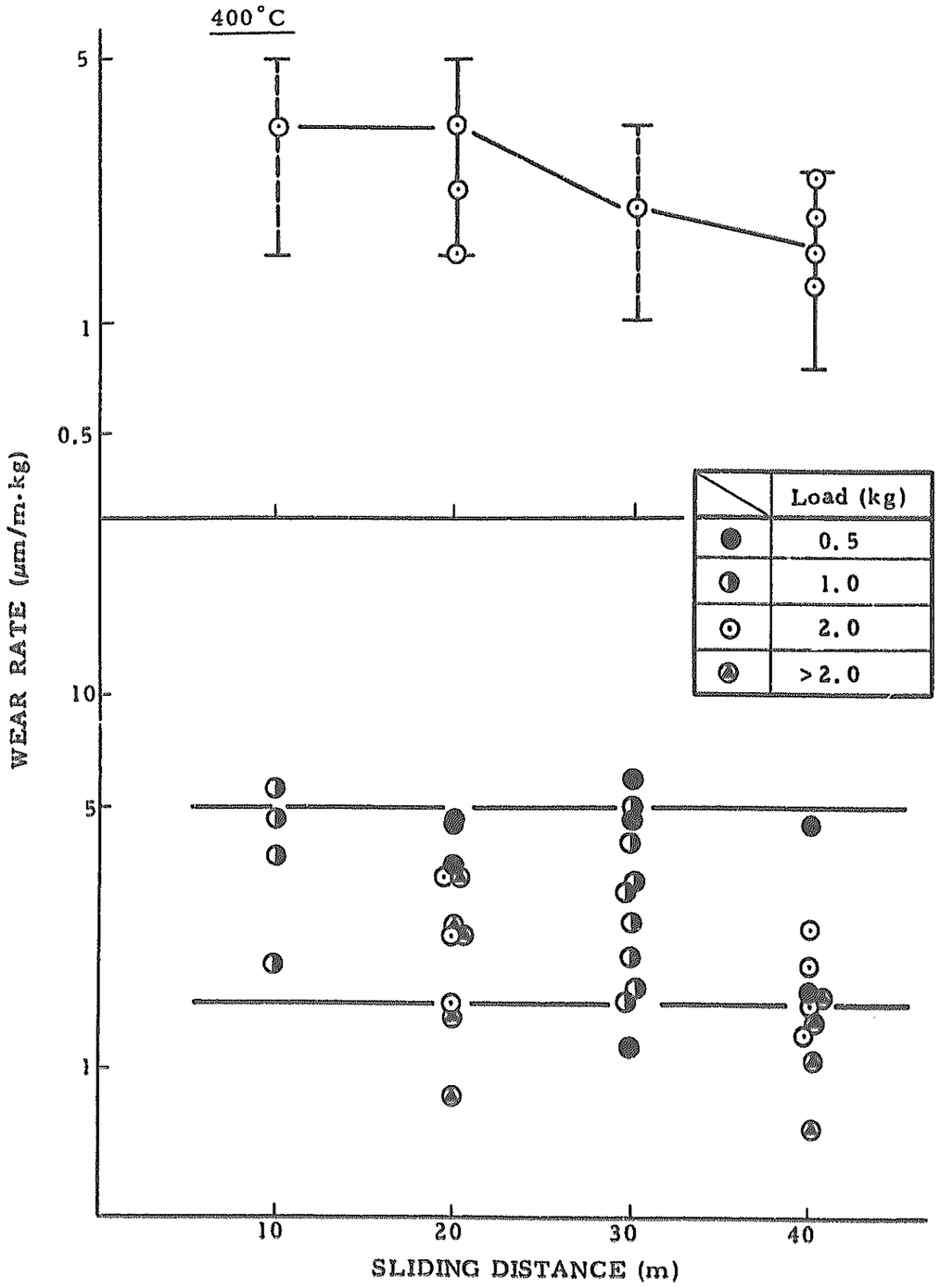

Fig. 6.12 Wear rate of grid dimple at 400°C.

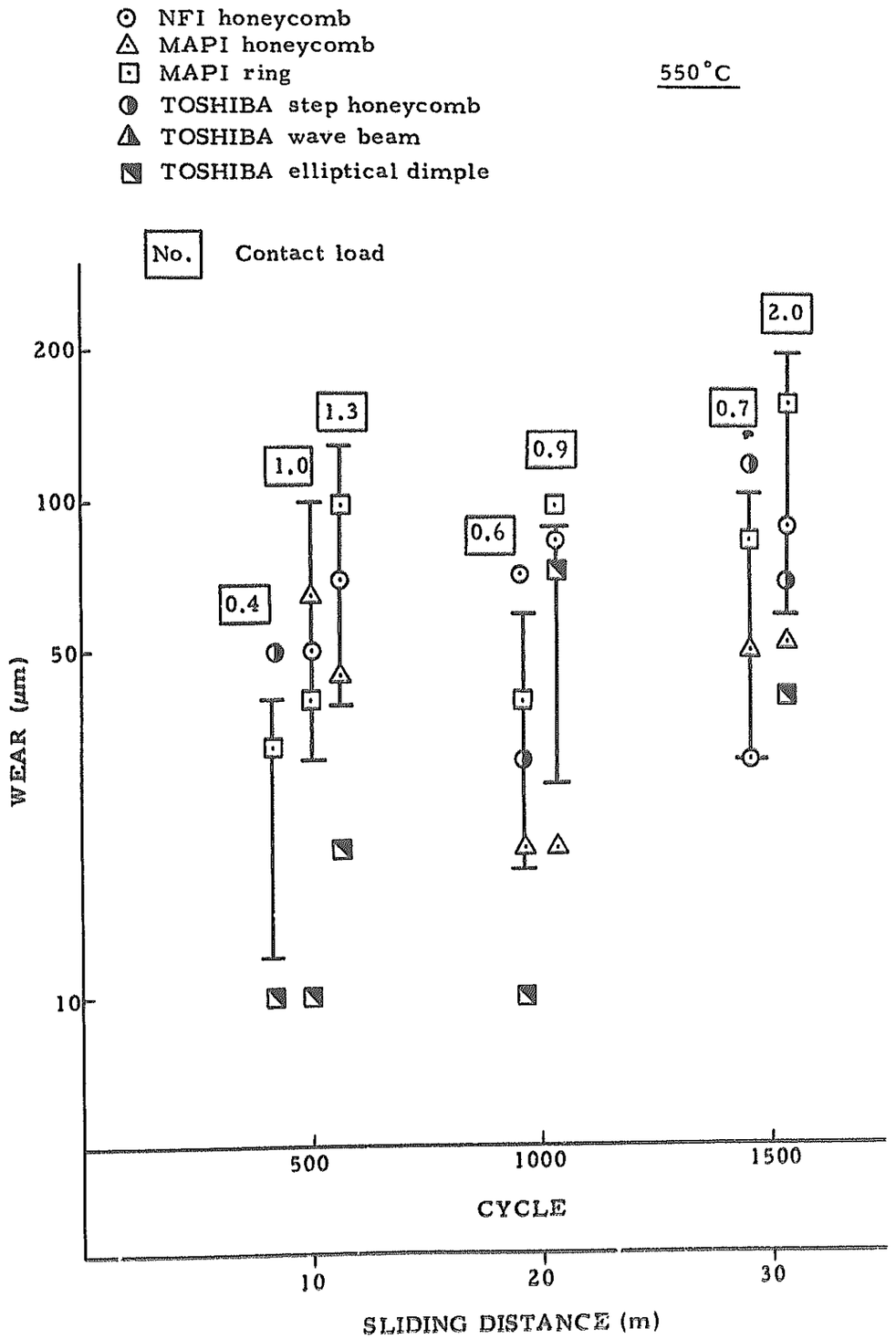

Fig. 6.13 Wear of grid dimple at 550°C.

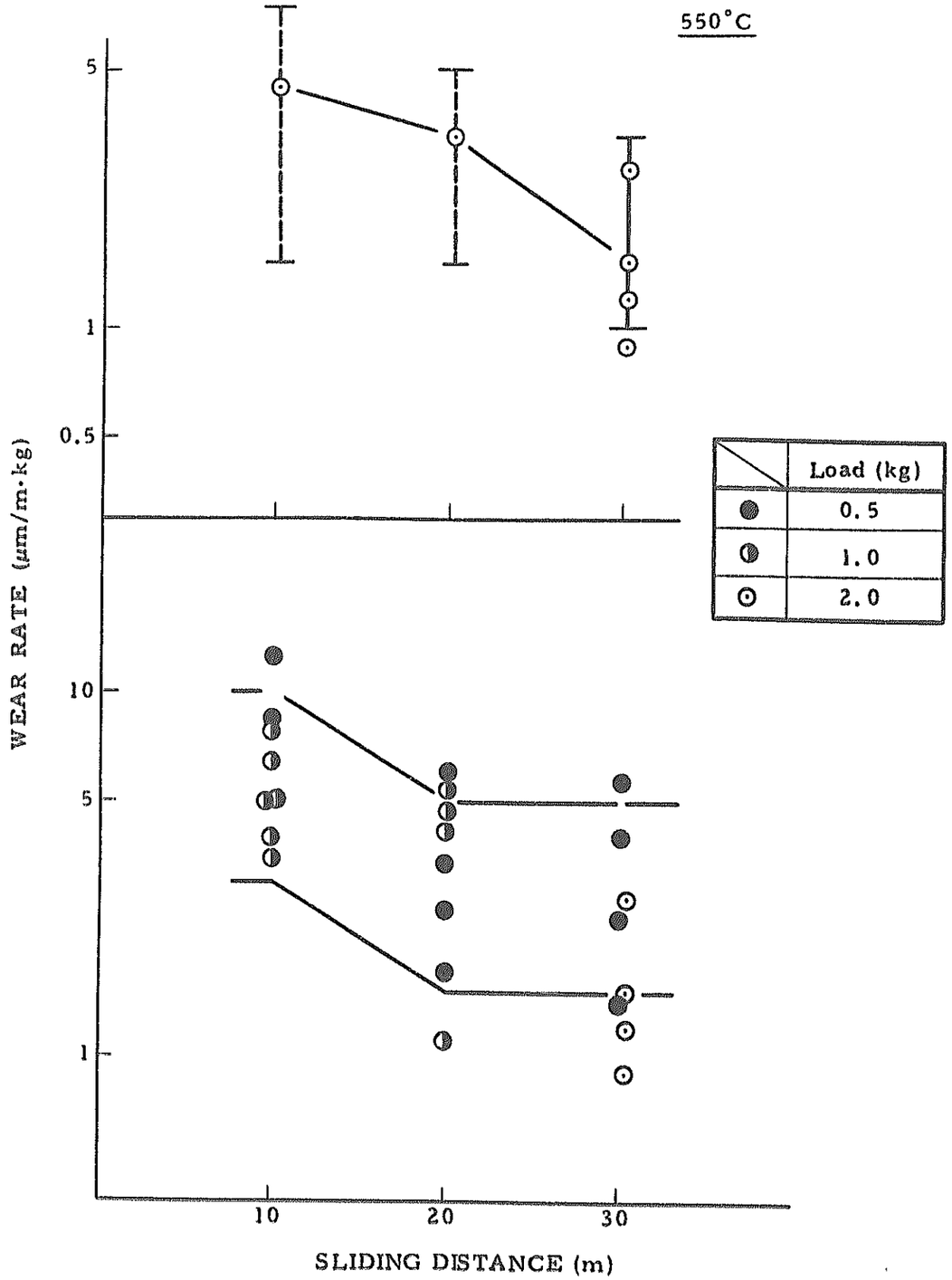

Fig. 6.14 Wear rate of grid dimple at 550°C.

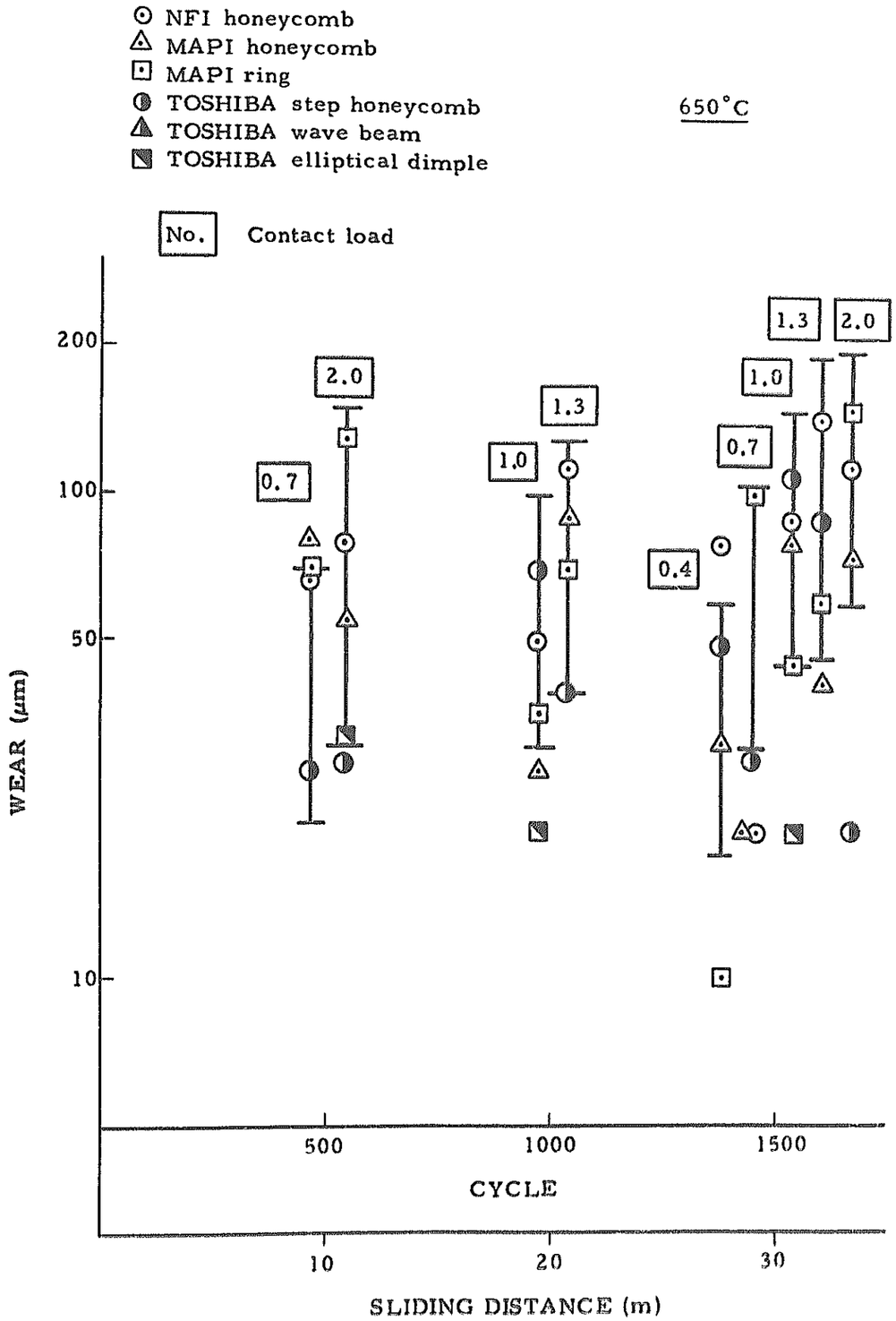

Fig. 6.15 Wear of grid dimple at 650°C.

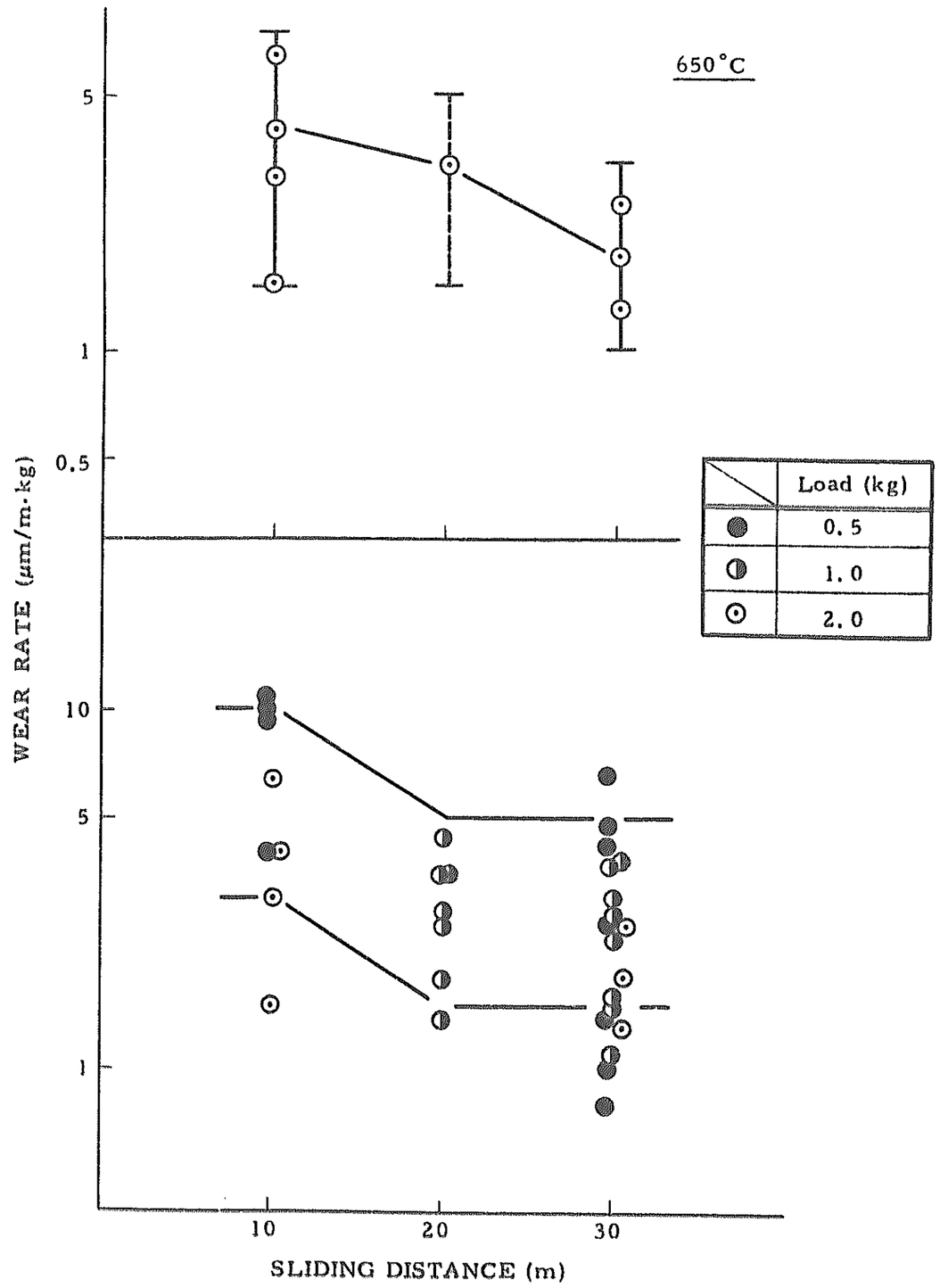

Fig. 6.16 Wear rate of grid dimple at 650°C.

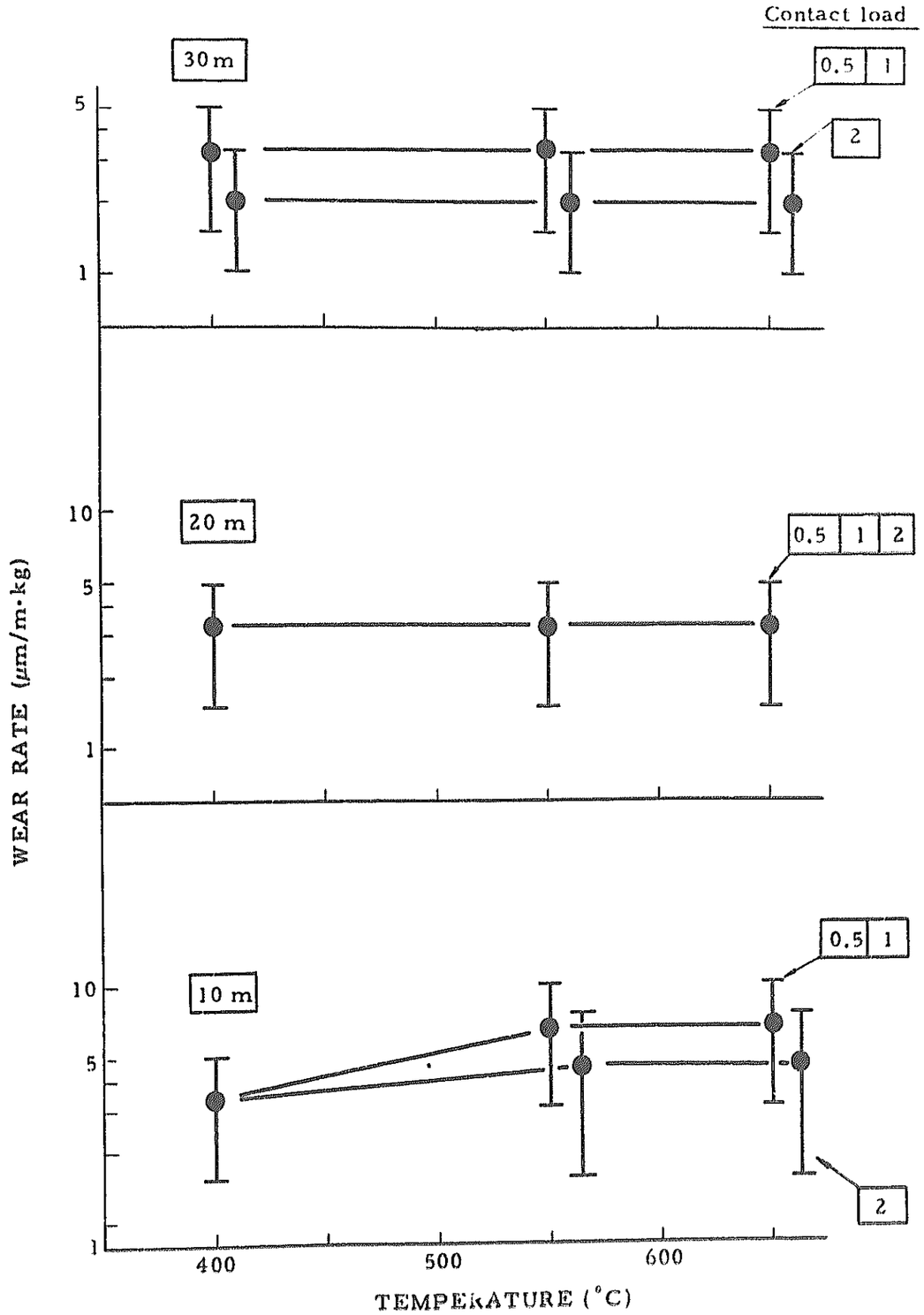

Fig. 6.17 Wear rate of grid dimple vs sodium temp. and contact load.

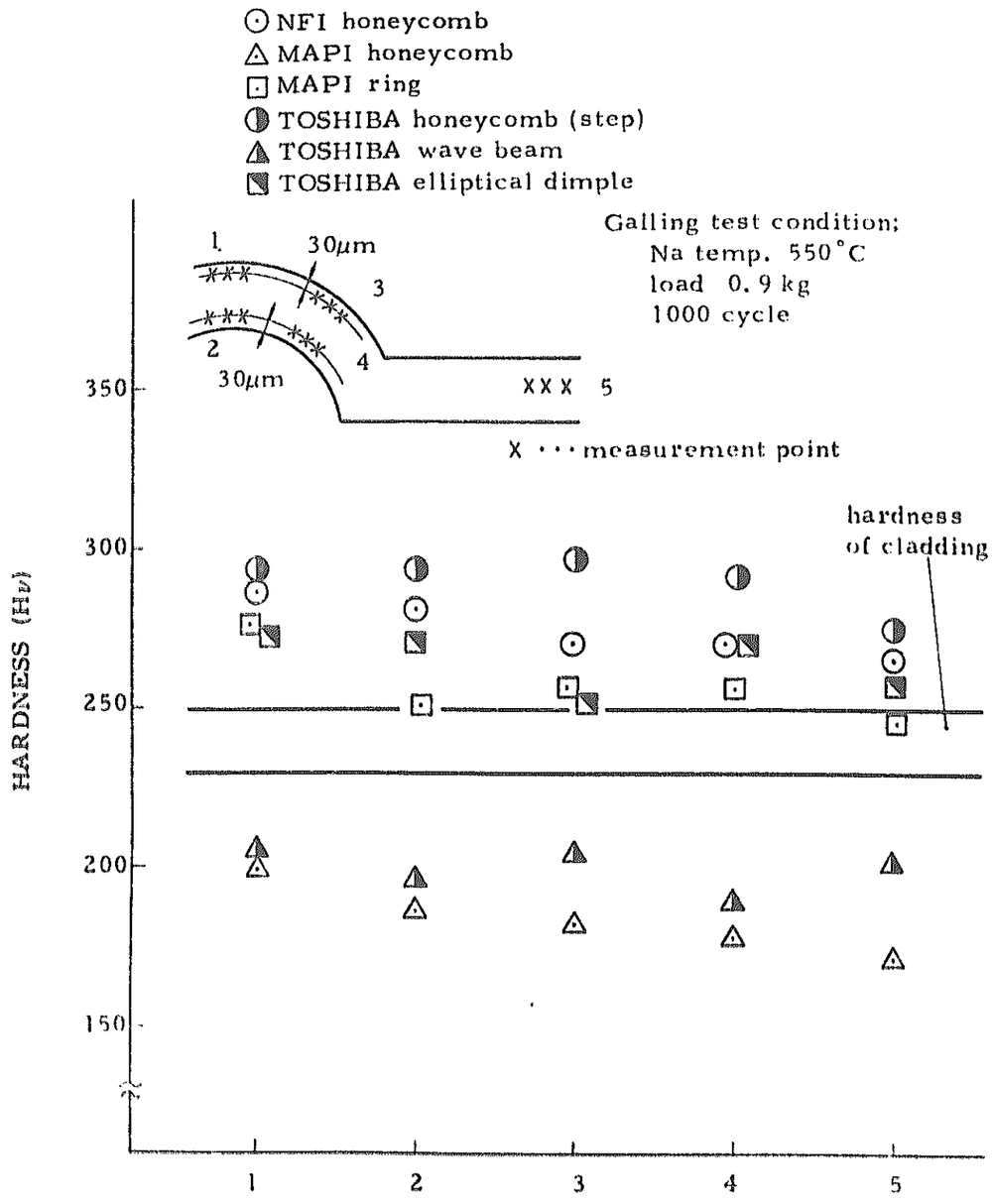

Fig. 6.18 Hardness of grid dimple and cladding (after galling test)

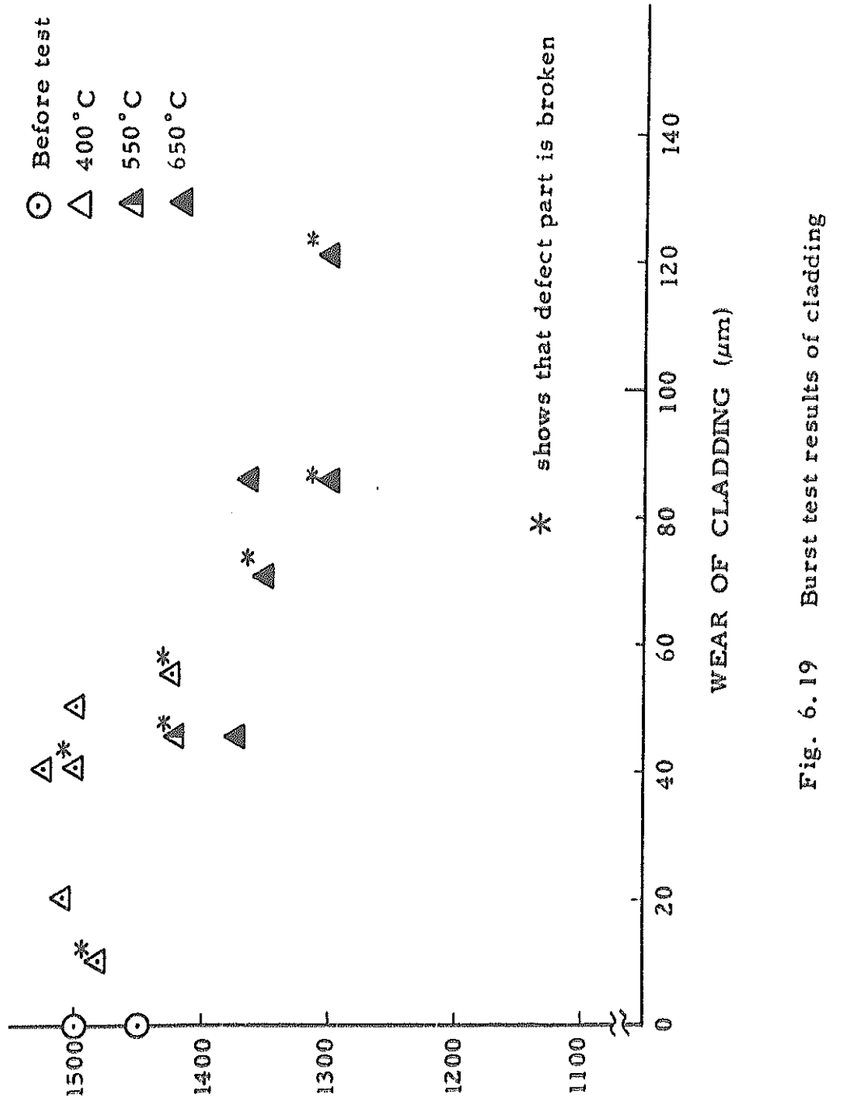

Fig. 6.19 Burst test results of cladding

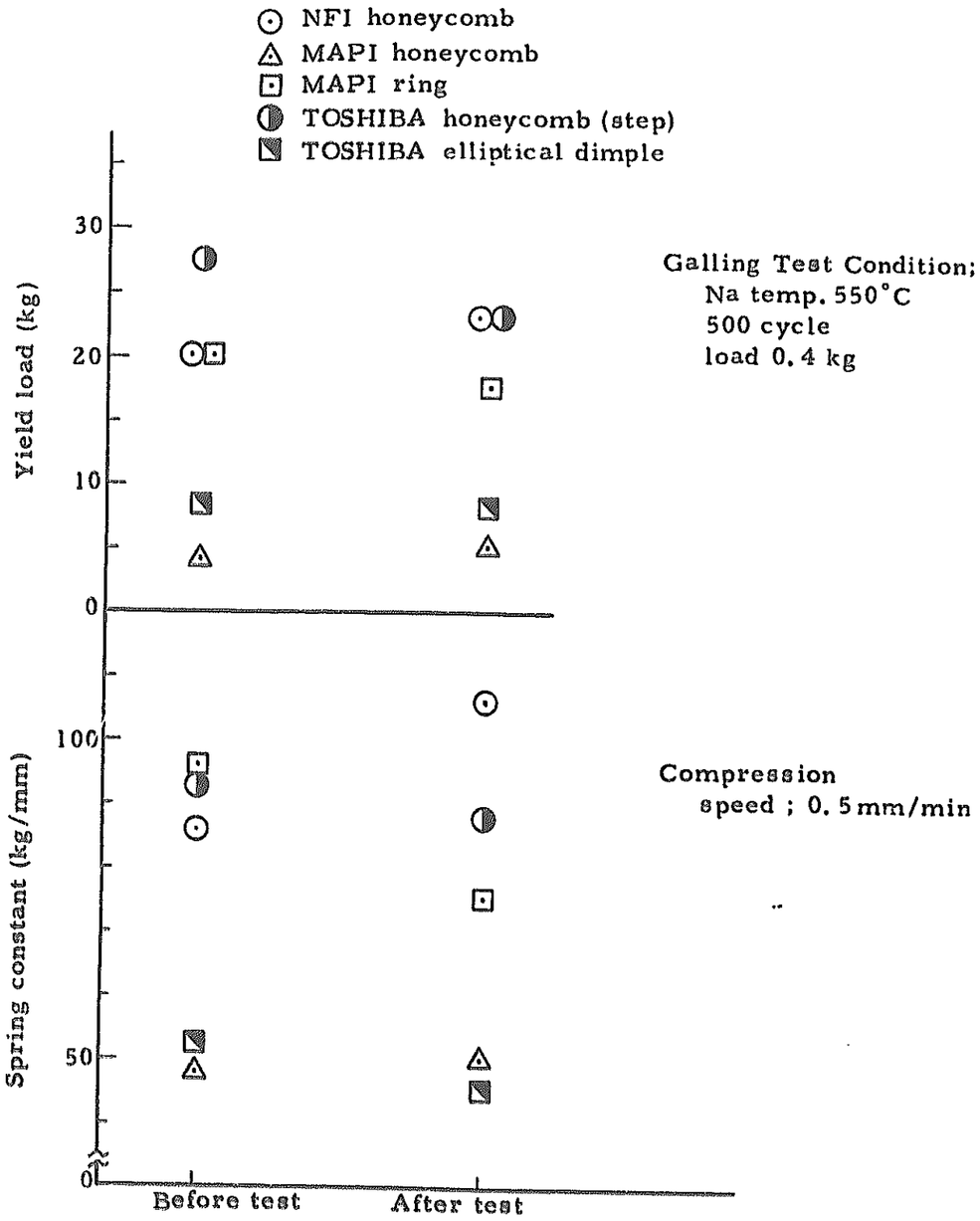

Fig. 6.20 Compression test results of grid dimple.

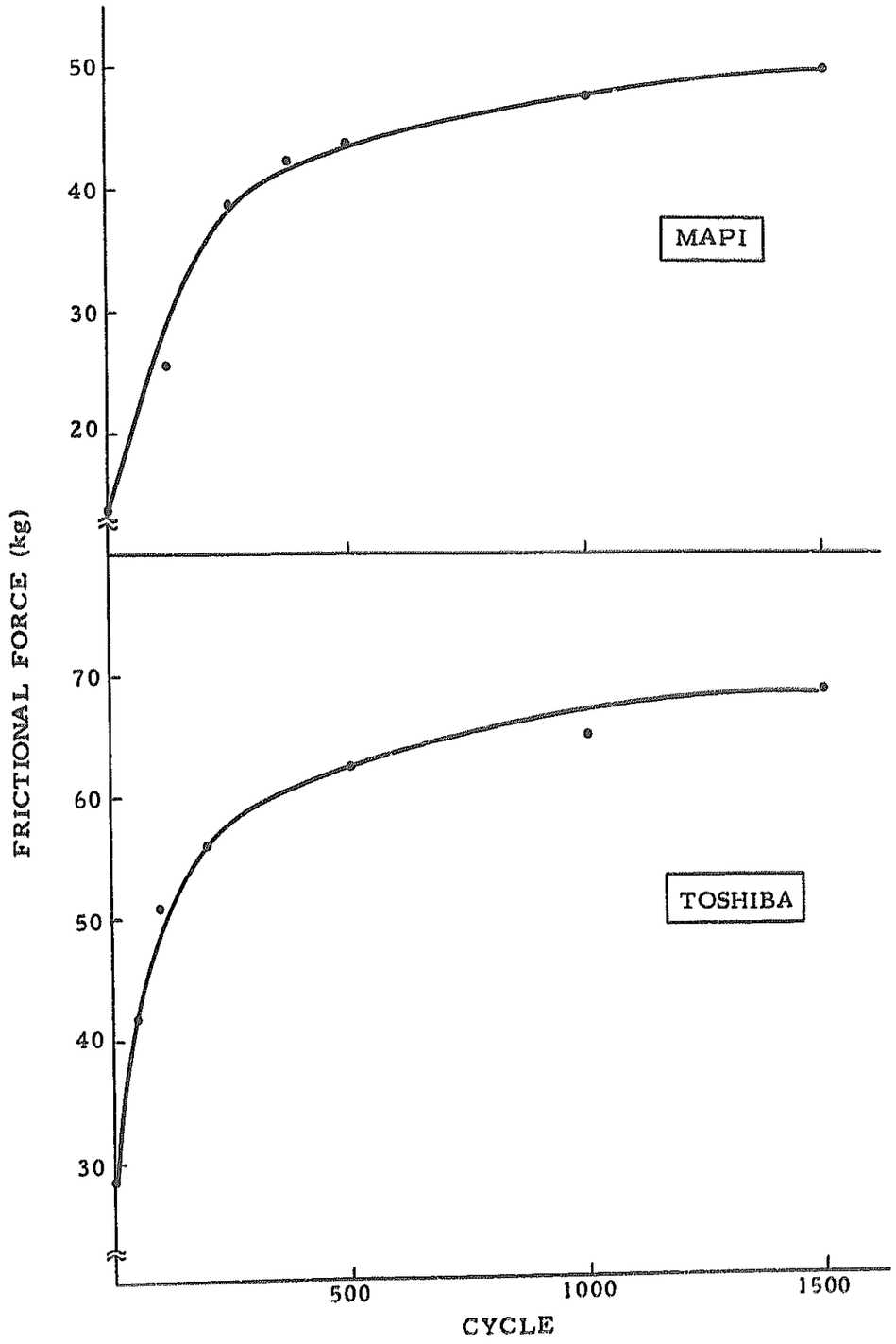

Fig. 6.21 Change of frictional force between grid spacers and rod bundle vs operational cycle at 550°C.

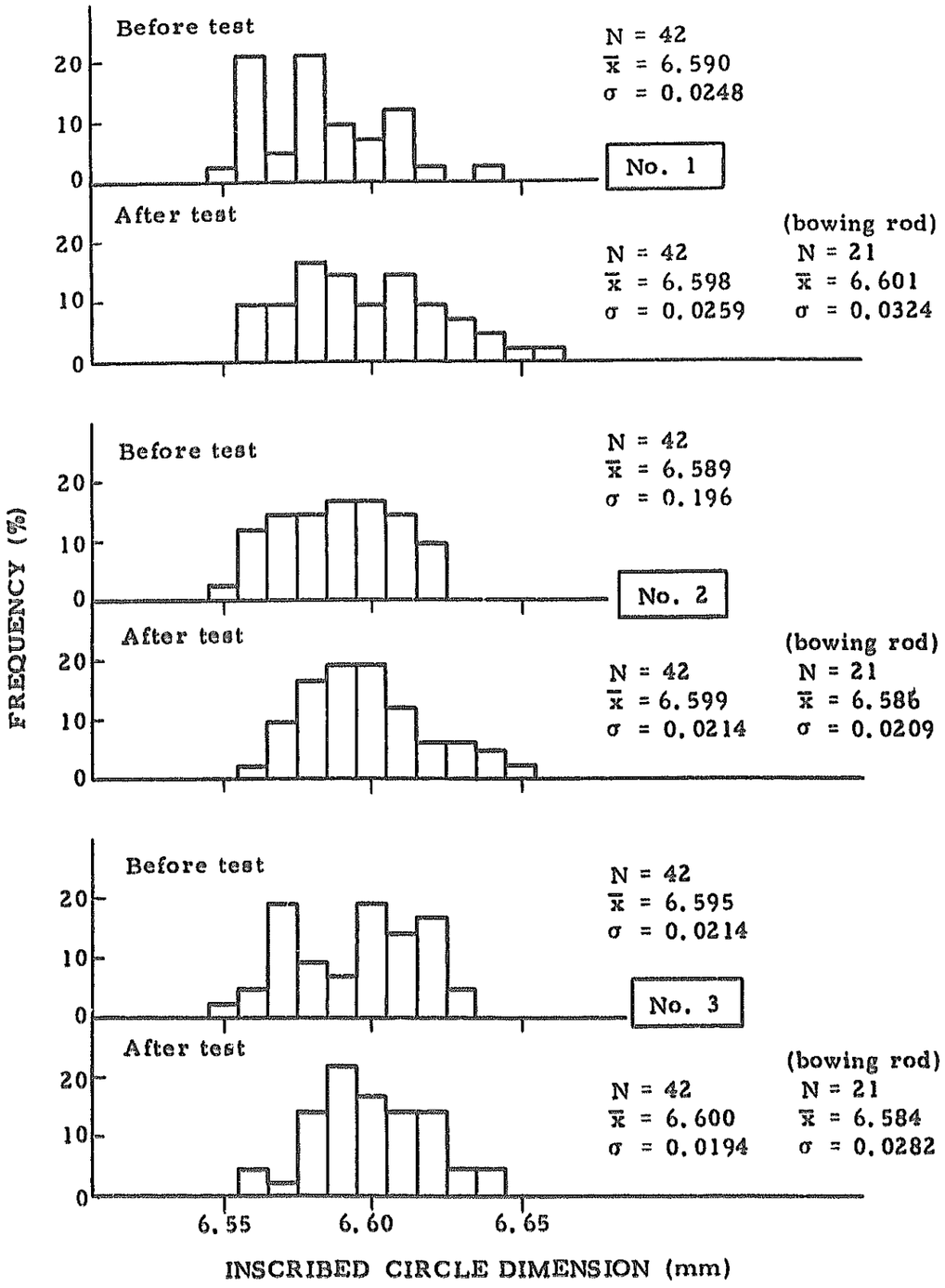

Fig. 6.22 Frequency data of inscribed circle dimension in Toshiba grid spacers.

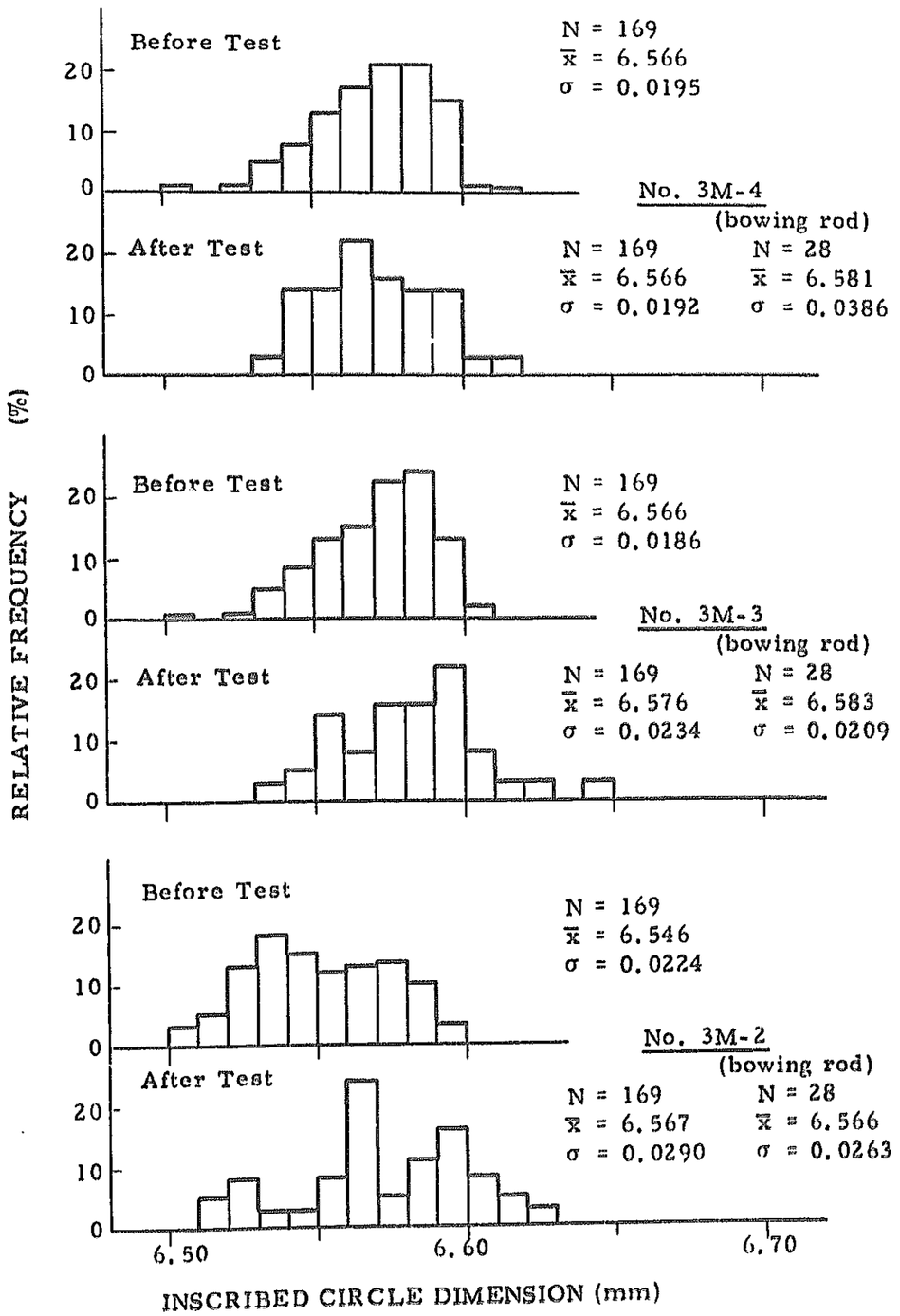

Fig. 6.23 Frequency data of inscribed circle dimension in MAPI ring type grid spacers.

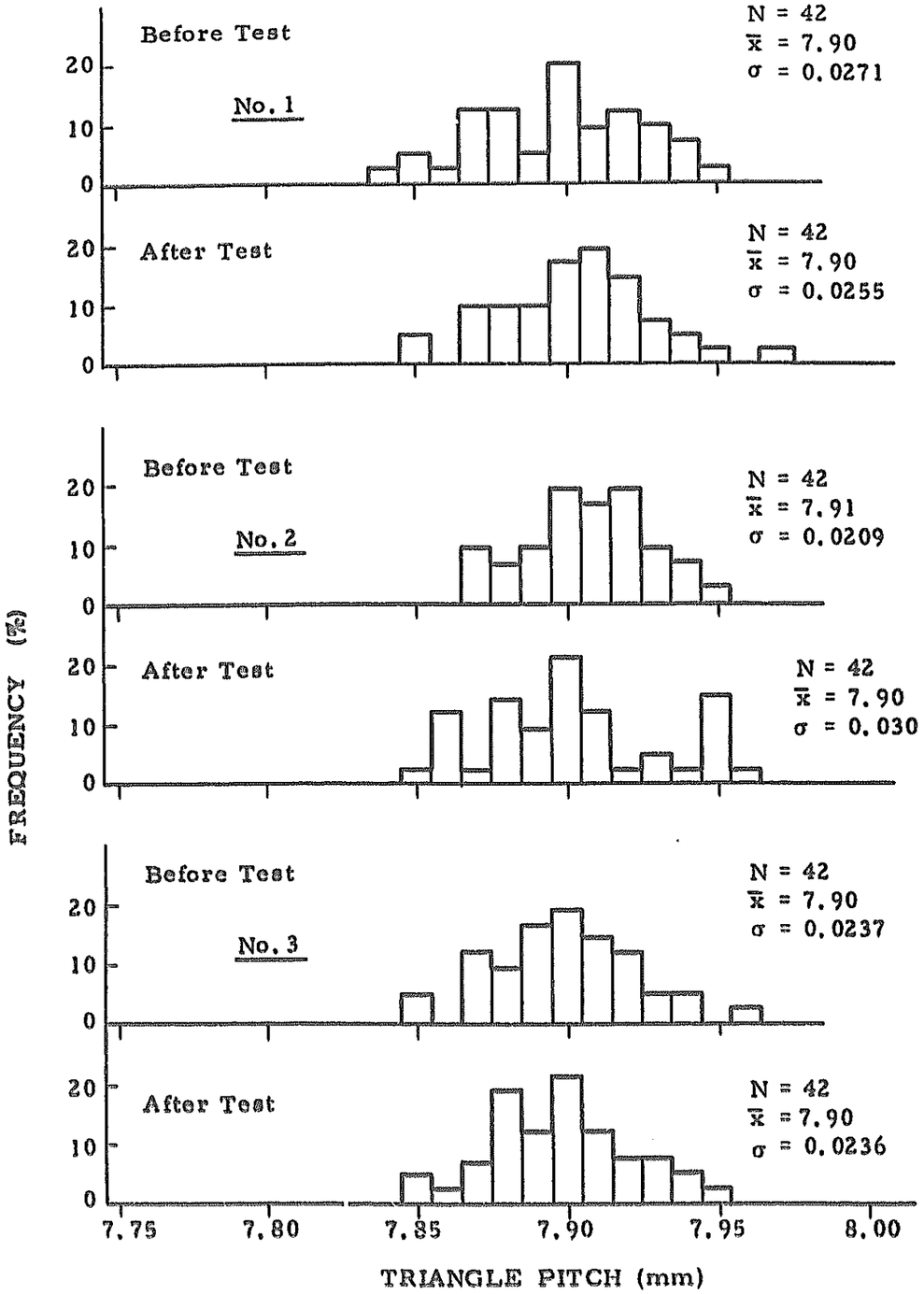

Fig. 6.24 Frequency data of triangle pitch in Toshiba grid spacers.

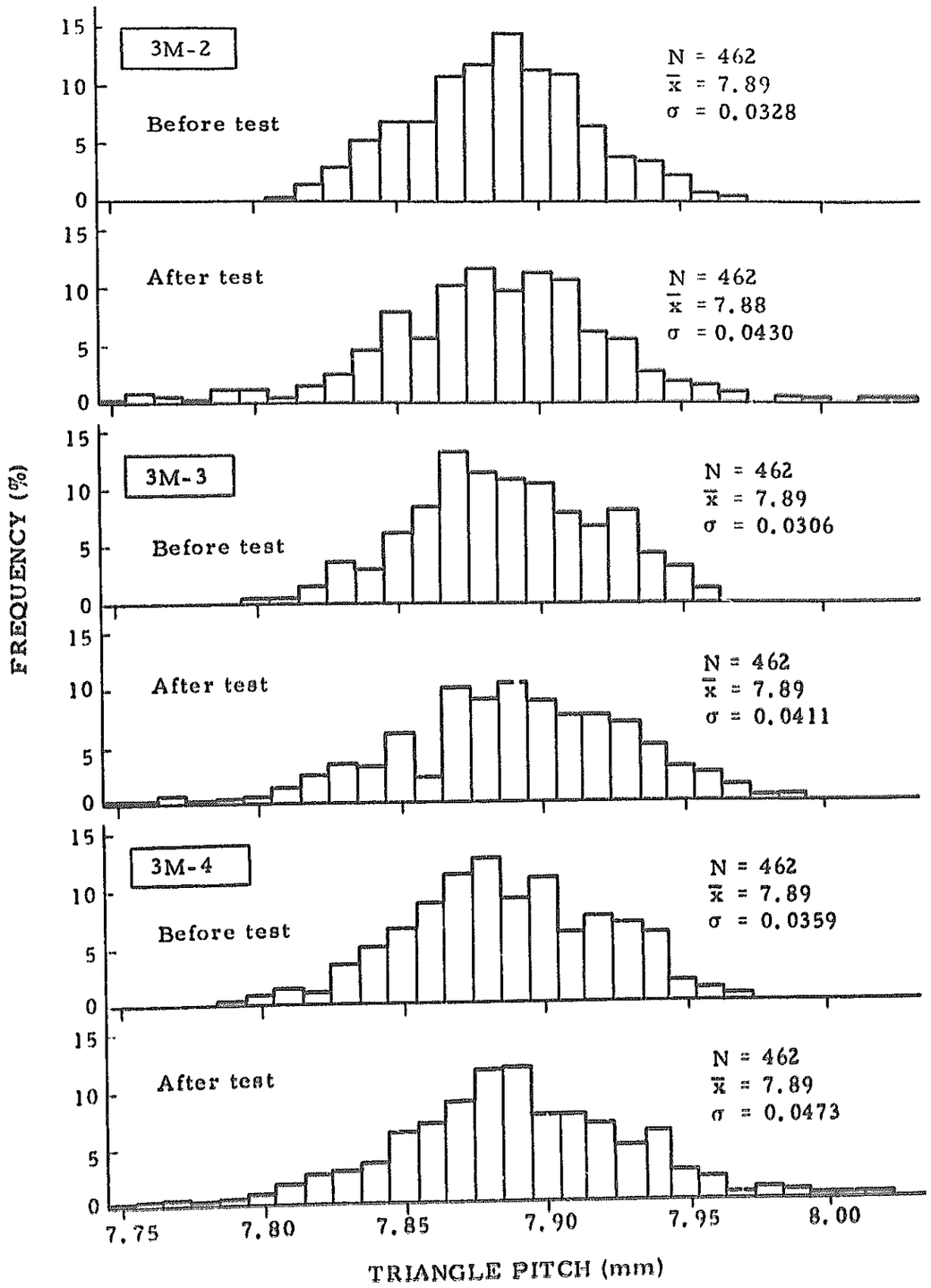

Fig. 6.25 Frequency data of triangle pitch in MAPI ring type grid spacers.

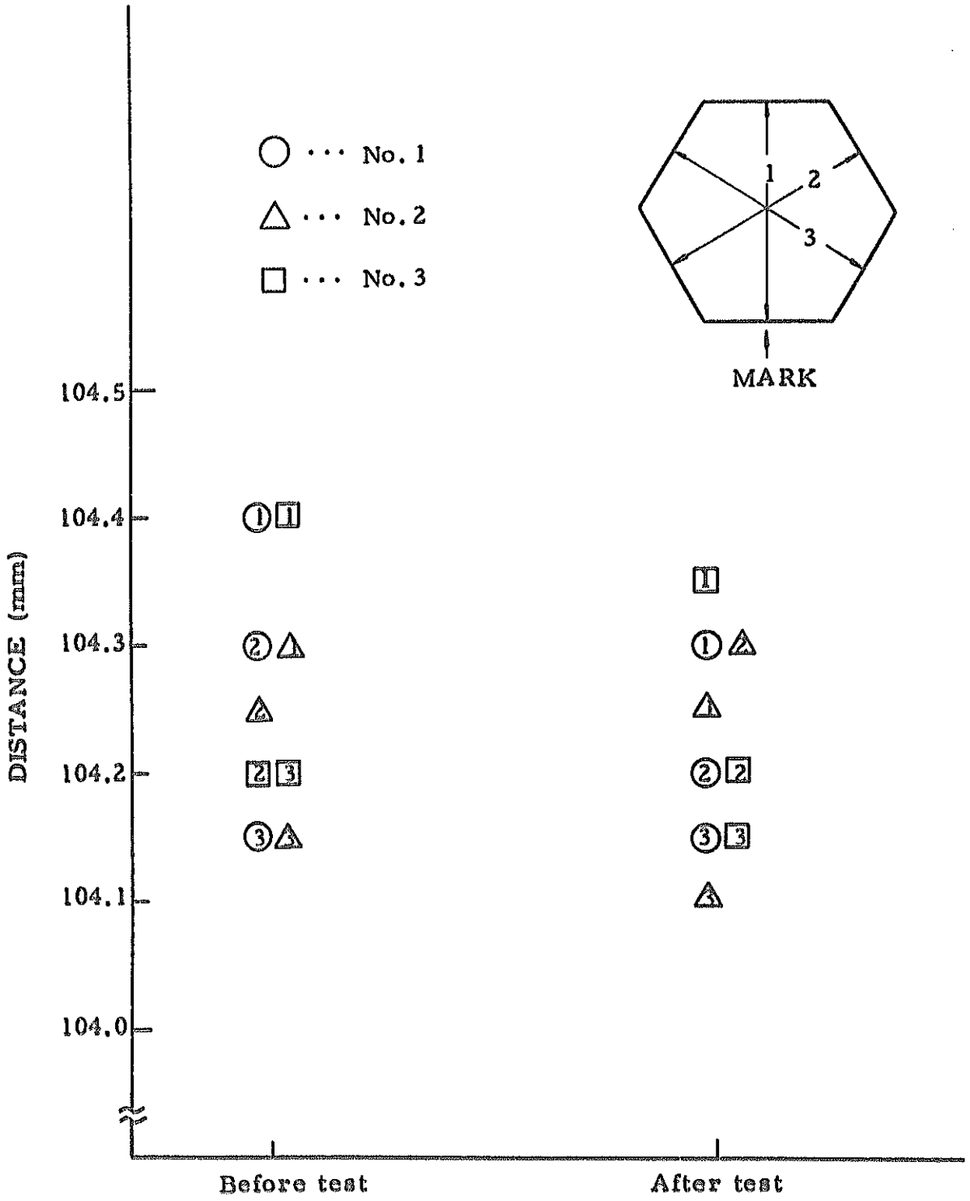

Fig. 6.26 Distance of between opposite surfaces.
(Toshiba grid spacers)

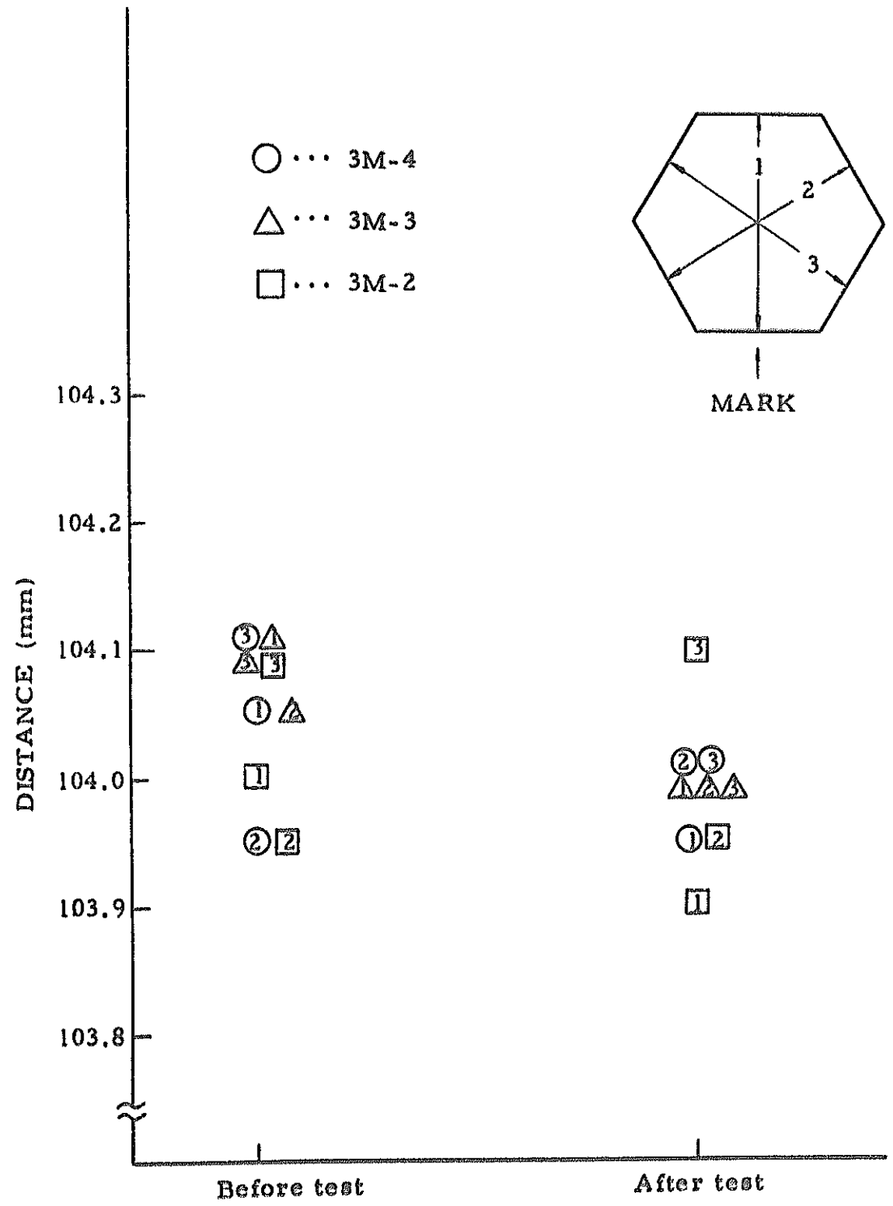

Fig. 6.27 Distance of between opposite surfaces.
(MAPI ring type grid spacers)

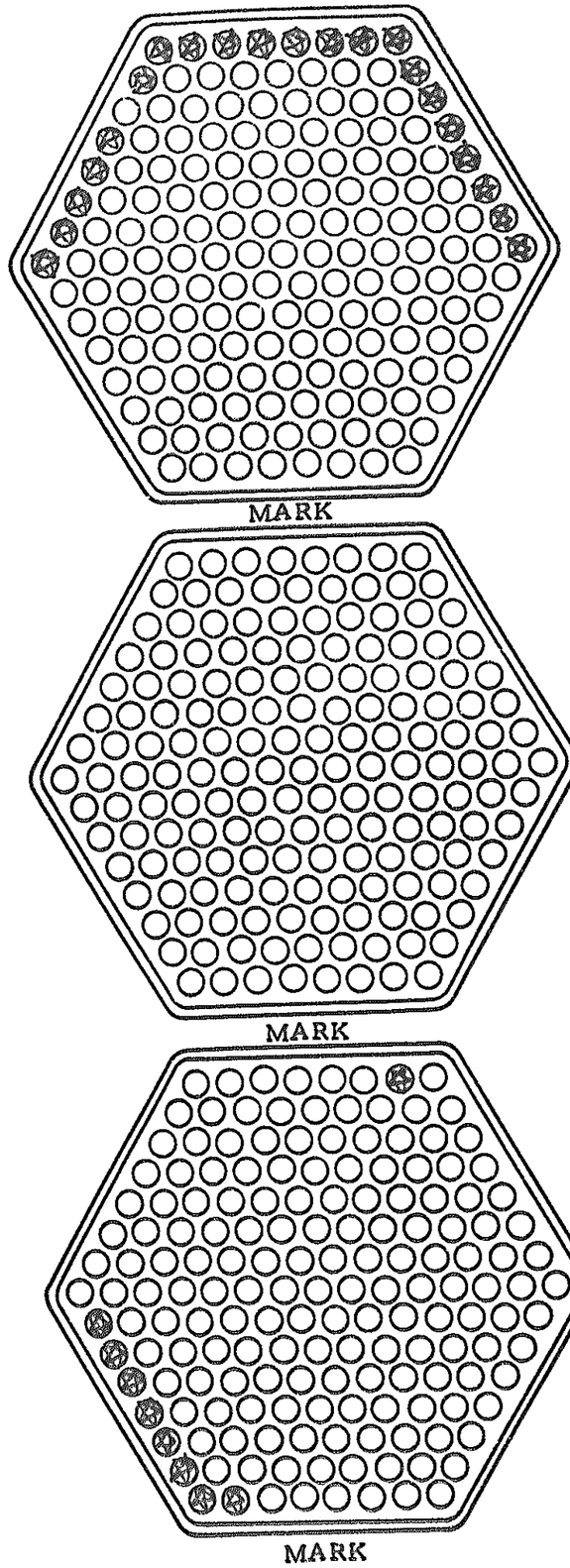

Fig. 6.28 Grid deformation after galling test.
(MAPI ring type grid spacers)

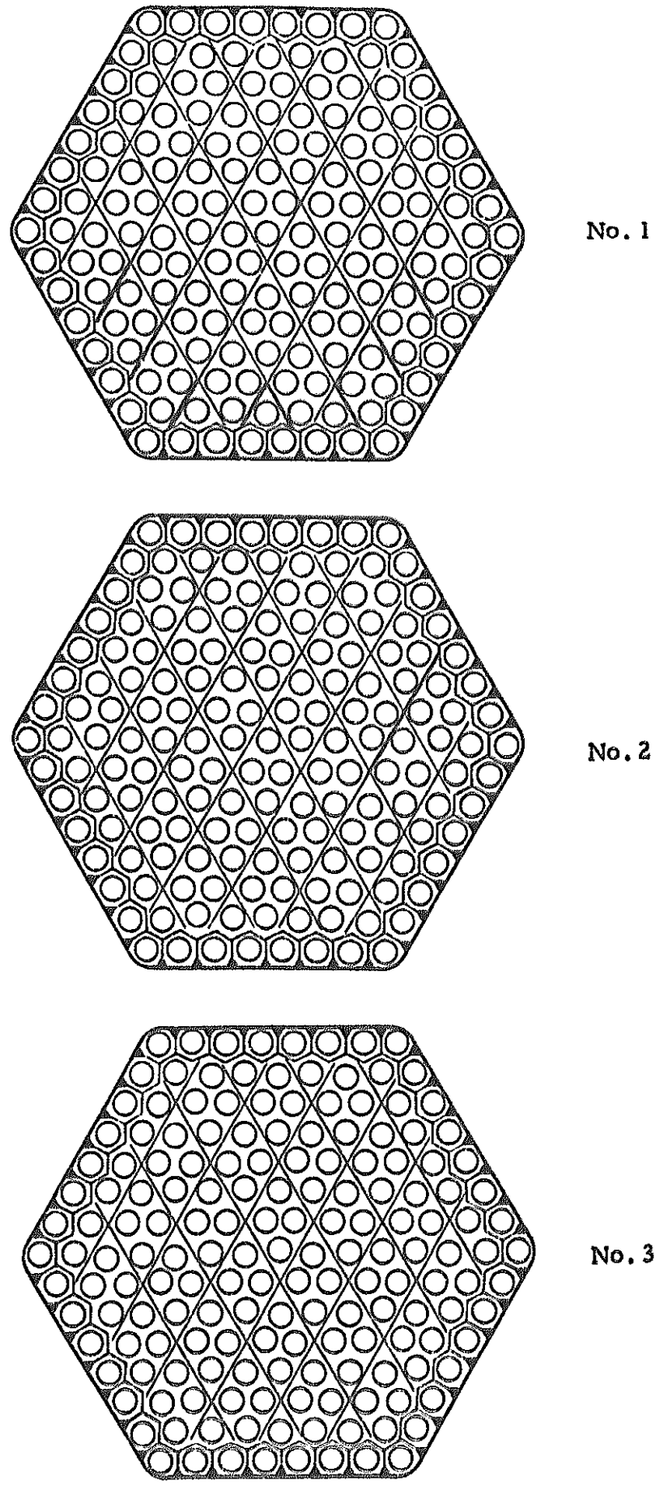

Fig. 6.29 Grid deformation after galling test.
(Toshiba grid spacers)

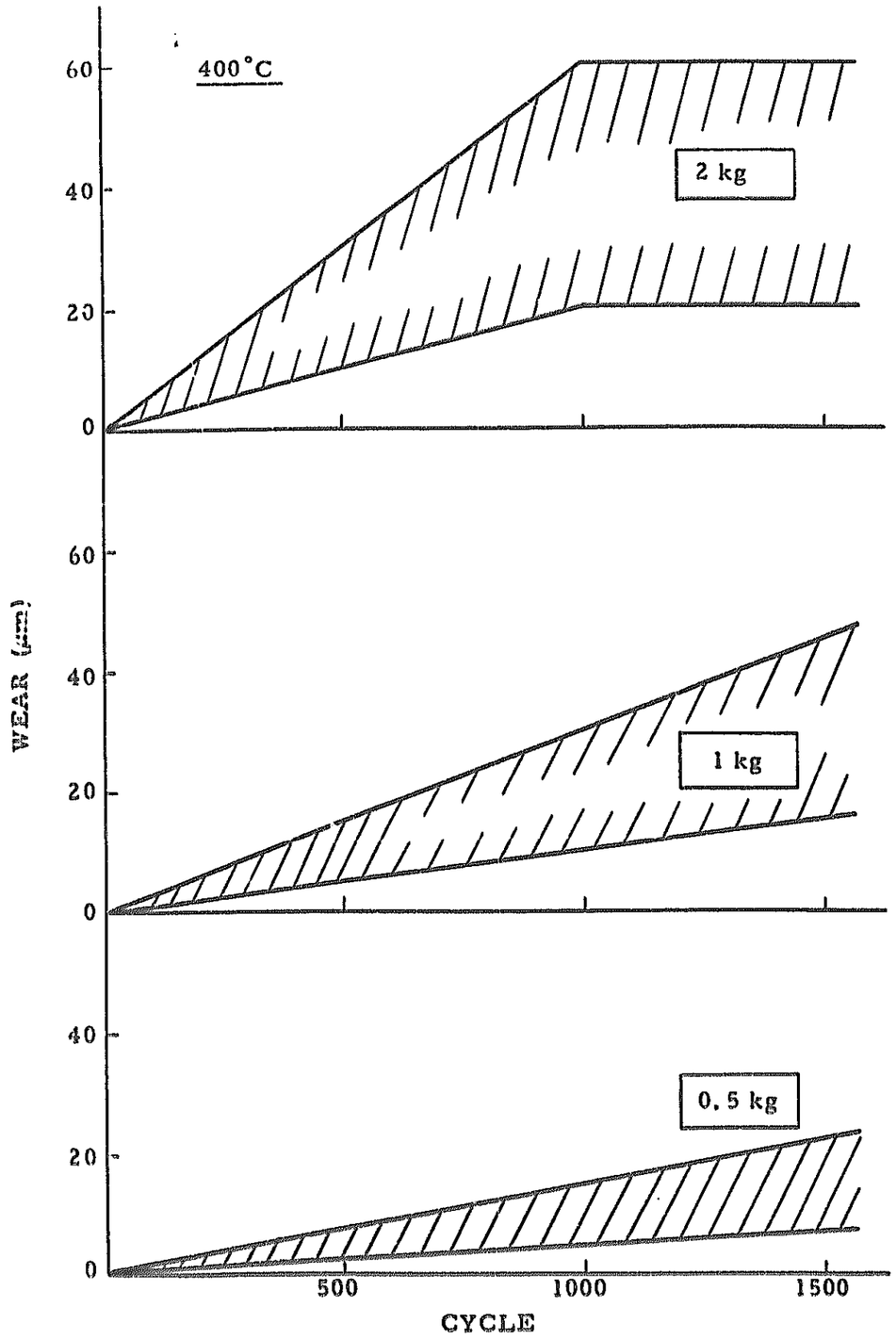

Fig. 7.1 Available data of cladding wear at 400°C.

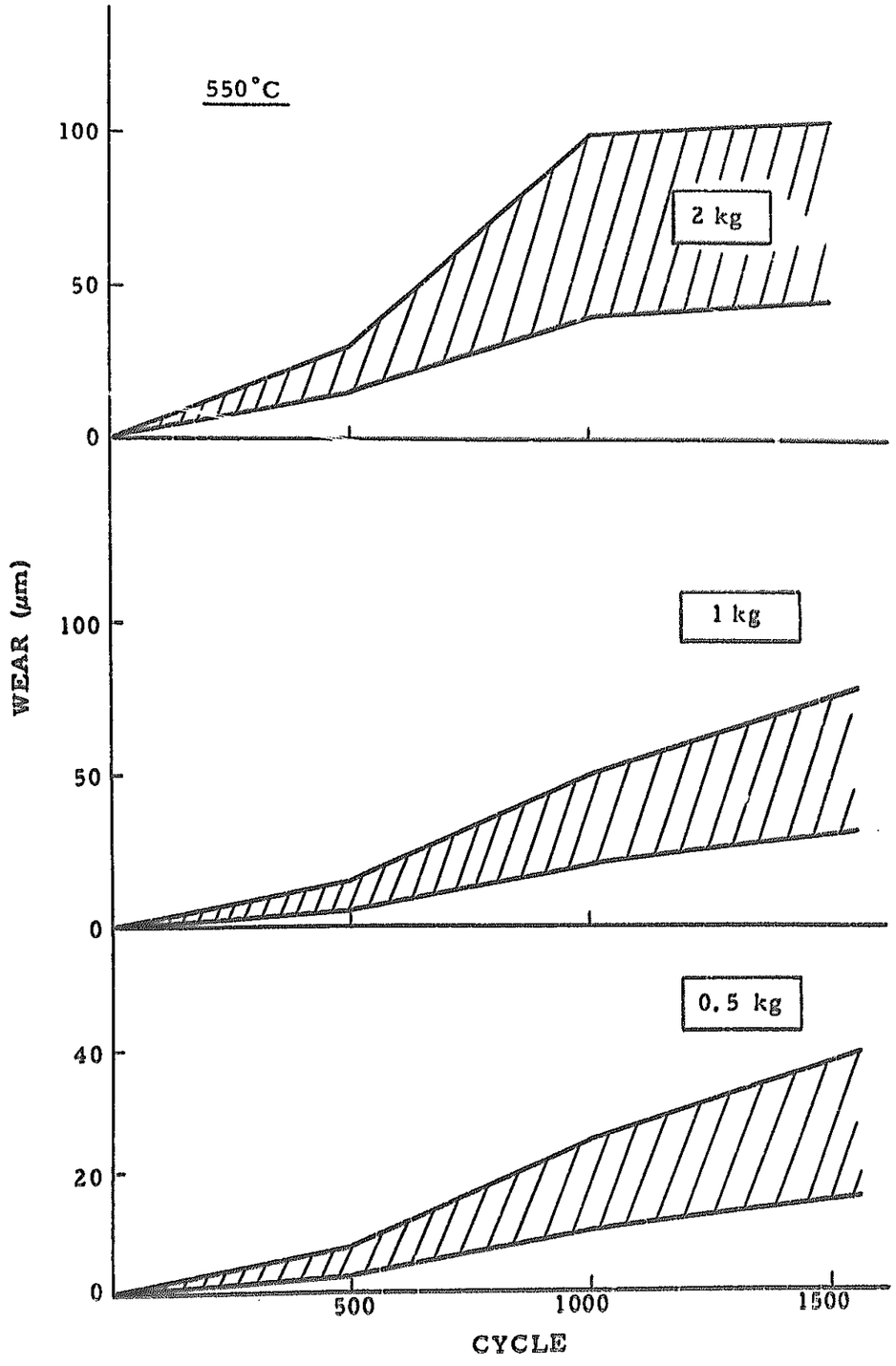

Fig. 7.2 Available data of cladding wear at 550°C.

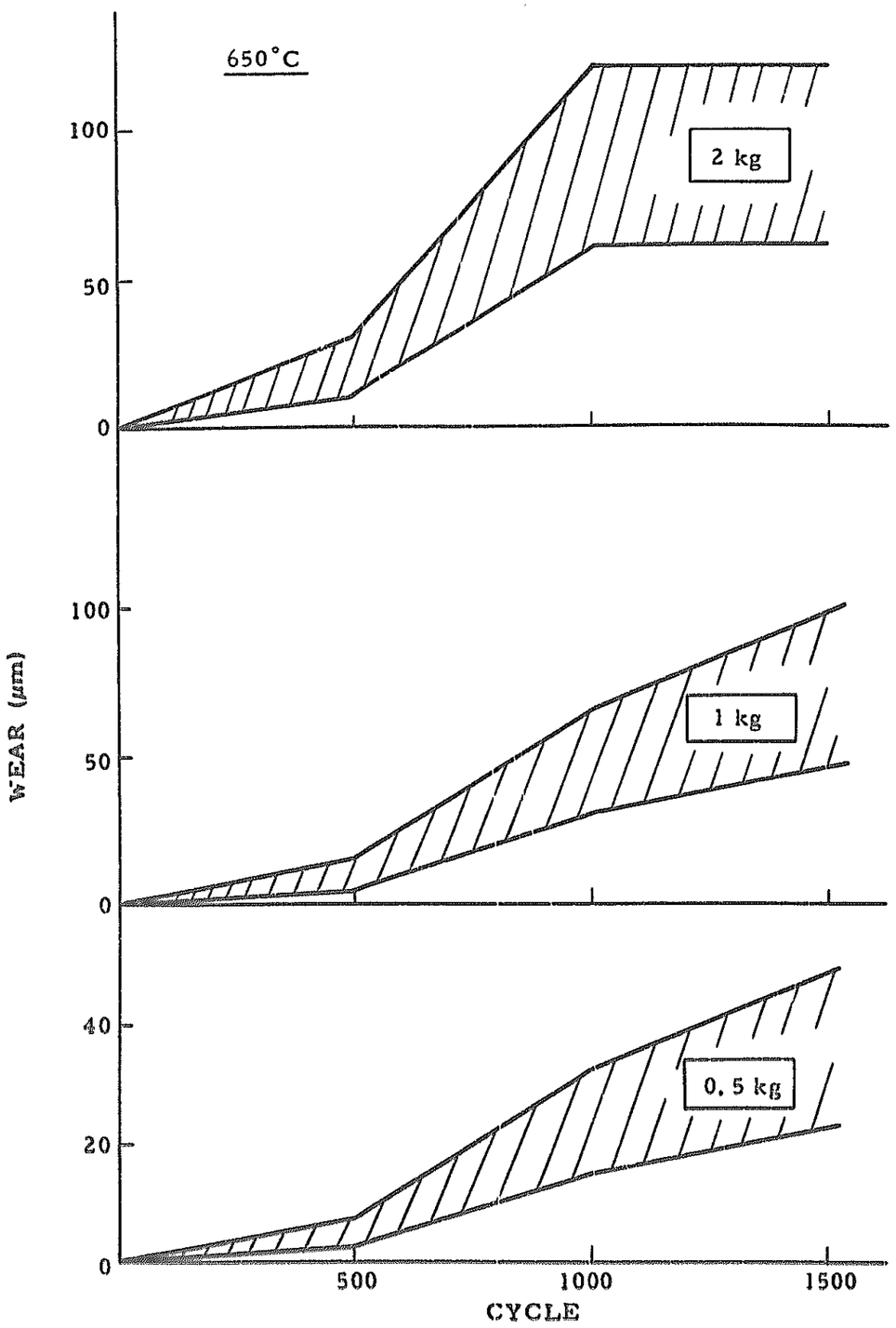

Fig. 7.3 Available data of cladding wear at 650°C.

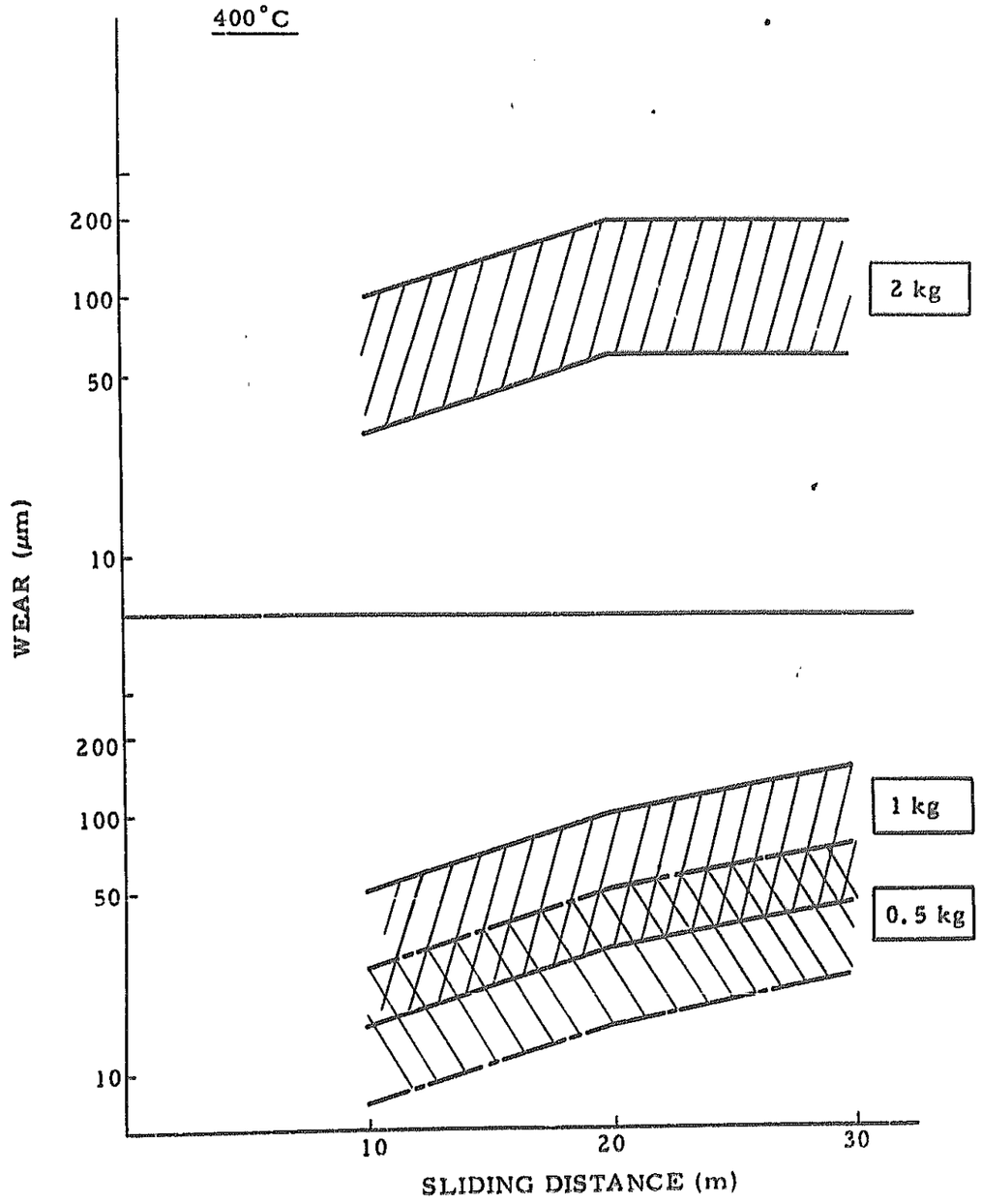

Fig. 7.4 Available data of grid wear at 400°C.

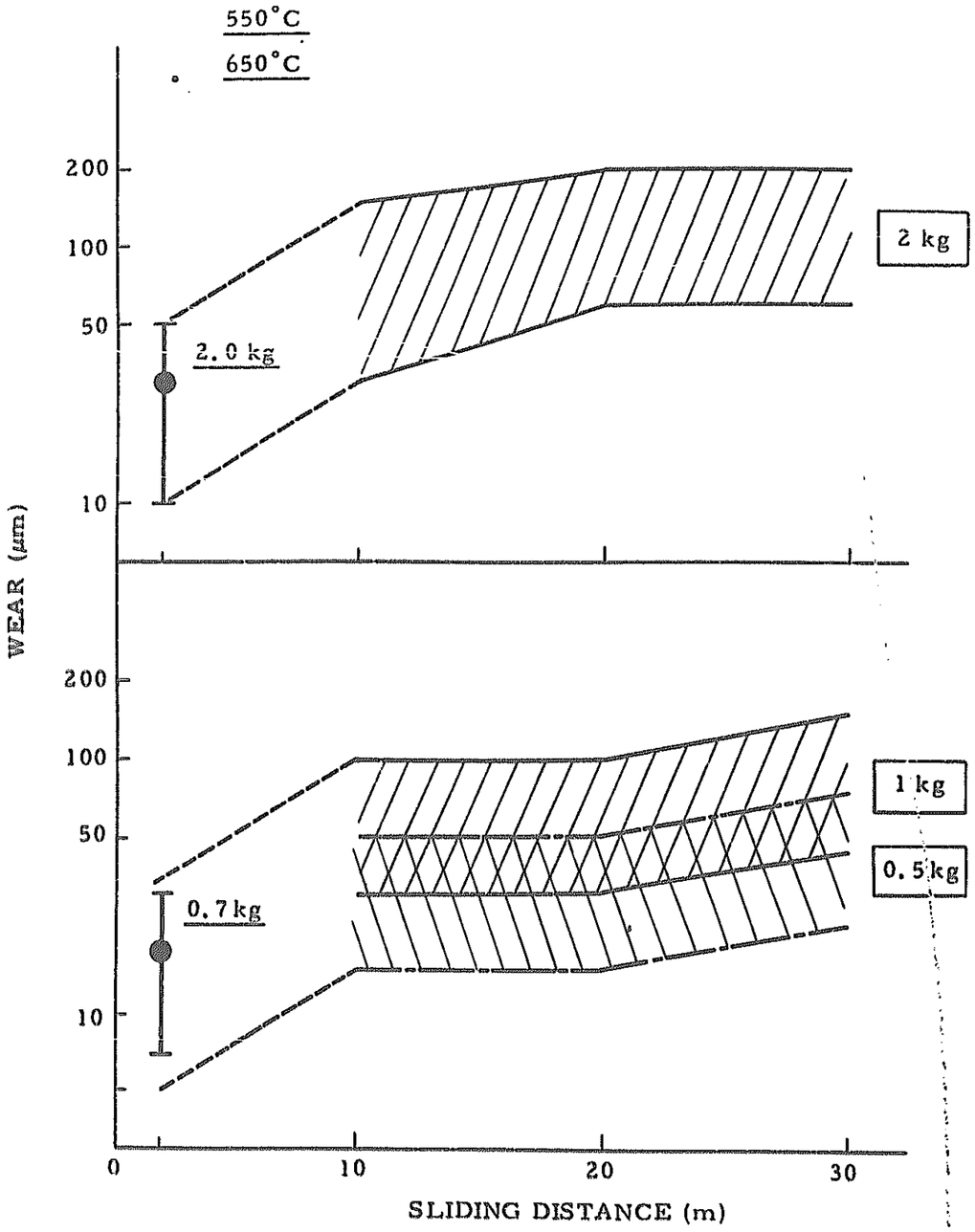

Fig. 7.5 Available data of grid wear at 550°C and 650°C.

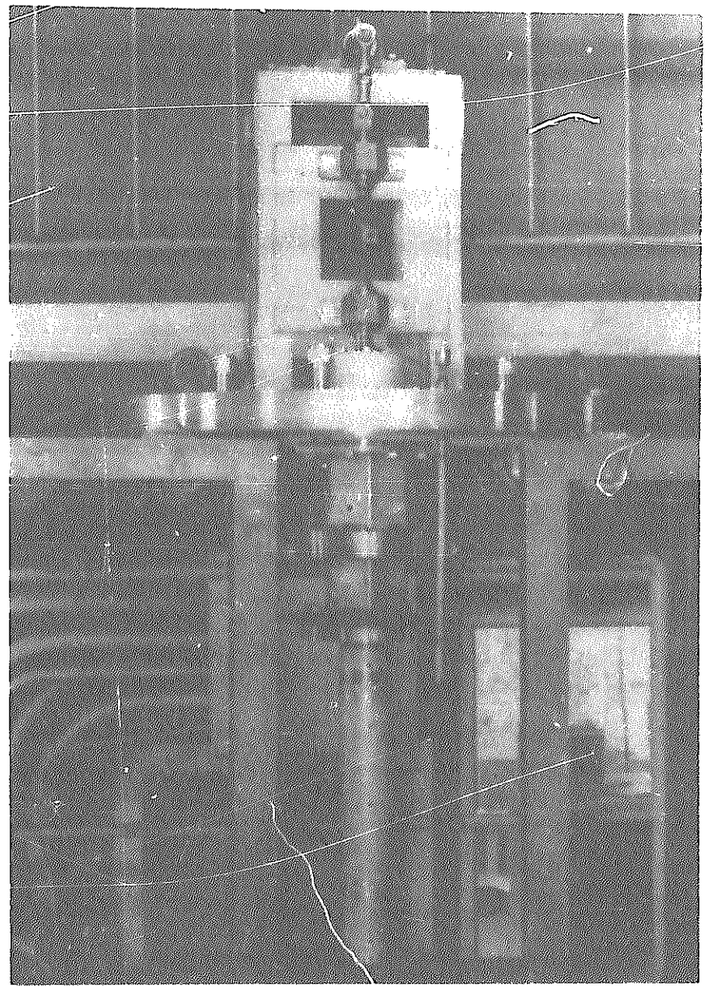

Photo 1 Overview of the apparatus and test section

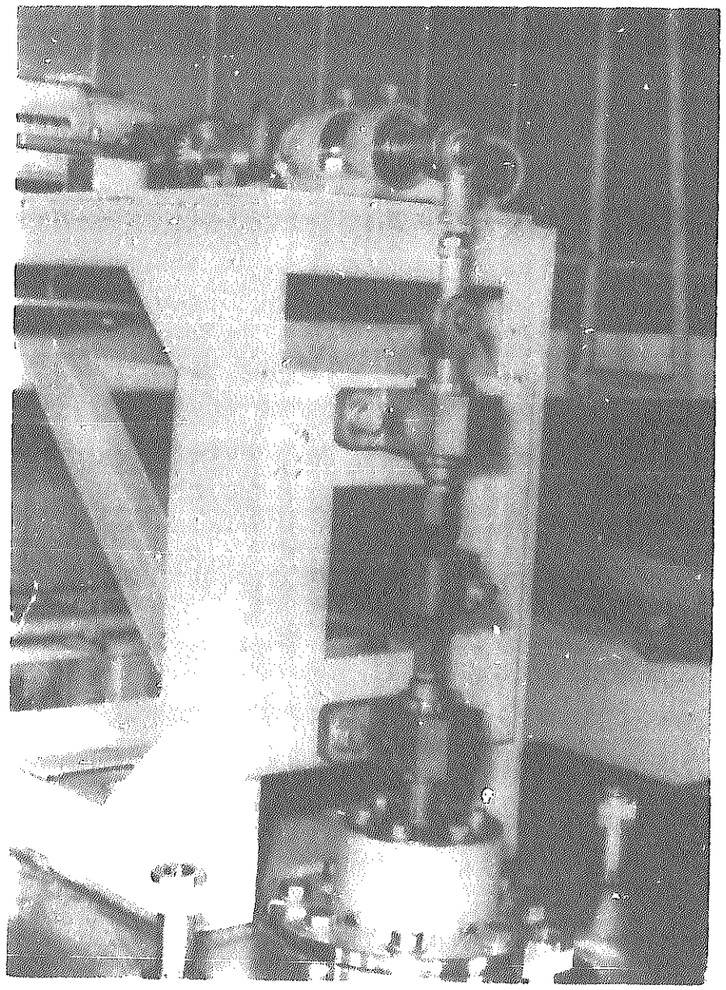

Photo 2 Driving mechanism and load cell

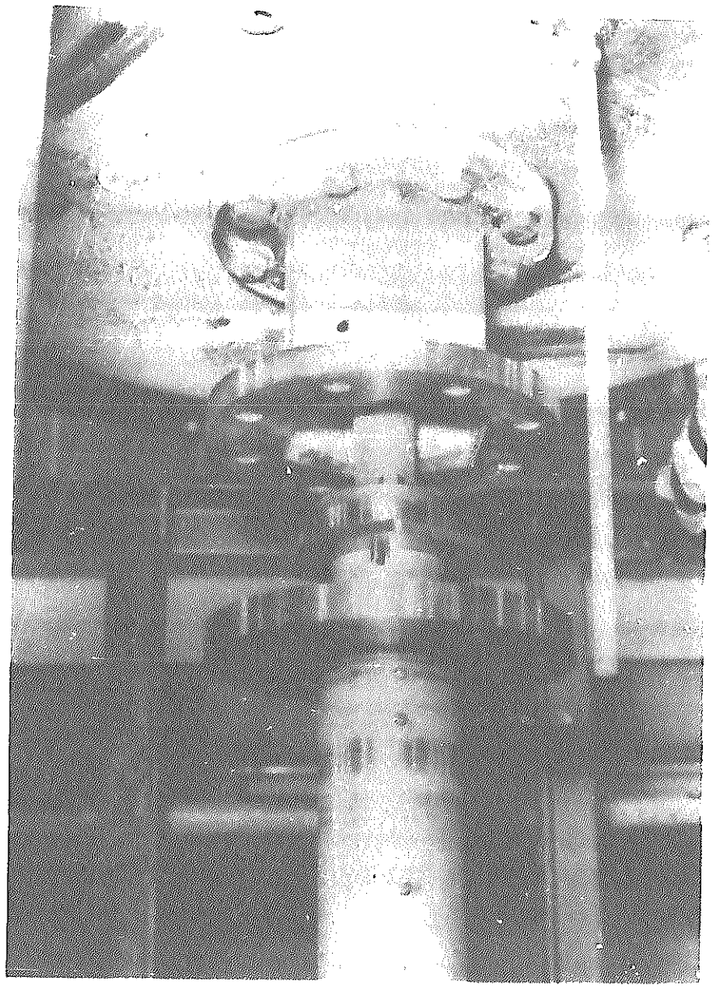

Photo 3 Connection of the test section and the driving shaft

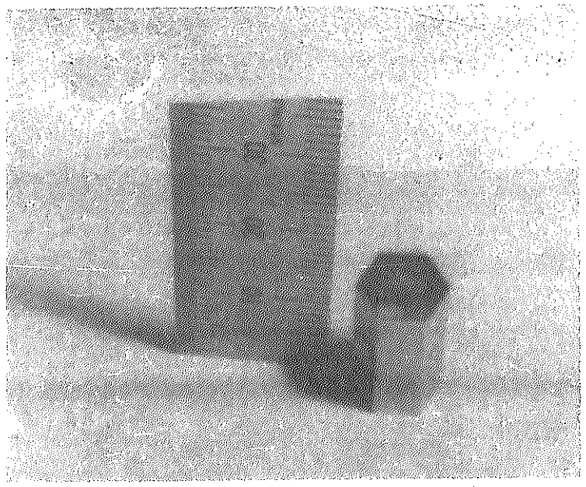

Photo 4 Grid element (MAPI honeycomb type)

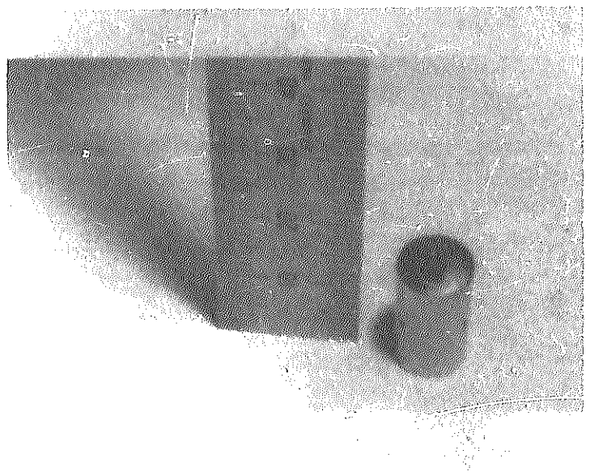

Photo 5 Grid element (MAPI ring type)

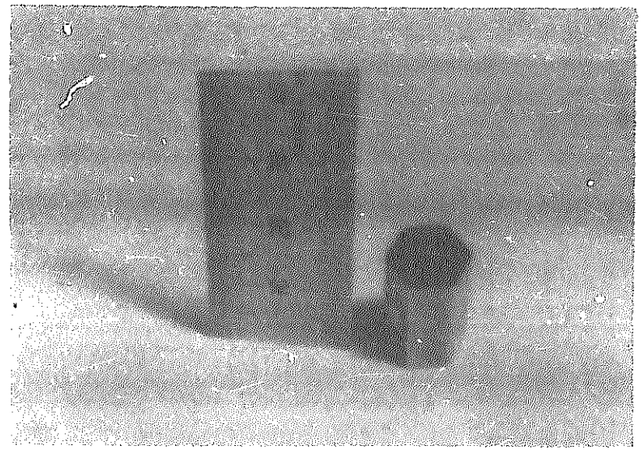

Photo 6 Grid element (Toshiba honeycomb type-elliptical dimple)

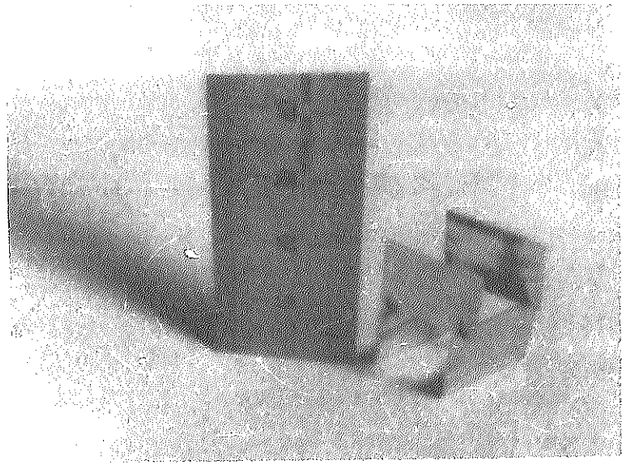

Photo 7 Grid element (Toshiba wave beam type)

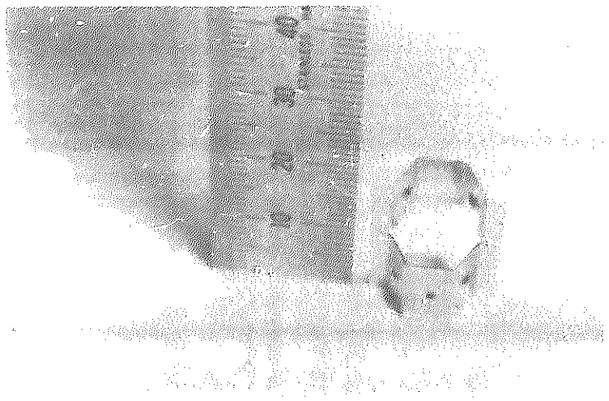

Photo 8 Grid element (Toshiba honeycomb type)

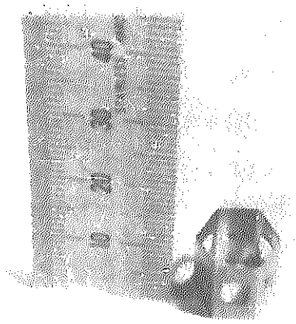

Photo 9 Grid element (NFI honeycomb type)

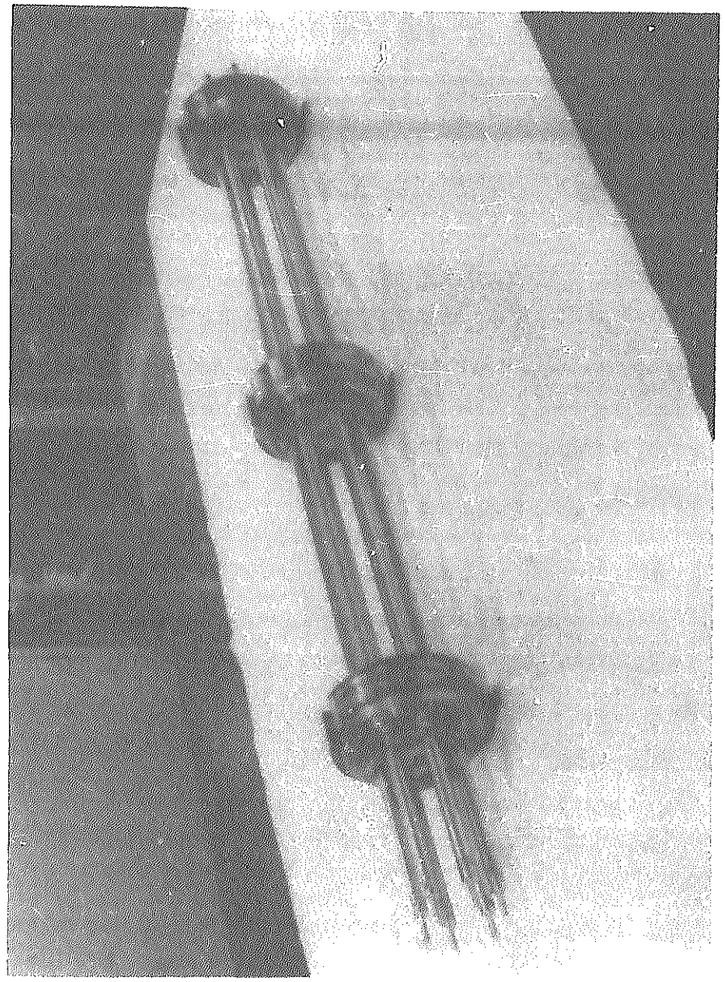

Photo 10 Structure of the test section (grid element test)

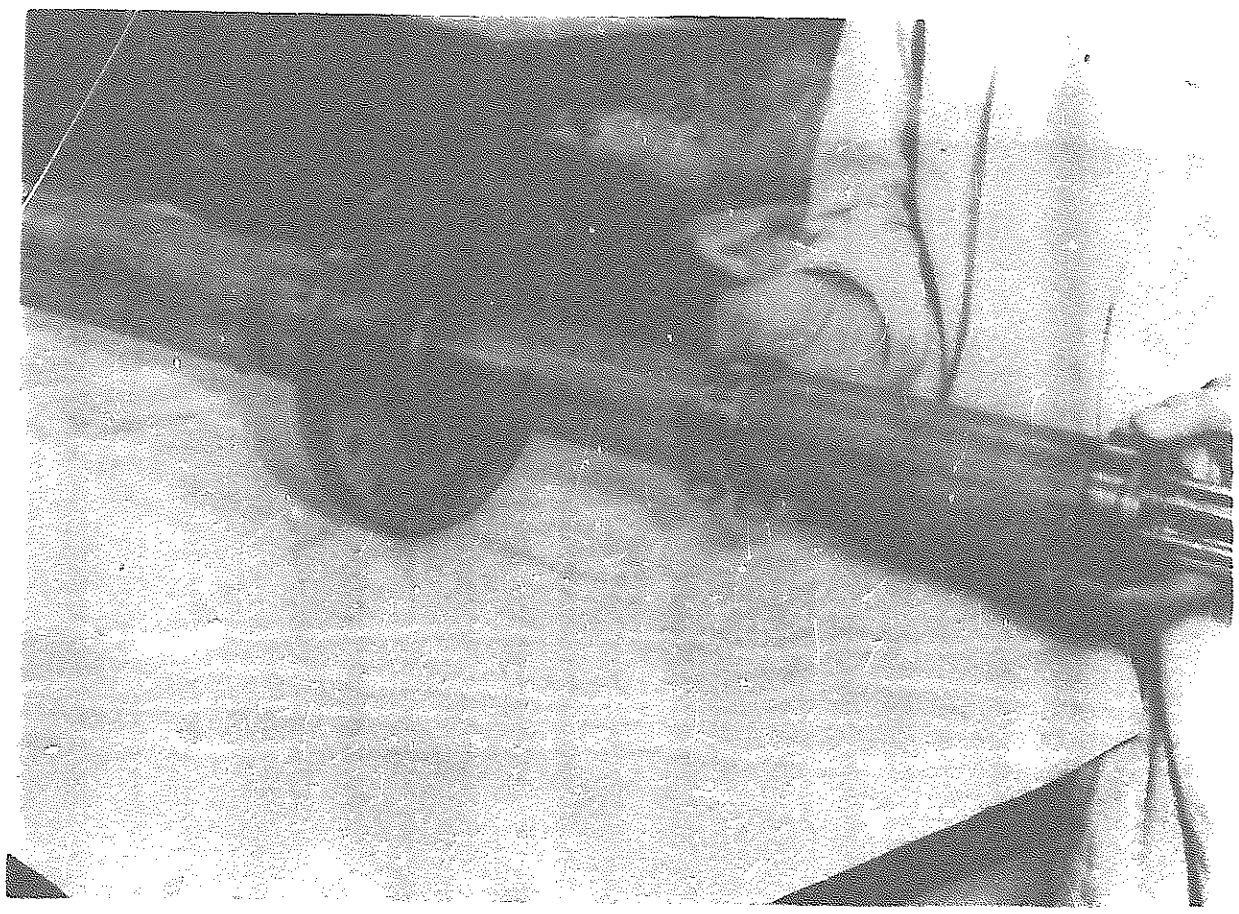

Photo 11 Assembly of the test section (grid element test)

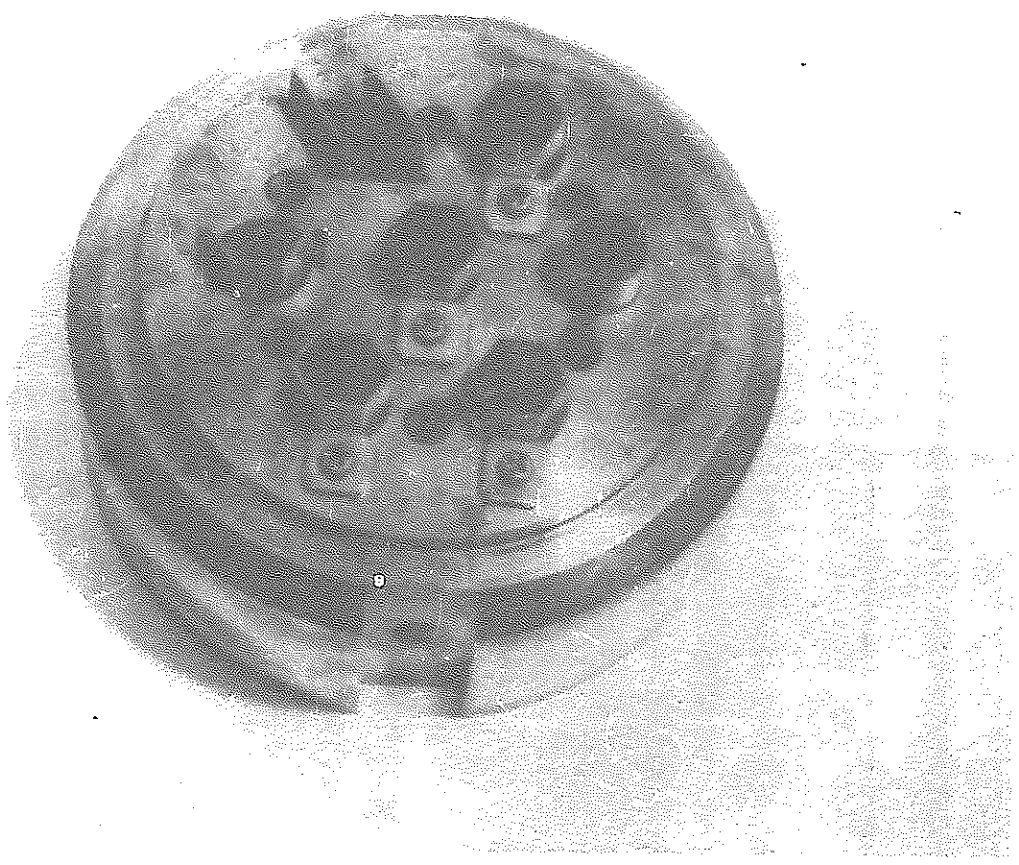

Photo 12 Grid element support (1)

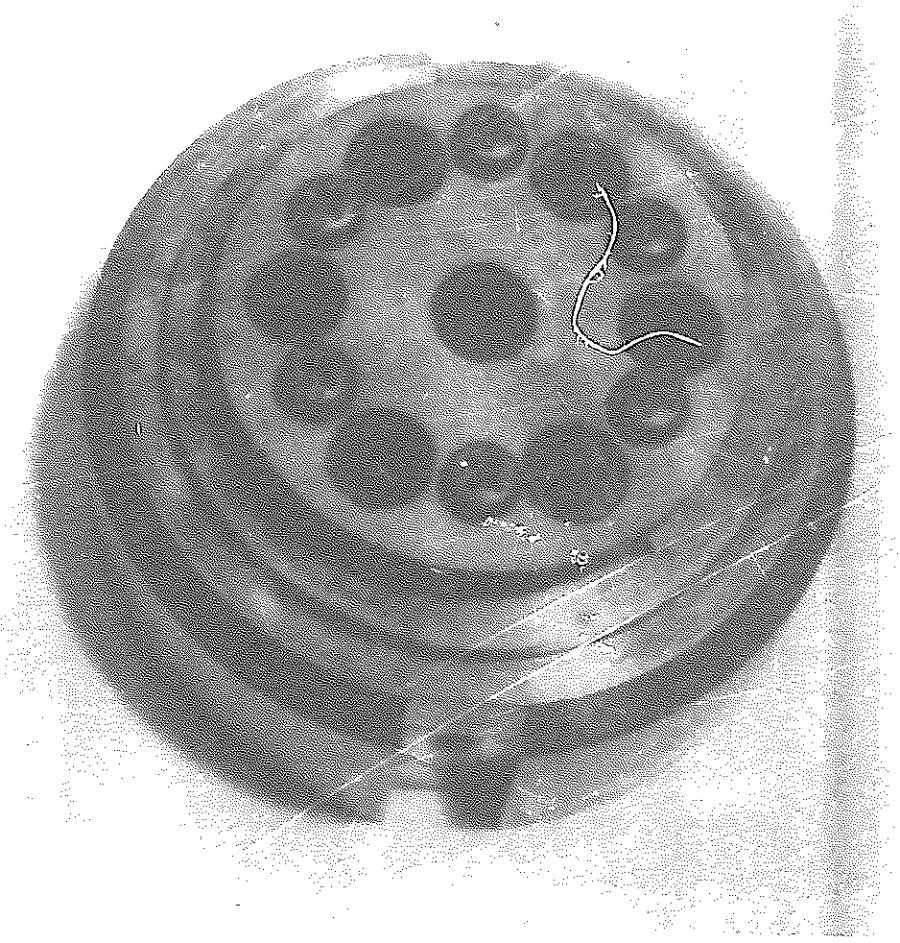

Photo 13 Grid element support (2)

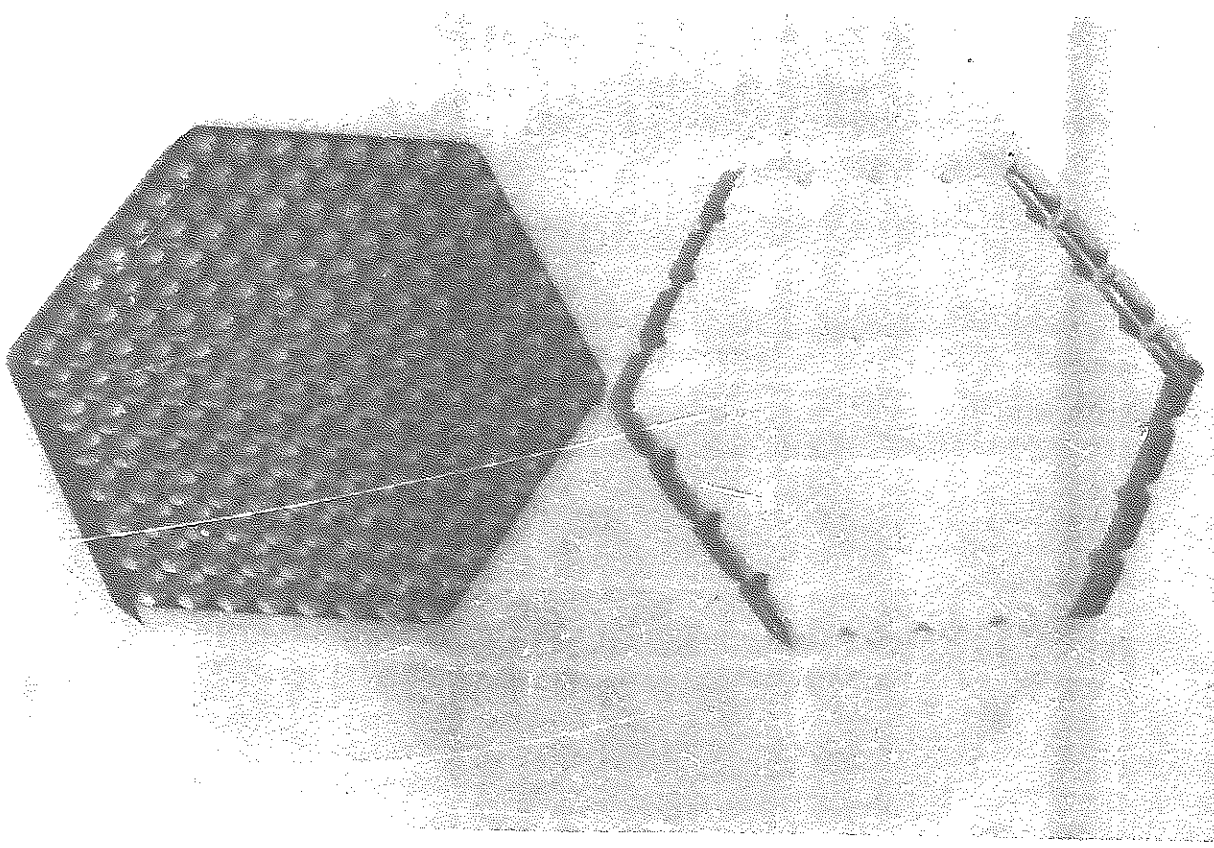

Photo 14 MAPI ring type grid spacer

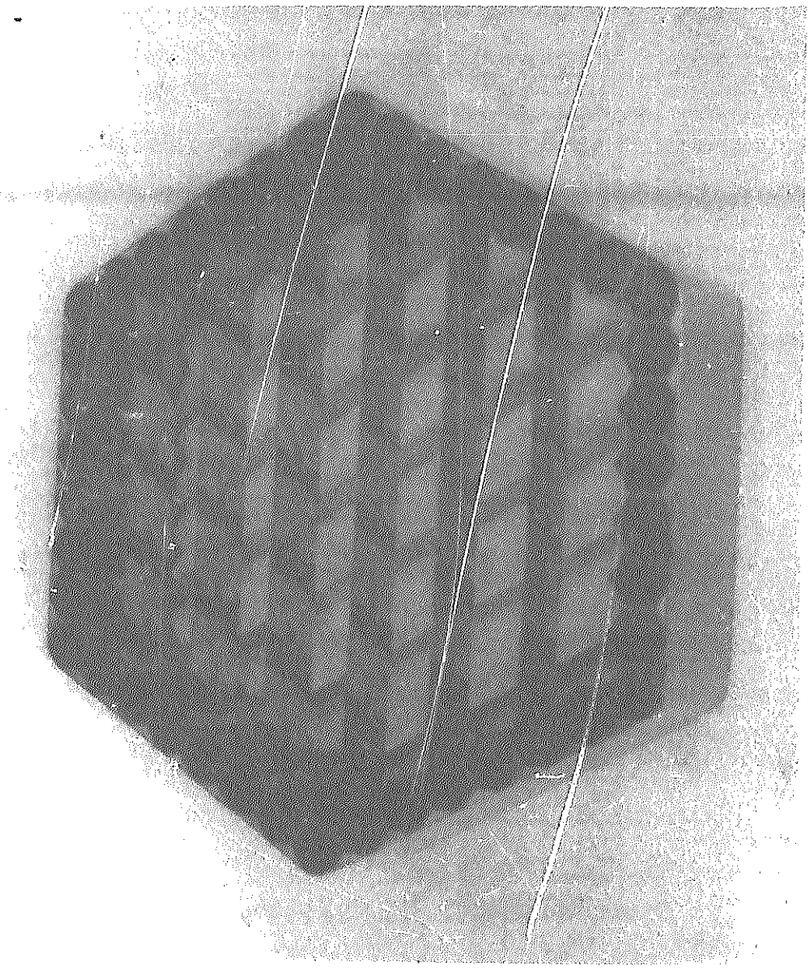

Photo 15 Toshiba honeycomb-rohmbus composed type grid spacer

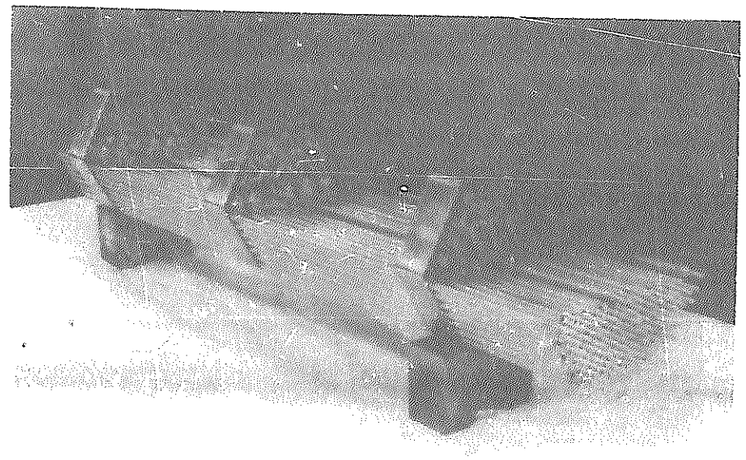

Photo 16 Assembly of the test section (bundle test) (1)

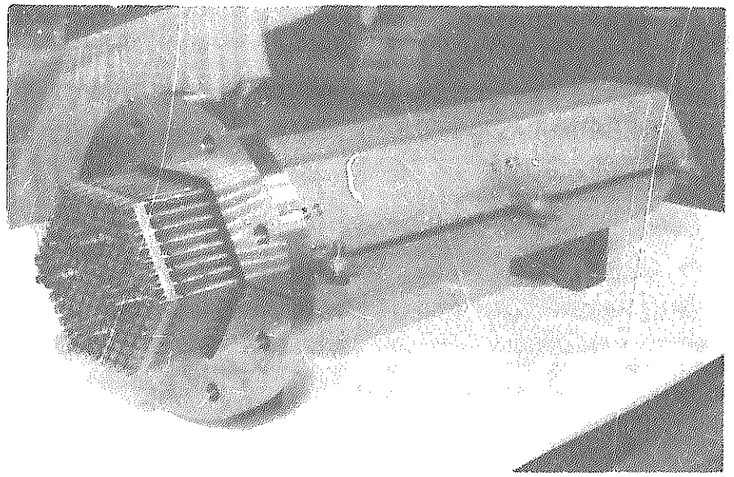

Photo 17 Assembly of the test section (bundle test) (2)

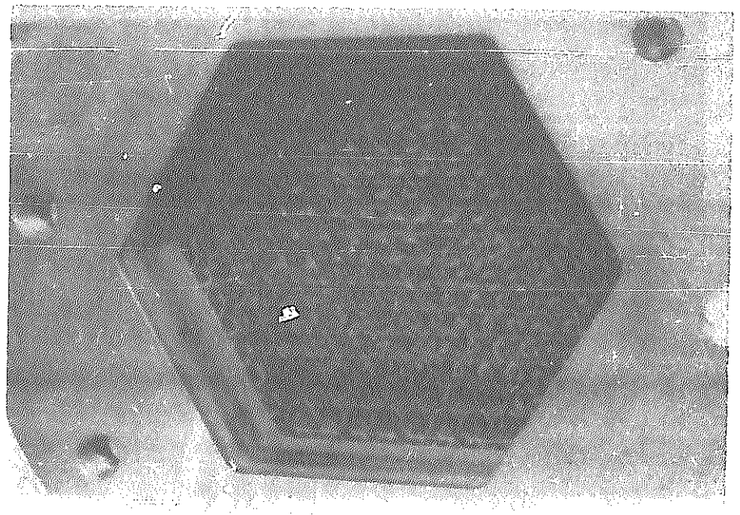

Photo 18 Grid spacer support (MAPI ring type grid spacer)

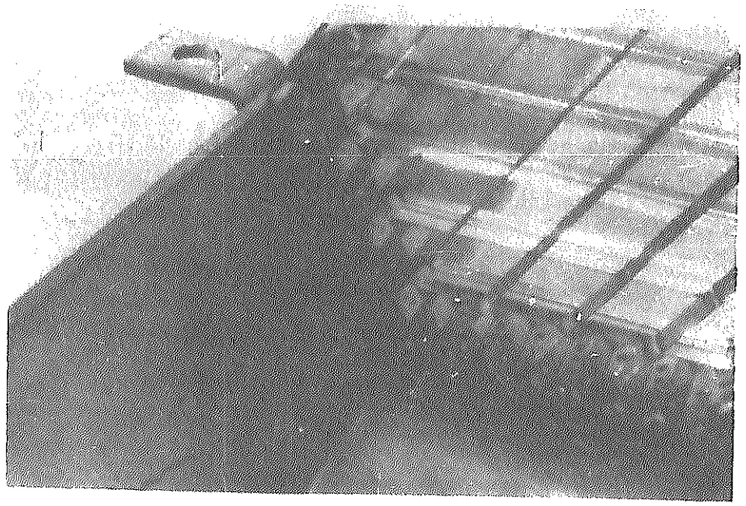

Photo 19 Grid spacer support (Toshiba honeycomb-rohmbus composed type grid spacer)

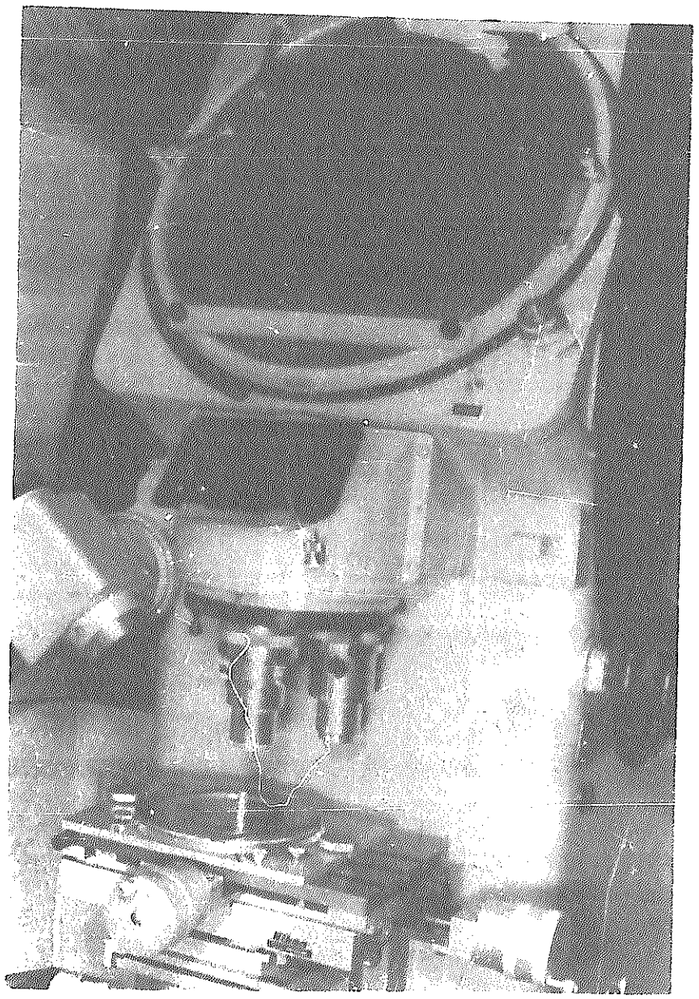

Photo 20 Measurement of wear for grid element

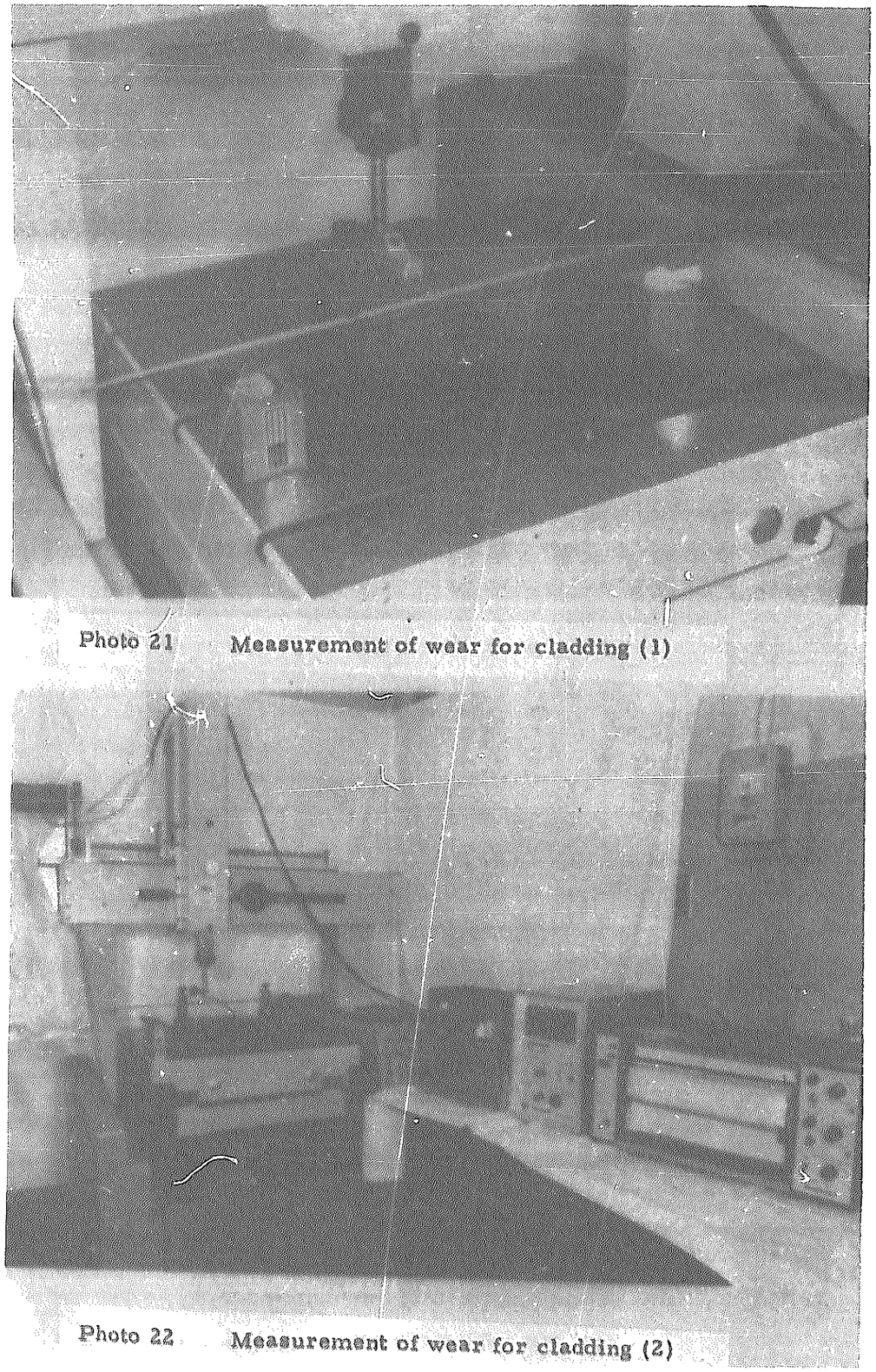

Photo 21 Measurement of wear for cladding (1)

Photo 22 Measurement of wear for cladding (2)

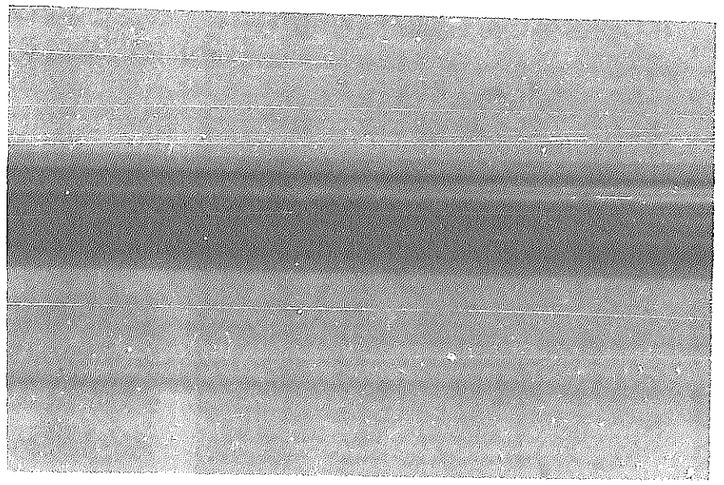

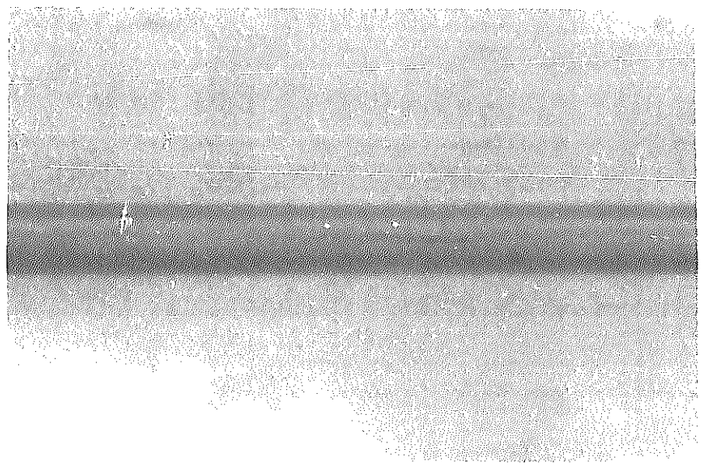

Photo 23 Macroscopic observation at cladding surface after galling test

Condition;
load 2.7 kg
Na temp.
400 °C
1000 cycle
wear ~130 μm

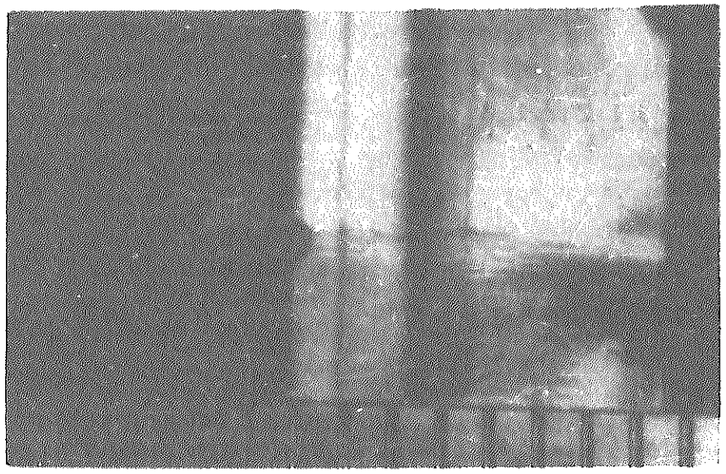

Condition;
load 2.0 kg
Na temp
650 °C
1500 cycle

Photo 24 Macroscopic observation at grid surface after galling test

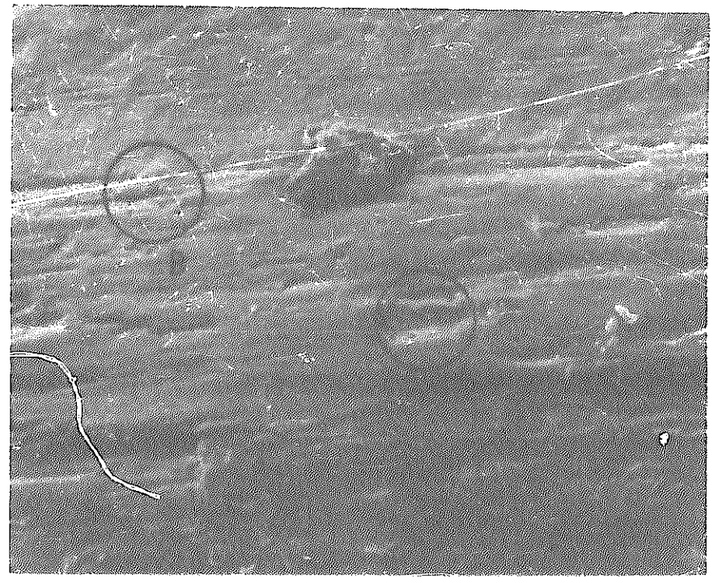

×100

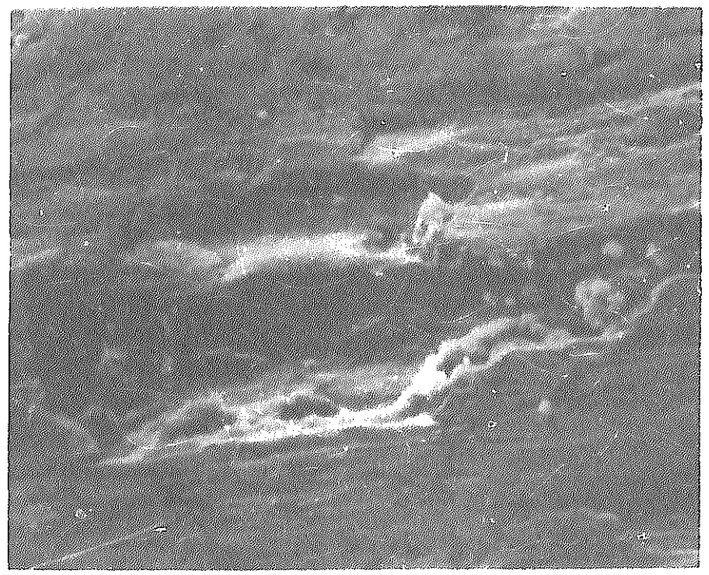

Condition;
load 1.0 kg
Na temp. 400 °C
1500 cycle
wear ~ 50 μm
TOSHIBA elliptical dimple

part A × 500

Photo 25 S.E.M. observation at grid surface after galling test

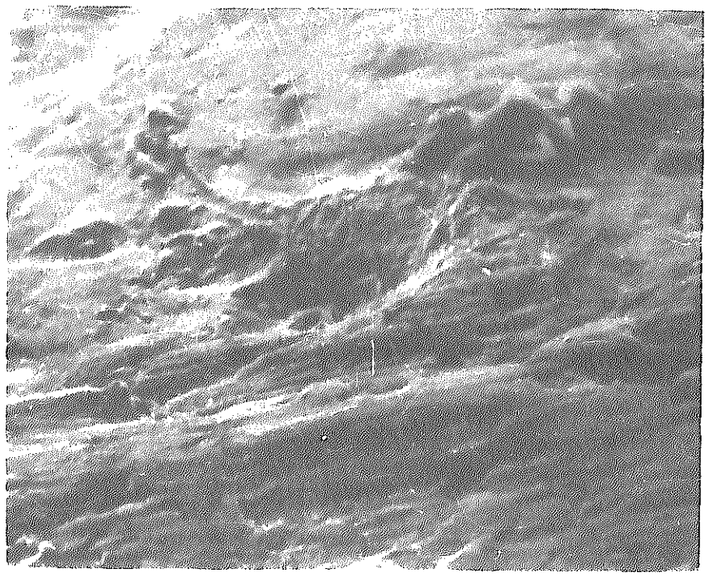

× 500

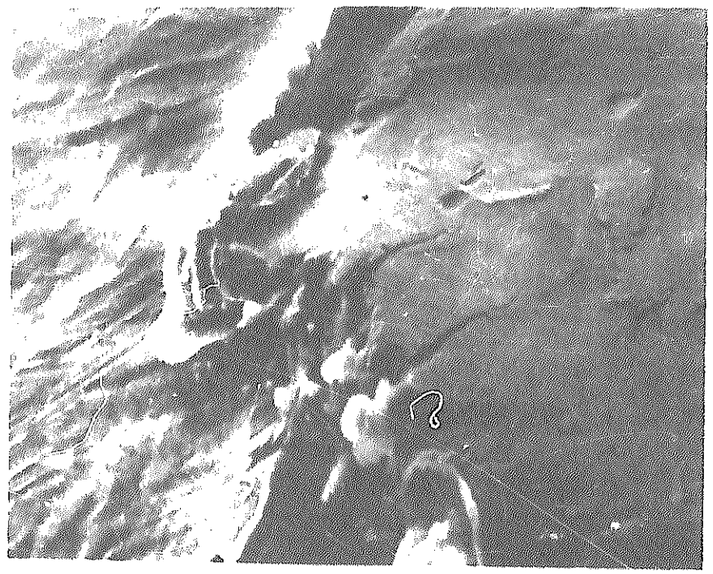

× 500

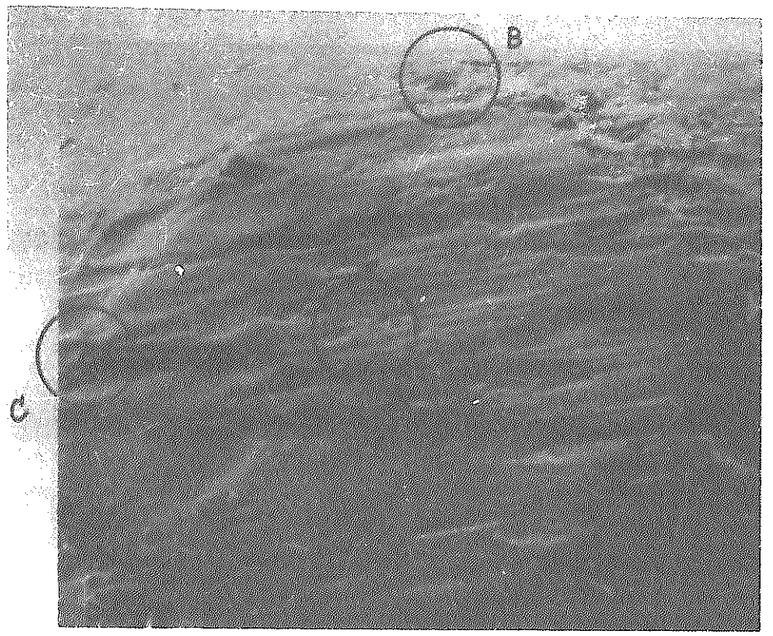

×100

part A

× 500

Condition :
load 1.0 kg
Na temp. 400°C
1500 cycle
wear ~ 50 μm
MAPI : hemp cond

Photo 26 S. E. M. observation at grid surface after galling test

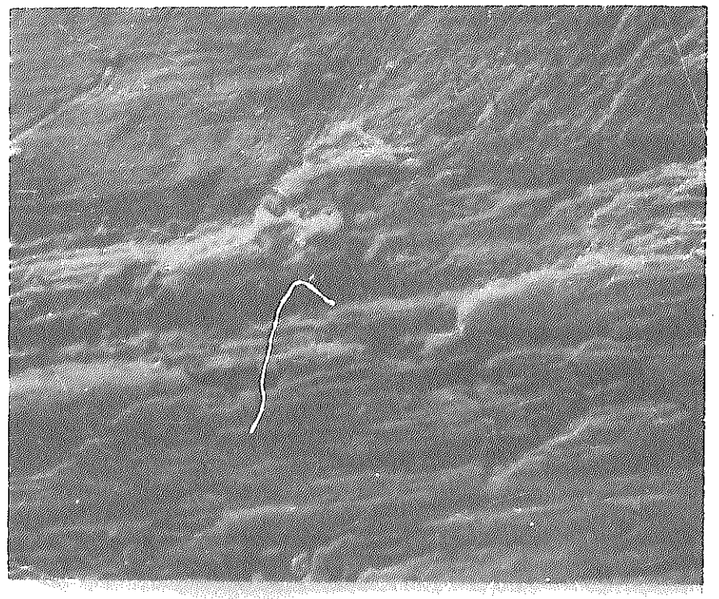

part B ×500

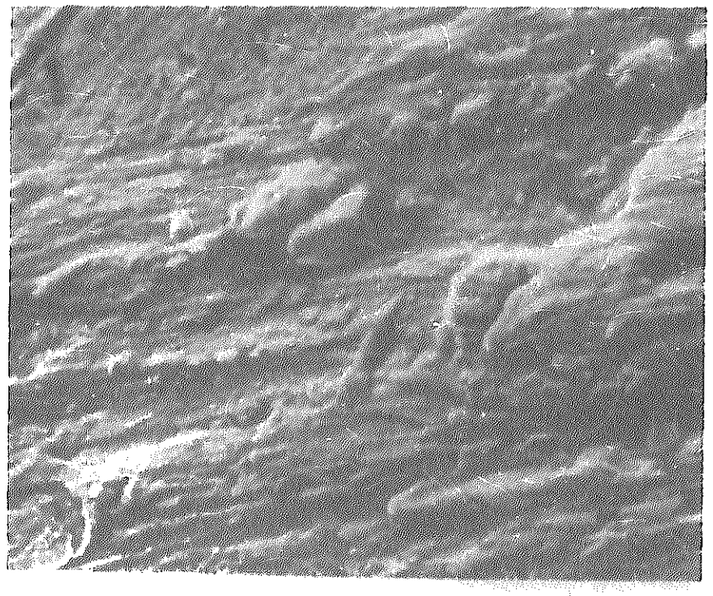

part C ×500

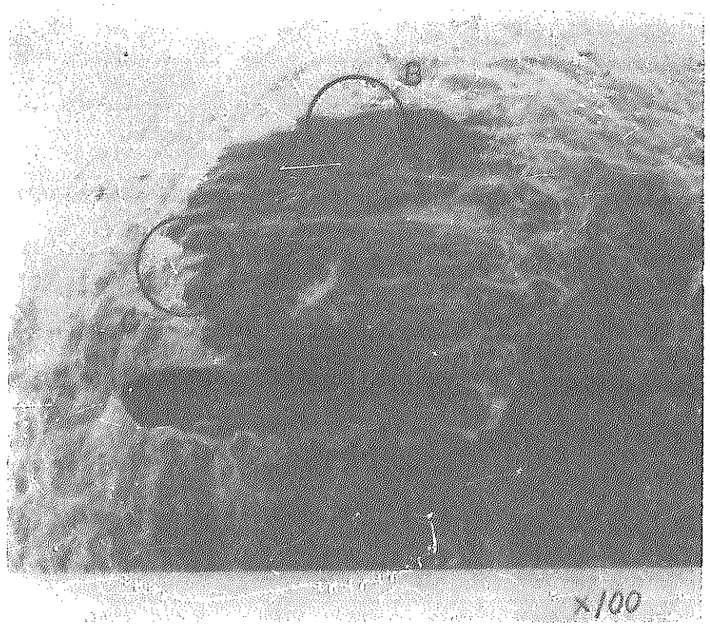

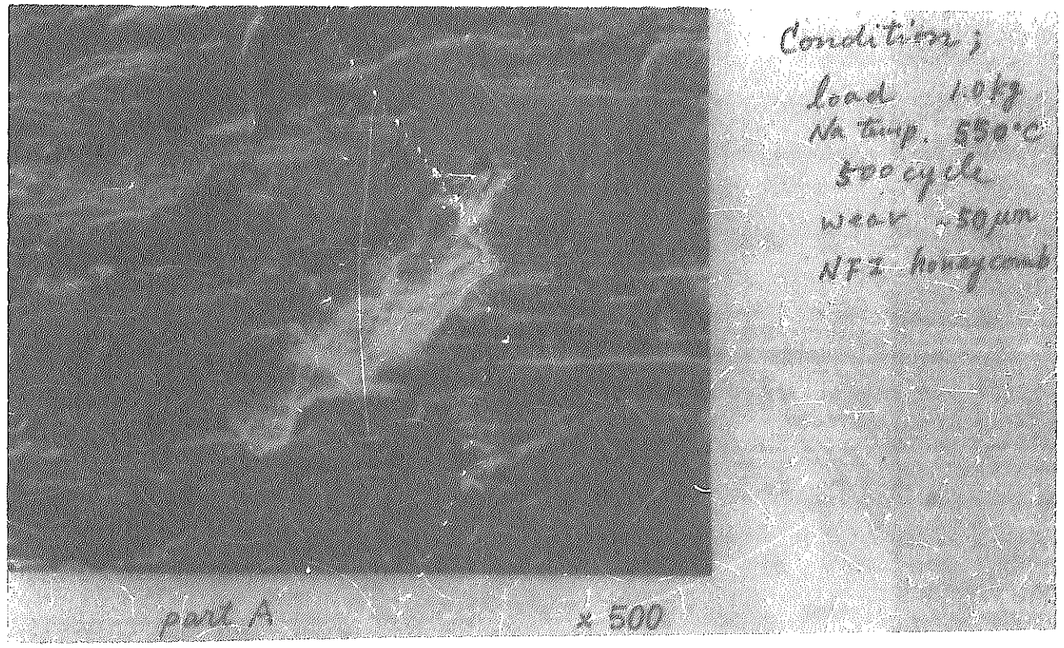

Photo 27 S. E. M. observation at grid surface after galling test

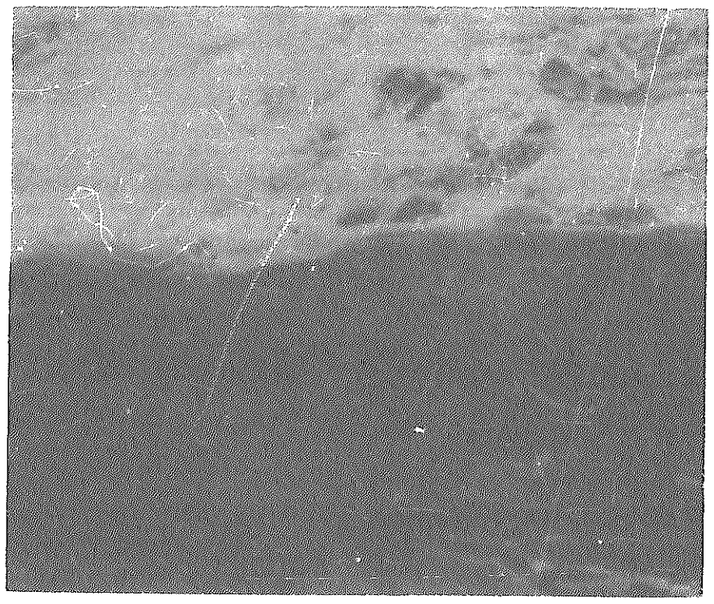

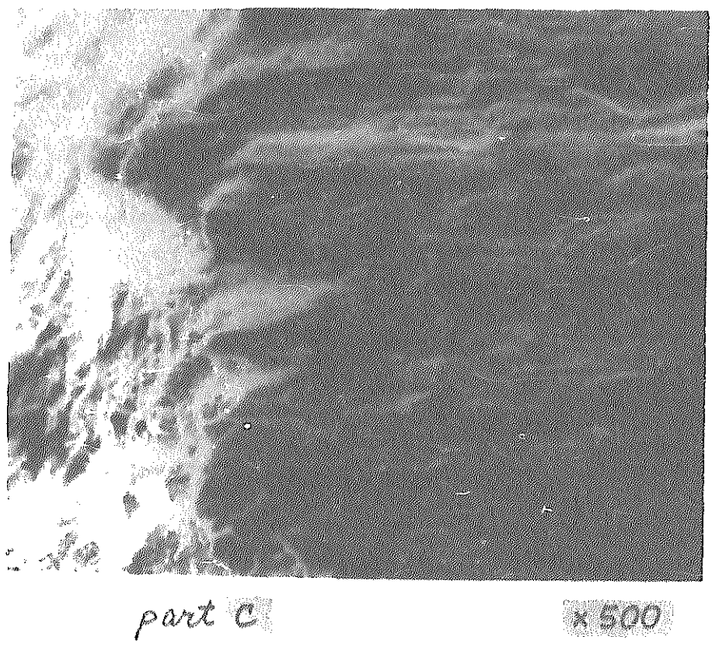

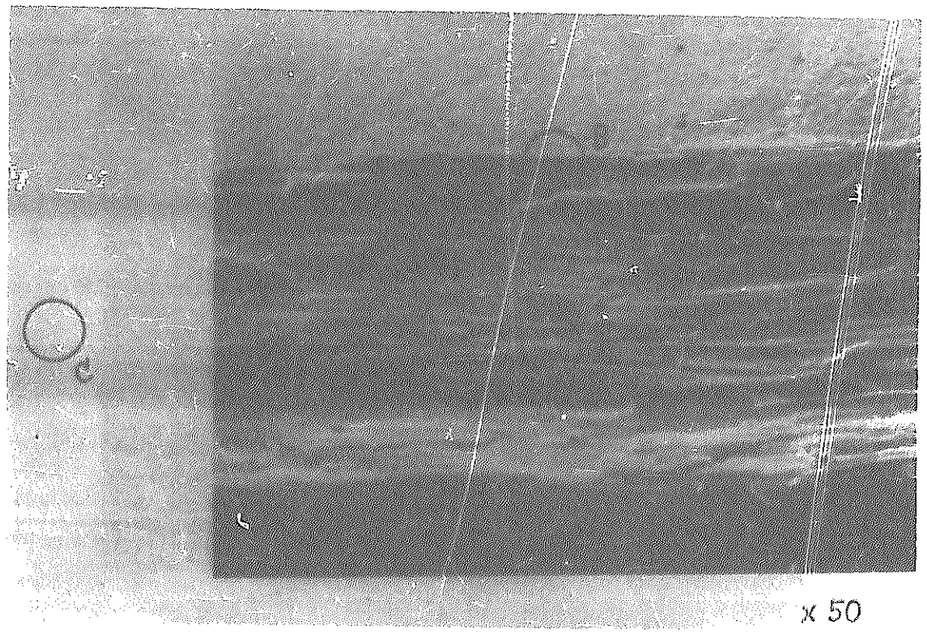

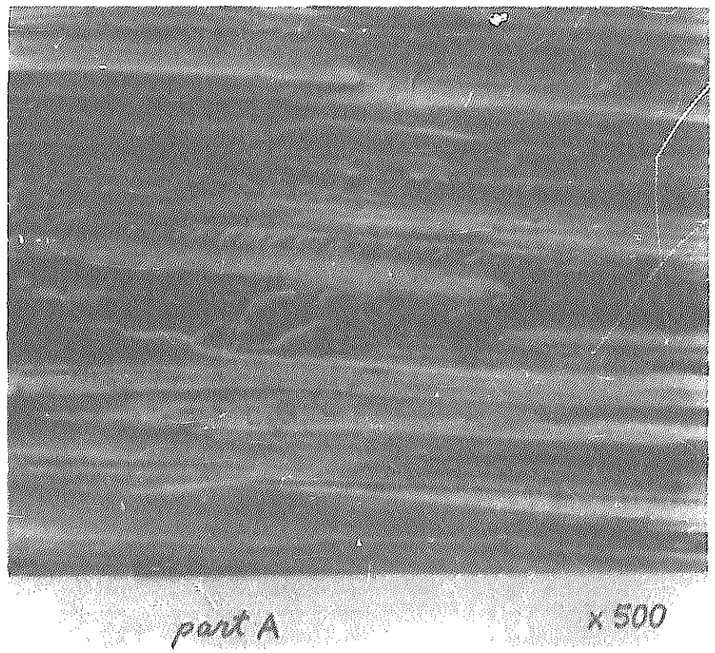

Photo 28 S.E.M. observation at cladding surface after galling test

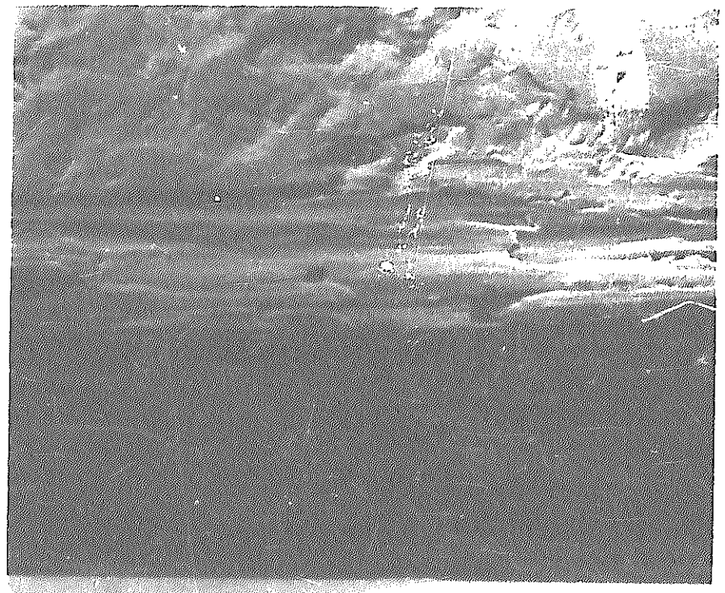

part B

× 500

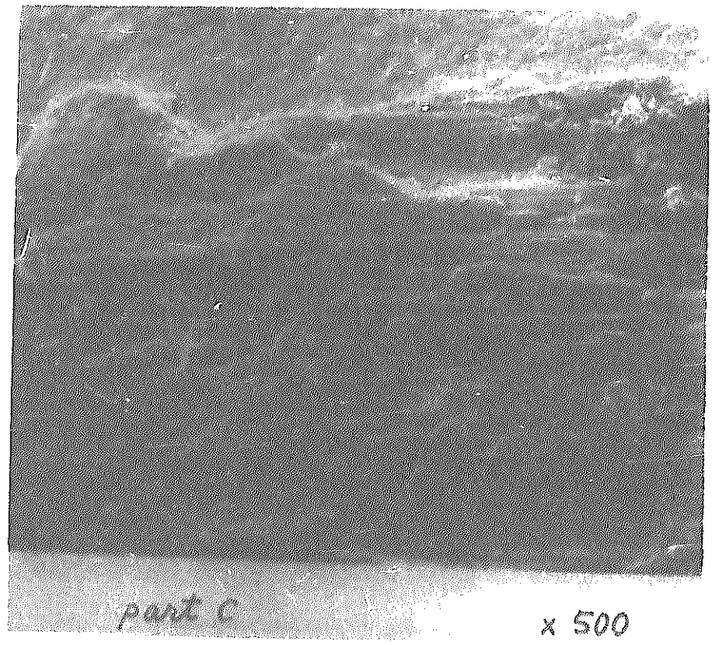

part C

× 500

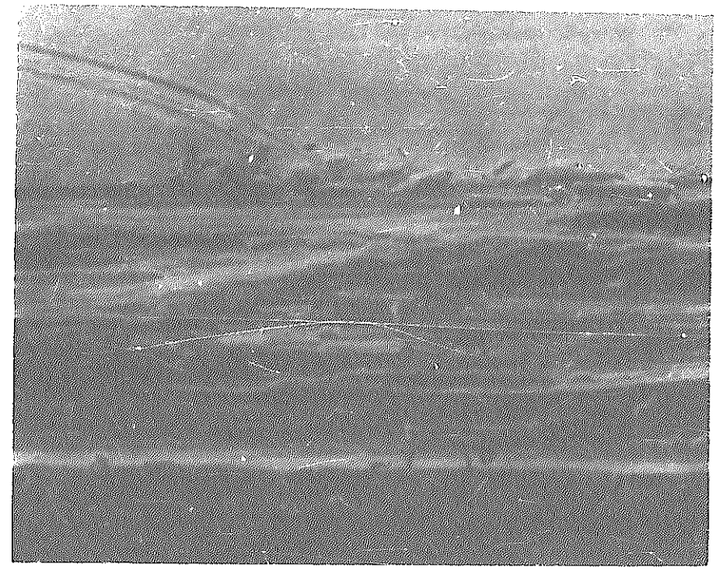

C

× 50

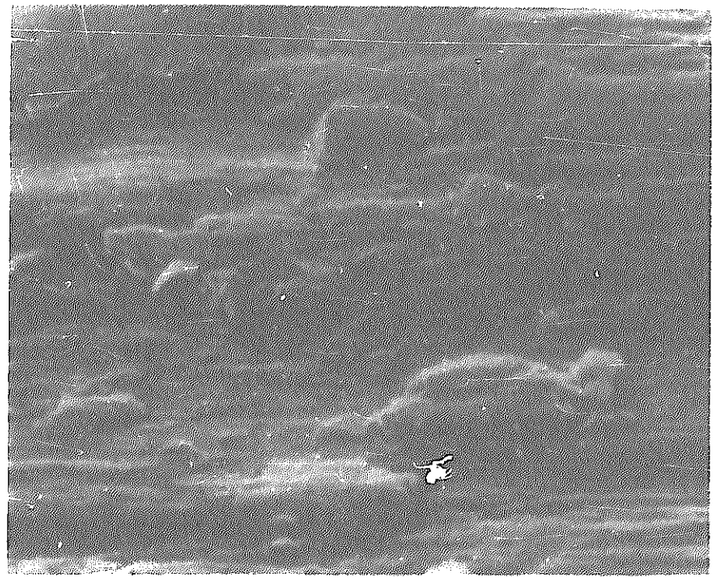

Condition ;
load 2.0kg
Na temp. 400°C
2000 cycle
wear ~25μm
TOSHIBA wave beam

part A

× 500

Photo 29 S. E. M. observation at cladding surface after galling test

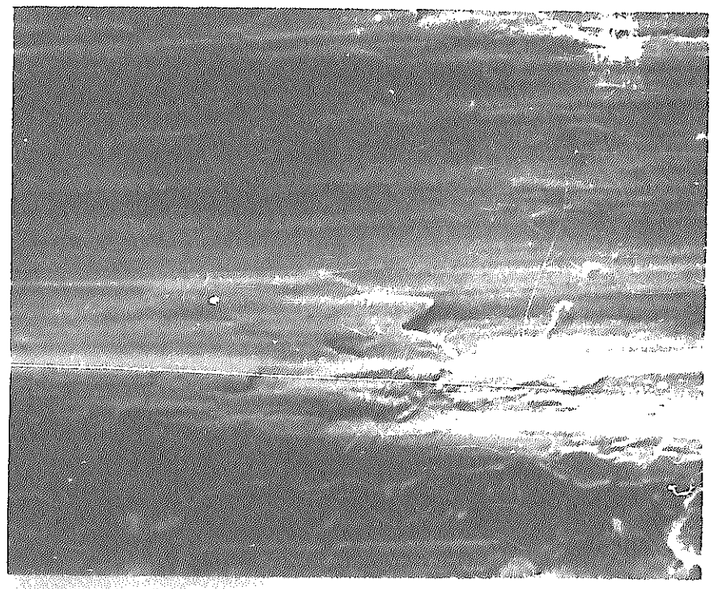

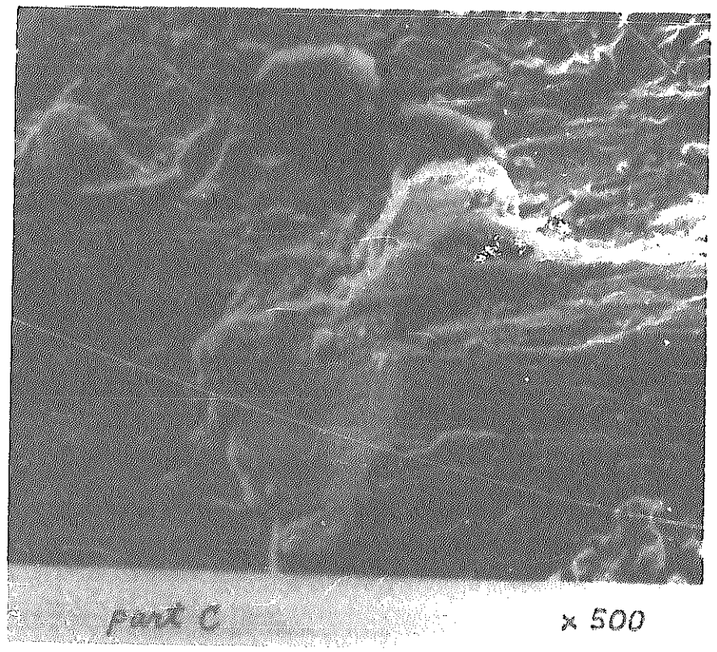

C

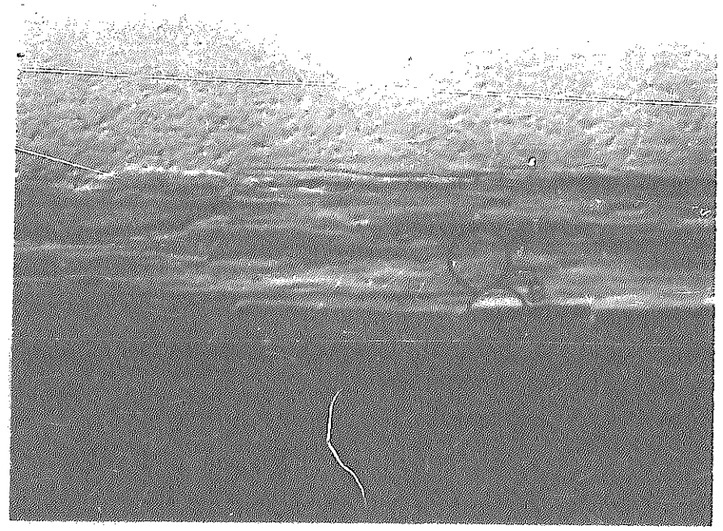

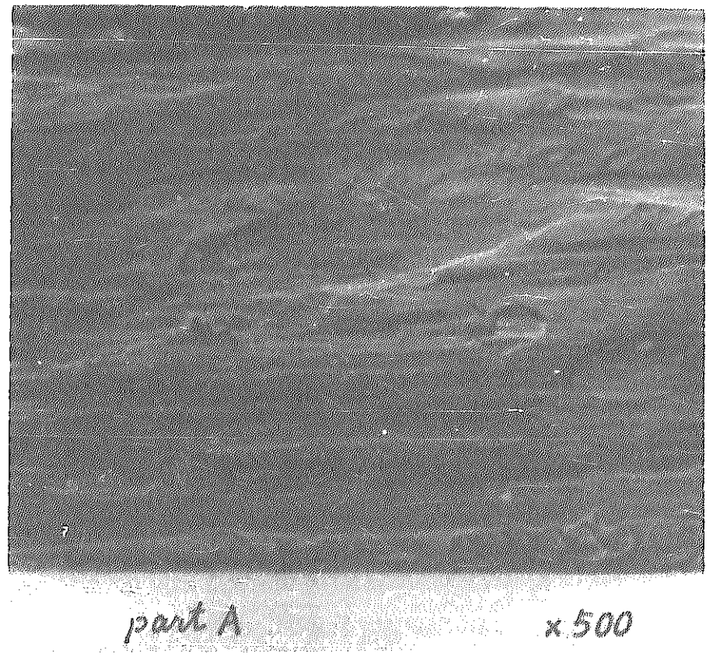

Condition ;
load 1.0 kg
Na temp. 650°C
500 cycle
wear ~5μm
NFZ honeycomb

Photo 30 S.E.M. observation at cladding surface after galling test

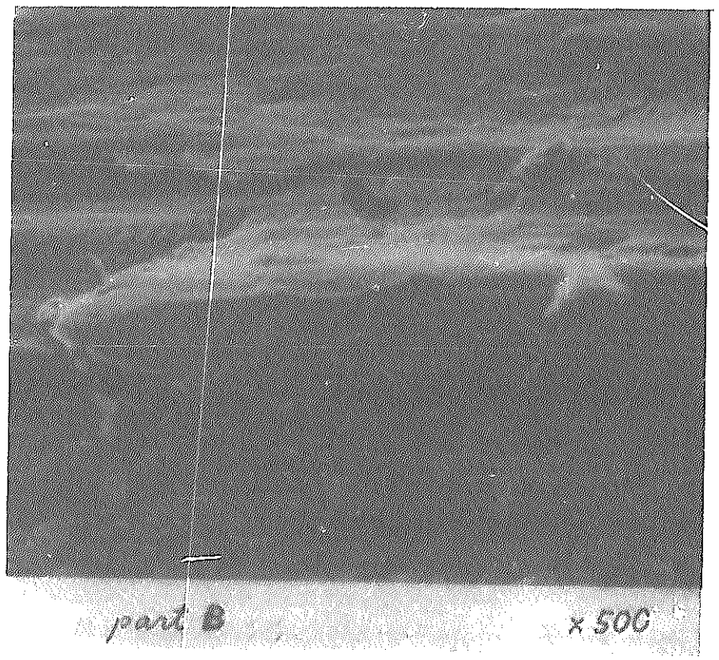

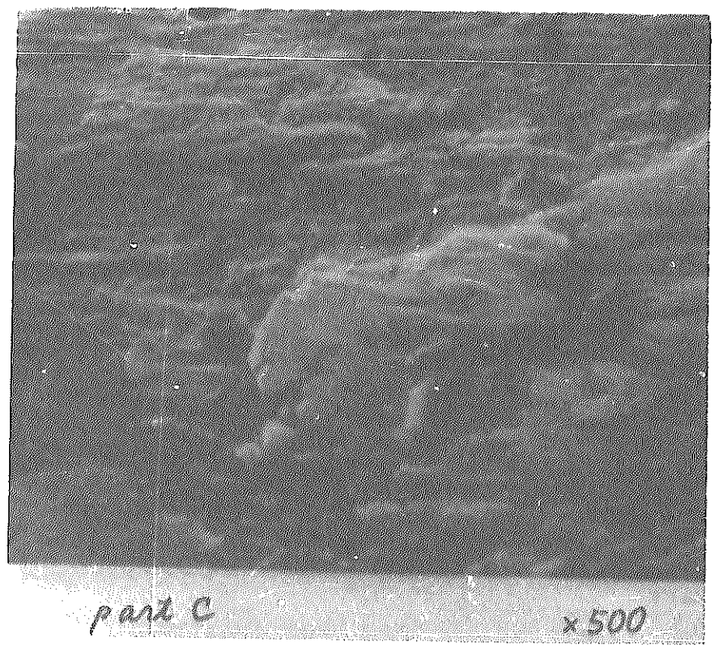

Condition ;
load 0.7 Kg
temp. 400 °C
1000 cycle
wear ~50 μm
TOSHIBA
step honeycomb

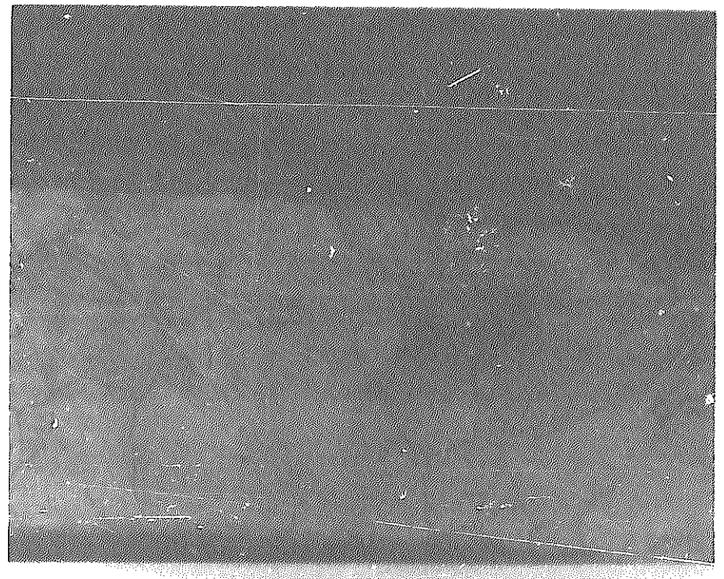

Condition ;
load 1.0 Kg
temp. 650°C
1000 cycle
wear ~80 μm
MAPI honeycomb

Photo 31 Metallographic observation of the cross section after galling test (grid element)

Condition :
load 0.7Kg
temp. 600°C
1000 cycle
wear ≈30 μm
MAPI ring type

traverse cross section x 250

Condition :
load 2.0 Kg
temp. 600 °C
1000 cycle
wear ≈30 μm
rotating
strip honeycomb

longitudinal cross section x 500

Photo 32 Metallographic observation of the cross section after galling test (cladding tube)

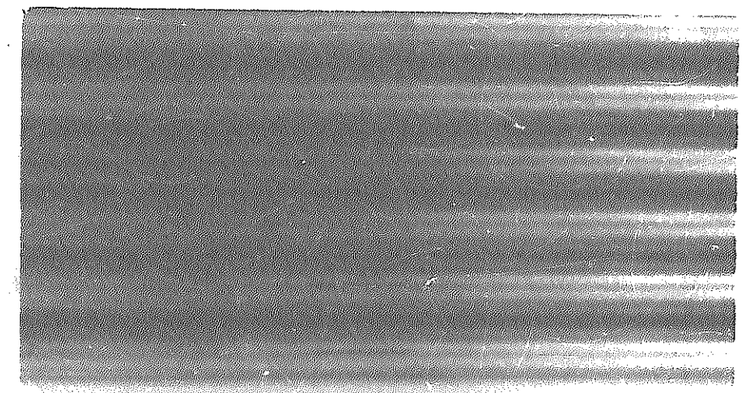

Inner Fuel Pin

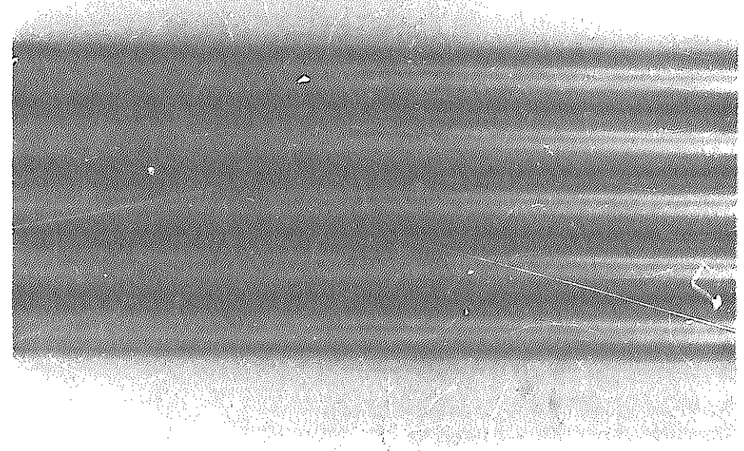

Outer Fuel Pin

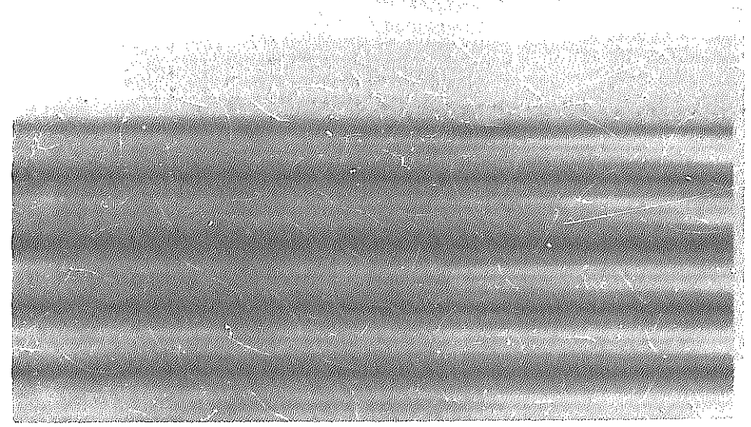

Bowed Fuel Pin

Photo 33 Macroscopic observation of cladding surface after galling test (MAPI ring type)

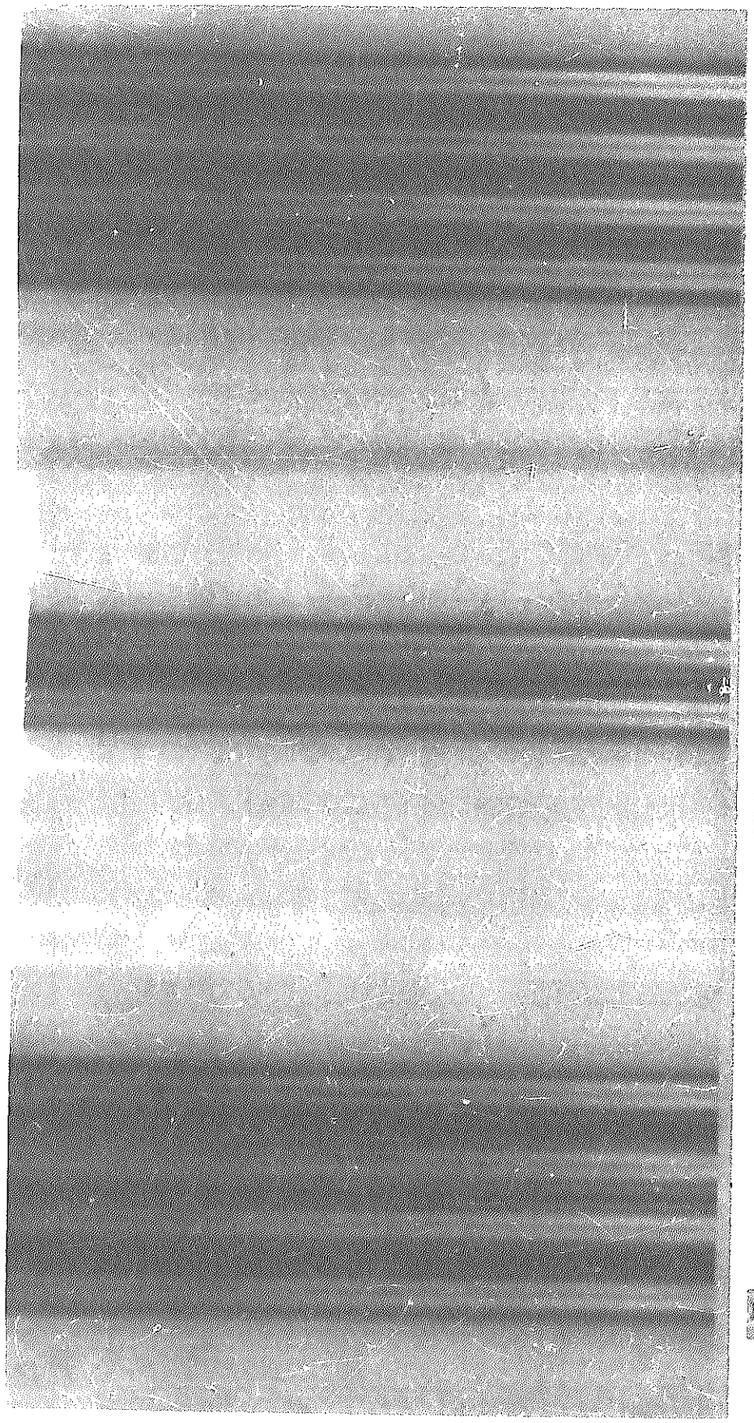

Photo 34 Macroscopic observation of cladding surface after galling test (Toshiba honeycomb-rohmbus composed type)

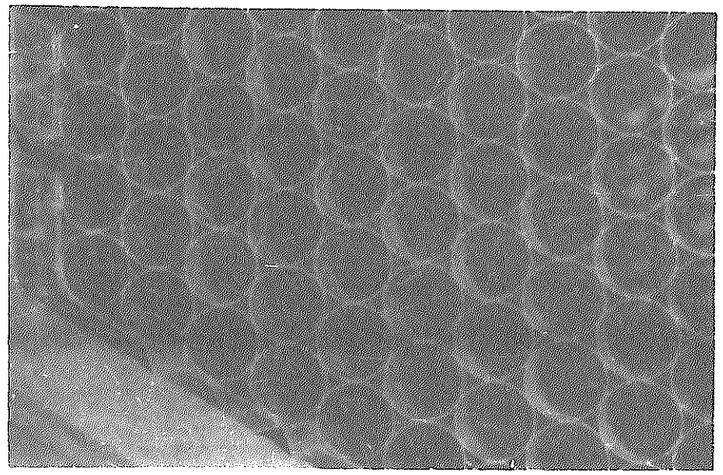

(MAP I)

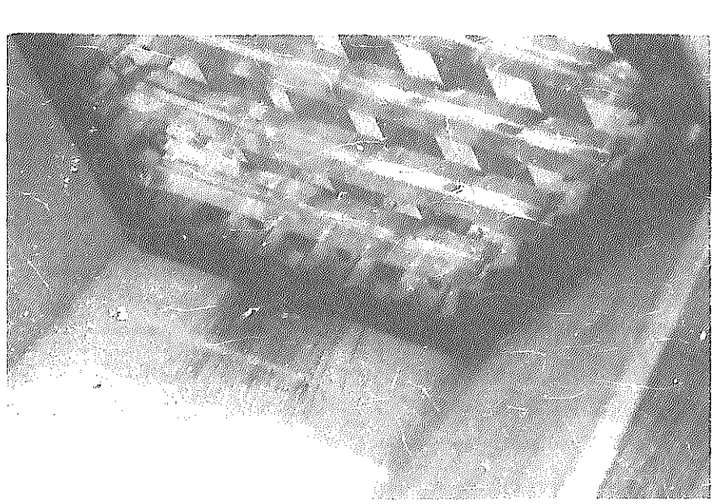

(TOSHIBA)

Photo 35 Grid spacer support for Bundle test